Doctoral Thesis

# Dosimetric Evaluation in Rats and Humans for Radio-Frequency Exposure with Multiphysics Simulation

複合物理解析を用いたヒト・ラットに対する高周波ドシメトリ評価

January 2019

Sachiko Kodera

# Contents

# List of Figures

# List of Tables

# Chapter 1

# Introduction

## 1.1. Background

The rapid development of wireless technology, including telecommunications, industrial applications etc., has changed the electromagnetic environment around humans, and has led to widespread concerns regarding adverse human health effects caused by exposure to electromagnetic fields. In the low-frequency exposure (below 100 kHz), the dominant factor is electro-stimulation caused by induced current in the body, whereas thermal effect caused by power absorption in radio-frequency (RF) exposure (above 100 kHz).

Microwave (MW) has been used for various purposes such as telecommunications and medical applications including diagnosis, hyperthermia therapy etc. Therefore, the temperature elevation in biological bodies is an important factor to be considered, while discussing human protection form RF exposure.

### 1.1.1. International Guidelines/Standards for Human Exposure

There are two international guidelines/standards that have been mentioned by the World Health Organization (WHO) as international recommendations for human protection from electromagnetic fields: ICNIRP guidelines [1] and IEEE standards [2]. The guidelines/standards indicate the temperature elevation above 100 kHz, although some studies have explored the

possibility of non-thermal effects.

The specific absorption rate (SAR), defined as power absorption per unit mass in W/kg, averaged over 10 g of tissue and whole-body is used as dose metrics, which is surrogate for local and core temperature elevations [1]–[3], respectively. Table 1.1 and Table 1.2 show the basic restrictions (BRs) in the international guidelines/standards [1], [2]. In the current guidelines/ standards, the SAR averaged over 10 g of tissue (localized SAR) for RF localized fields ranging from 100 kHz to 3 GHz [2] or 10 GHz [1]. At frequencies higher than 3 or 10 GHz, the surface heating becomes dominant; therefore, incident power density is used as a metric for human protection instead of SAR. The limit of the localized SAR is 10 W/kg for occupational exposure or in restricted areas, and a reduction factor of five is applied for the general public or in unrestricted areas. Wireless devices used in our daily life are designed to comply with the localized SAR limit for general public.

By current international standards, the averaging time for local exposure is 6 min for frequencies up to 3 GHz in controlled environments [2] or 10 GHz [1]. The rationale for this averaging time is not clearly mentioned in the guidelines/standard; according to [4], it was originally 0.1 h. Recent studies discuss the effectiveness of this averaging time [5], [6].

Table 1.1 Basic restrictions in ICNIRP guidelines

| | Frequency range | Current density for head and trunk (mA/m$^2$) | Whole-body averaged SAR (W/kg) | Localized SAR (head and trunk) (W/kg) | Localized SAR (limbs) (W/kg) | Power density (W/m$^2$) |
|---|---|---|---|---|---|---|
| Occupational exposure | up to 1 Hz | 40 | – | – | – | – |
| | 1–4 Hz | 40/$f$ | – | – | – | – |
| | 4 Hz–1 kHz | 10 | – | – | – | – |
| | 1–100 kHz | $f$/100 | – | – | – | – |
| | 100 kHz–10 MHz | $f$/100 | 0.4 | 10 | 20 | – |
| | 10 MHz–10 GHz | – | 0.4 | 10 | 20 | – |
| | 10–300 GHz | – | – | – | – | 50 |
| General exposure | up to 1 Hz | 8 | – | – | – | – |
| | 1–4 Hz | 8/$f$ | – | – | – | – |
| | 4 Hz–1 kHz | 2 | – | – | – | – |
| | 1–100 kHz | $f$/500 | – | – | – | – |
| | 100 kHz–10 MHz | $f$/500 | 0.08 | 2 | 4 | – |
| | 10 MHz–10 GHz | – | 0.08 | 2 | 4 | – |
| | 10–300 GHz | – | – | – | – | 10 |

Table 1.2 Basic restrictions for frequencies between 100 kHz and 3 GHz in IEEE standard

| | Frequency range | Whole-body averaged SAR (W/kg) | Localized SAR (peak spatial-average) (W/kg) | Localized SAR (extremities and pinnae) (W/kg) | RMS power density (W/m$^2$) |
|---|---|---|---|---|---|
| Persons in controlled environments | 100 kHz–3 GHz | 0.4 | 10 | 20 | – |
| | 3–6 GHz | 0.4 | 10 | 20 | 100 |
| | 6–300 GHz | – | – | – | 100 |
| Action level (general public) | 100 kHz–3 GHz | 0.08 | 2 | 4 | – |
| | 3–6 GHz | 0.08 | 2 | 4 | 10 |
| | 6–100 GHz | – | – | – | 10 |
| | 100–300 GHz | – | – | – | (90$f_G$-7000)/200 |

Unlike body-core temperature elevation, whose time constant is of the order of an hour or longer [7], the time required for local temperature to reach a steady state is the order of a few dozen minutes [8], [9] and depends on frequency and exposure area/volume [10].

## 1.1.2. Revision of Guidelines/Standard

There are differences between ICNIRP guidelines and IEEE standards. Examples are the upper frequency boundary for SAR, averaging scheme of localized SAR and incident power density, and averaging time. These are caused by lack of rationale above 6 GHz. These frequency ranges will be used in the fifth generation mobile communication systems. The ICNIRP guidelines and the IEEE standards are currently being revised. The IEEE draft standard C95.1 and the public consultation document of the ICNIRP were issued on February (and later updated) and July 2018, respectively. The main differences from current guidelines/standards for RF exposure are as follows:

- SAR is applied from 100 kHz to 6 GHz.
- Averaging time is 30 min for whole body RF exposure and 6 min for local exposure.
- Averaging scheme of localized SAR corresponding to 10 g of tissue in a cube shape is also adopted in the ICNIRP.
- Transmitted power or energy density (TPD or TED), which is a new physical quantity corresponding to the local temperature elevation, is introduced as a basic restriction from

6 GHz to 300 GHz.

## 1.1.3.   Related Previous Studies and Research Necessity

*Extrapolating Thermal Damage in Animals to Humans*

Many studies examine thermal damages in animals and extrapolate the findings to humans, primarily for ethical reasons concerning health risks to human subjects [11]–[14], as also summarized in the guidelines/standards (see the review in ICNIRP [15] and IEEE standard [2]). For example, the point SAR measurement and local temperature elevation in anesthetized rabbit eyes have been cited in the ICNIRP 1998 guidelines [1]. The SAR threshold value, estimated with a probe of finite dimension, was 137 W/kg [16]. Animal studies are one of the important topics in safety assessment as reviewed in [17], [18]. In most animal studies, SARs are evaluated computationally to estimate the heat load. In experiments, the number of locations for measuring the temperature is limited. Thus, it is useful to develop a computational model for multiphysics (electromagnetics and thermodynamics) and thermal response to follow temperature and blood perfusion for MW exposure, particularly for intense localized exposure. Till date, only a few computational models considering multiphysics and thermal response have been developed (e.g., on rats [19]–[21] and rabbits [14]). Even for humans, only very few groups have run successful studies on this [22]–[25]. Clarification of the difference in temperature elevation and its time evolution in humans and animals may contribute to the scientific rationale of international guidelines/standards.

*Thermal Damage and Time Constant*

For discussion of thermal damages, the intensity and exposure duration of MW are essential. Thermal damage, for example, occurs when rabbit eyes are exposed to high-intensity RF waves for $\geq 30$ min (e.g., [16], [26]). Also, many studies examine thermal damage in rats (e.g., [27]–[29]). The thermal damage of tissues is characterized by CEM43 as reviewed in [30]. The WHO

workshop in 2002 [31], ICNIRP thermal damage workshop [18], and FDA thermal damage workshop concluded that thermal limits should consider both temperature and time of exposure, whenever possible.

Foster et al [4] derived an analytic formula to estimate the thermal time constant using a one-dimensional homogeneous model for intense brief exposures, especially for millimeter waves. Some studies using human anatomical models computed the thermal time constants for handset antennas without considering thermoregulation [5], [8], [9], [32]. However, no reports have compared thermal time constants between humans and animals, making direct extrapolation of findings from animals to humans difficult. Note that thermal damages are caused by the exposure time-temperature elevation relationship [30], which are not considered in the international guidelines/standards. This is because the limits for SAR and incident power density are set so that allowable temperature elevation is well below the limit for thermal damage. Clarifying the difference in temperature elevation and its time course between rats and humans exposed to local RF fields is important, in order to estimate the conservativeness of current limits for local exposure, in the international guidelines/standards.

*Limit of Temperature Elevation in Internal Tissue*

The localized SAR limits are intended to prevent excessive heating, especially in internal tissue (e.g., brain and eye, which have high sensitivity). Temperature elevation computed in the brain is listed on Table C.2 in Annex C of the IEEE standard C95.1 [2]. The temperature elevation at 10 W/kg of the localized SAR is approximately 1 °C. In the IEEE standard [2], temperature elevation in the eye without anesthesia has been reported to be smaller [12]. Later, Hirata reported that this is caused due to the effect of thermoregulation in non-anesthetized rabbits [14]. No computational study listed therein considered the effect of thermoregulation, which is inherent in homeotherms such as humans, on the human temperature elevation for localized exposures.

The heating factor, which is defined as the ratio of temperature elevation to SAR, has been introduced and discussed extensively [33]. After obtaining this factor, temperature elevation can

be estimated in the regime where thermoregulation can be neglected. As one of the drawbacks of this concept, temperature under thermoneutral conditions depends on the body part and is not directly related to thermal damage. For example, information of the location where maximum temperature appeared is missed. When thermoregulation is ignored, the heating factor becomes conservative when tissue temperature becomes large enough to activate thermoregulation. Thermoregulation, especially for vasodilation, can move heat away and maintain homeostasis. Many researchers developed a thermoregulatory response model that included vasodilation. These models are based on the measurements of internal tissues during animal studies. Some of these studies used an invasive approach with anesthesia (e.g., [34]). Even though a limited amount of data on thermoregulation is available for internal tissues in humans, it is known that thermoregulation in humans is superior to that of other species [35]. Previous studies have not evaluated the temperature elevation in human head models for local exposure, while considering thermoregulation. It should be noted that several studies computed the temperature elevation for whole-body exposures [7], [22], [25], [36], [37].

*Limit of Absorbed Energy for Brief Exposure*

The averaging time for local exposure is defined as 6 min in the guidelines/standards. If all the energy over an averaging time of 6 min was concentrated into a short duration (e.g., several seconds), the local temperature elevation for a pulse may exceed the temperature elevation due to constant exposure [4]. This is because the effect of blood flow is marginal for brief exposures (e.g., several seconds), and thus an adiabatic condition is approximately valid. Indeed, the temperature elevates almost linearly with time in such cases. The electromagnetic energy is thus concentrated on the superficial part of the 10 g-averaged SAR volume, which is due to the decrease in penetration depth as a function of frequency. Also, in adiabatic conditions the uneven distribution of localized SAR in conducting tissues such as skin, in contrast to low conducting fat, increases local peak temperature before the heat diffusion washes them out. Human protection for such pulses that are shorter than the averaging time has been discussed in Global Coordination of Research and Health Policy on RF Electromagnetic Fields (GLORE) in

6

November 2017 (Washington DC, USA). Further analysis is therefore needed to understand the temperature elevation due to brief intervals in order to protect humans from pulses that are shorter than the averaging time.

For frequencies above 10–30 GHz, the radiant exposure (incident energy density) averaged over a specific area is currently being discussed (e.g., GLORE in November 2017). This physical quantity is a good metric to describe skin temperature elevation, as it is supported by surface heating theory [38] and a computational model [39]. For brief exposure above 6 GHz, the correlation between TED and temperature elevation is computed [40].

For frequencies below 6 GHz, the corresponding physical quantities would be specific (energy) absorption (SA) [2]. It was mentioned in the ICNIRP 1998 guidelines [1] that "*For frequencies exceeding 10 MHz, $S_{eq}$ (equivalent power density) as averaged over the pulse width should not exceed 1,000 times the reference levels or that field strengths should not exceed 32 times the field strength reference levels. For frequencies between about 0.3 GHz and several GHz, and for localized exposure of the head, in order to limit or avoid auditory effects caused by thermoelastic expansion the specific absorption from pulses must* (be) *limited.*" The IEEE C95.1 standard [2] mentioned that "*For short duration exposures the BRs* (basic restrictions) *and MPEs* (maximum permissible exposures) *are related to energy, i.e., specific absorption (SA) or energy density.*" In the ICNIRP public consultation document, the MW hearing effect [41] caused by thermoelastic waves are not considered as an harmful tissue damaging effect. The SA is also used to limit temperature elevation from brief pulses, but for a different purpose. Specifically, it is set to limit temperature elevation to 5 °C and 2 °C for superficial and deeper tissue, respectively. The reduction factor 2 is applied for occupational exposure. The SA limit was mentioned in the IEEE C95.1 standard, and equivalently instantaneous peak power density is limited to remain below a certain level. However, to the best of our knowledge, no study has evaluated temperature elevation for a pulse or pulse trains with energy concentrated shorter than the averaging time (6 min). It would prove to be a useful to ensure human safety when exposed to RF energy, if the best way to set the metric in order to limit temperature elevation from brief exposures is determined.

## 1.2.   Contents of Thesis

This study evaluated temperature elevations and thermoregulation using the multiphysics simulation from the viewpoint of RF safety. The motivations of this study are as follows:

1.  To estimate temperature elevation in a rat cortex for localized exposure to high-intensity MW by considering heat transfer and thermoregulation. Thus, the development of improved multiphysics code in regional cerebral blood flow is needed.

2.  To clarify the difference in temperature elevation and thermal time constants between rats and humans. The target tissues are the skin, in which power absorption is concentrated at high frequencies, and the brain, which has high sensitivity to heat.

3.  To investigate brain temperature elevation for excessive SAR exposure levels and to find out how vasodilatation can affect temperature elevation and how it relates to the exposure limits.

4.  To evaluate temperature elevation for a pulse or pulse trains with energy concentrated shorter than the averaging time (6 min), and determine how best to set the metric in order to limit temperature elevation from brief exposures.

The contents of this thesis are as follows.

Chapter 1 introduces the background and motivation of this study.

Chapter 2 explains numerical human/rat models and computational methods. First, the numerical rat, multilayer cube, and four individual human models are presented. Next, the finite-difference time-domain (FDTD) method for computing the absorbed RF power in the numerical models is explained. The bioheat transfer equation by considering thermoregulation is described.

Chapter 3 proposes a thermoregulatory response model in the rat brain based on local brain and body core temperatures. First, parameters that accurately reflect changes in regional cerebral blood flow (rCBF) are extracted from experimental data using rats (anesthetized). Next, these parameters are incorporated into our thermophysiological model to simulate the temperature

elevation during and after local RF exposure. Finally, the effectiveness of the newly acquired computational model is examined by comparing the temperature changes simulated by the model with the measured values.

Chapter 4 estimates the thermal time constants of temperature elevation in human and rat models exposed to dipole antennas at 3–10 GHz. This chapter aims to clarify the difference in temperature elevation and its time course between rats and humans exposed to local RF fields.

Chapter 5 computes the brain temperature elevation for excessive SAR exposure levels to find out how vasodilation can affect temperature elevation and how it relates to the exposure limits. This chapter computes the temperature elevation in an anatomical human head model exposed to dipole antennas and truncated plane waves at 300 MHz–10 GHz.

Chapter 6 confirms the temperature elevation for brief exposure. This chapter proposes the limit from regression curves that is dependent on the duration of brief exposure to RF pulses. The limits based on the regression curve can be used as a metric to prevent excess temperature elevation for different brief exposure scenarios.

Chapter 7 shows the summary of this study.

# Chapter 2

# Models and Methods

## 2.1. Overview

In this study, we computed the temperature elevation for local MW exposure. We used the multiphysics simulation considering thermoregulation.

Our procedure is two-stepped approach. We first computed the SAR in anatomical models based on the Maxwell equation. We then solved the bioheat transfer equation taking SAR as a heat source, exchange to blood, heat conduction, and blood perfusion into account.

In this study, the Finite-Difference Time-Domain (FDTD) method was used [42] for solving electromagnetic fields. The FDTD method is one of the most common methods for solving electromagnetic problems. The FDTD method is introduced by Yee [43] and a method of discretizing Maxwell's equation in time and space and calculating it successively.

For solving of the time evaluation of temperature, the bioheat transfer equation was discretized in time. After the formulation of Pennes' bioheat equation [44], many improvements have been made to it for different purposes. Bioheat equations are often used to calculate temperature elevation in numerical models. The equation provides approximate temperature and is demonstrated to be a reasonable and powerful tool for analyzing temperature, especially in the shallow region of the body [45], [46]. This chapter describes the numerical human/rat models and computational methods.

## 2.2.    Numerical Human/Rat Models

### 2.2.1.    Numerical Rat Model

A numerical rat model was developed from computed tomography (CT) images [47], as seen in Figure 2.1. The model is composed of the following six tissues: muscle, skin, fat, eye, bone, and brain. These tissues were classified in semi-automatic procedure and then manual editing by an expert was partly added in a similar method to [48]. The voxelized model (94,276,000 elements) has a resolution of 0.25 mm. The whole-body and brain weights used in the rat model corresponded to 265 and 1.9 g, respectively.

Unit : mm



Side View

Front View

Cross-section
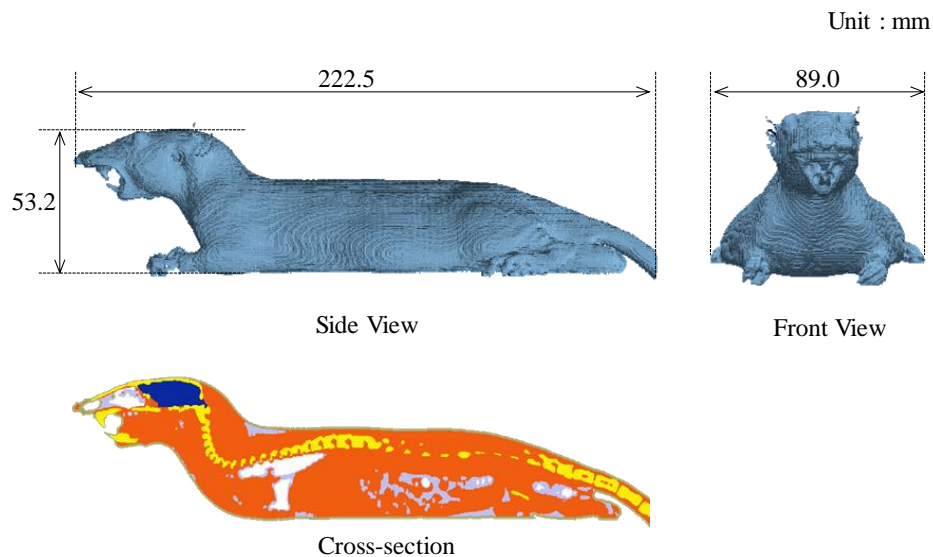
Figure 2.1 Numerical rat model

### 2.2.2.    Multilayer Cube Model

Figure 2.2 shows a three-dimensional multilayer cube model that was used for simulating a human head. This model is comprised seven-layers; the skin (1.5 mm), fat (1.5 mm), muscle (2.5 mm), skull (4.5 mm), dura (1.0 mm), cerebrospinal fluid (1.0 mm), and brain (58.0 mm).

Each thickness was determined based on the measurement at the region of the auricularis superior muscle [49].
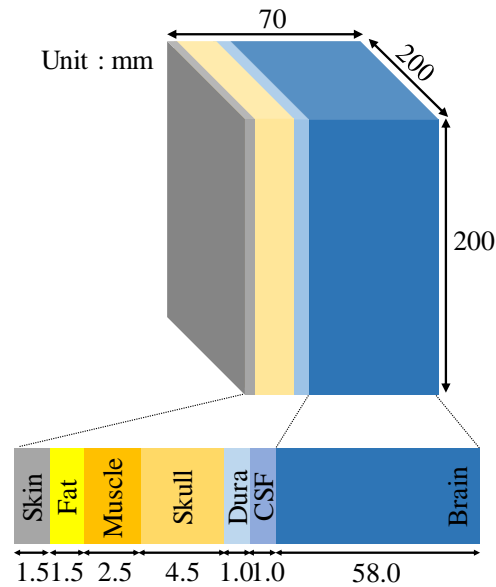


Figure 2.2 Multilayer cube model

### 2.2.3. Anatomical Human Head Models

In this study, realistic anatomical human models for different ages and gender were considered. Figures 2.3 and 2.4 show the Japanese male model (TARO) [50] and the European models of the Virtual Family (Duke, Ella, and Billie) [51], respectively. Taro was developed based on the magnetic resonance (MR) images of volunteer. Each image featured a slice thickness of 2 mm [50]. This model was segmented into 51 anatomical regions and had 2 mm resolution. A major source of computational error in the finite-difference time-domain (FDTD) method is the discretization error, which depends on the ratio between the cell size and the wavelength in biological tissue. A rule to suppress the numerical dispersion error in FDTD simulations is that the maximum cell size should be smaller than one-tenth of the wavelength [42]. Thus, the model resolution was adjusted to 0.5 mm to ensure computational accuracy. Duke, Ella and Billie were developed based on the MR images of volunteers. These model were segmented into 77, 74, and

73 anatomical regions, respectively, and they had 0.5 mm resolution.

The human models were truncated at the bottom of the neck because the rest of the body marginally affects the interaction with the dipole antenna [52] (see Appendix A). These truncated head models were composed of 23 tissues.
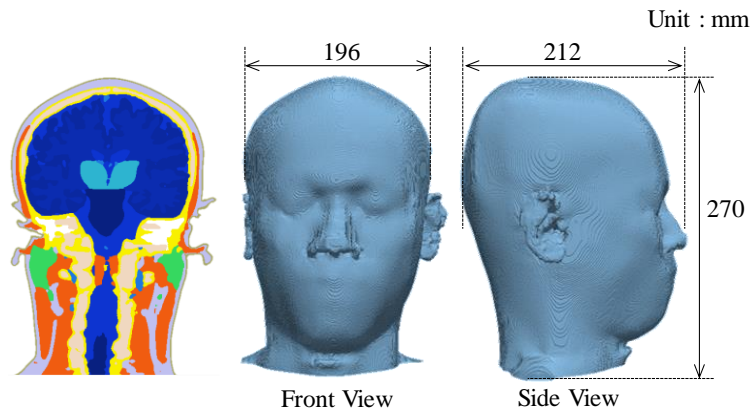


Figure 2.3 Japanese male head model (TARO)
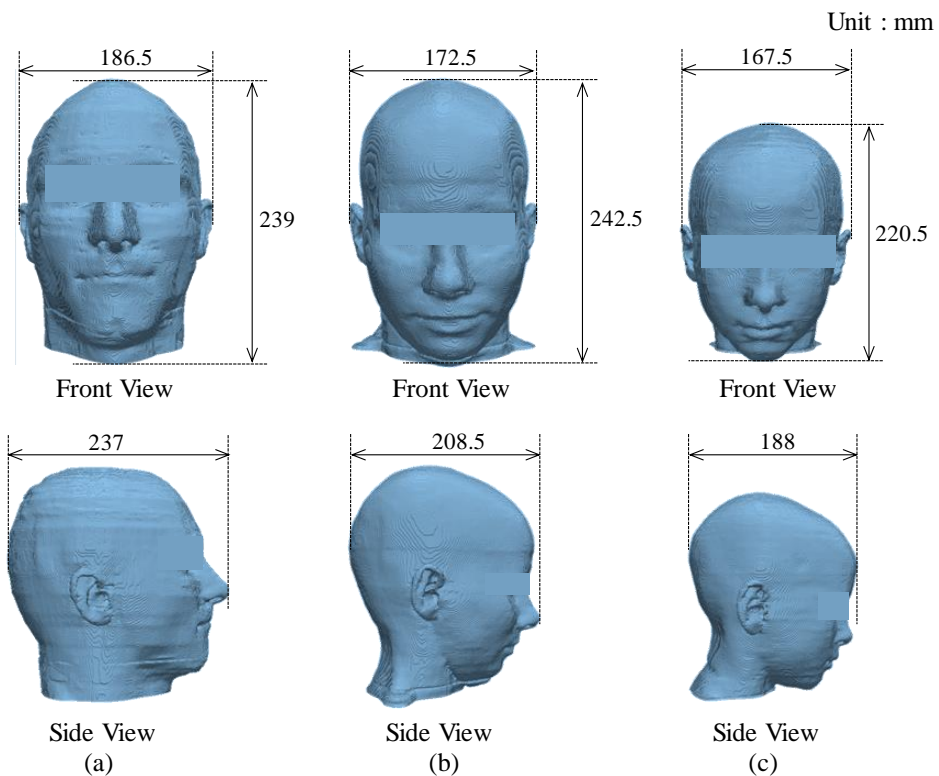


Figure 2.4 European head models (Virtual Family); (a)Duke, (b)Ella, and (c)Billie

## 2.3.    Computational Methods

### 2.3.1.    Electromagnetic Field Computation

*FDTD Methods*

There are various analysis methods such as the moment method and the finite element method for calculating the electromagnetic field. In this study, we analyzed using the FDTD method [42], which has a comparatively small computational capacity and is suitable for calculating electromagnetic fields for inhomogeneous medium such as living body. The electromagnetic field in the region can be solved by discretizing the Maxwell's equation into the time and the spatial domain.

Convolutional perfectly matched layers (CPML) were used as the absorbing boundary conditions for absorbing outgoing scattered waves to simulate an infinite space [53]. The dielectric properties of each type of tissue were determined with a Cole–Cole dispersion model in both rat and human models [54]. The variability caused by different sets of dielectric properties has been shown to be marginal [55]. The SAR was defined for sinusoidal waves as follows:

$$SAR(\mathbf{r}) = \frac{\sigma(\mathbf{r})}{2\rho(\mathbf{r})} |\mathbf{E}(\mathbf{r})|^2 \qquad (2.1)$$

where $|\mathbf{E}|$ denotes the temporal peak value of the electric field at position $\mathbf{r}$, and the parameters $\sigma$ and $\rho$ denote the conductivity and mass density of the tissue, respectively.

## 2.3.2. Temperature Computation

*Bioheat Transfer Equation*

The Pennes bioheat transfer equation considers heat exchange mechanisms, including heat conduction, blood perfusion, and resistive heating, as follows [44]:

$$C(\mathbf{r}) \cdot \rho(\mathbf{r}) \frac{\partial T(\mathbf{r},t)}{\partial t} = \nabla \cdot \left( K(\mathbf{r}) \cdot \nabla T \right) + A(\mathbf{r})$$

$$+ \rho(\mathbf{r}) SAR(\mathbf{r}) - B(\mathbf{r},t)\left( T(\mathbf{r},t) - T_B \right), \tag{2.2}$$

where $\mathbf{r}$ and $t$ denote the position vectors of tissue and time, respectively, and $T(\mathbf{r}, t)$ and $T_B(\mathbf{r}, t)$ denote the temperatures of tissue and blood, respectively. In addition, $C$ denotes the specific heat of the tissue, $K$ denotes the thermal conductivity of the tissue, $A(\mathbf{r}, t)$ denotes the metabolic heat, and $B(\mathbf{r}, t)$ denotes the factor related to blood perfusion. The $SAR(\mathbf{r}, t)$ determined from Equation (2.1) is substituted into the bioheat equation as a heat source.

The boundary condition between tissues and external air is

$$-K(\mathbf{r}) \frac{\partial T(\mathbf{r},t)}{\partial n} = H(\mathbf{r}) \cdot \left( T(\mathbf{r},t) - T_a \right) + EV(\mathbf{r},t), \tag{2.3}$$

where $T_a$, $H$, and $n$ denote the ambient temperature, heat transfer coefficient, and a vector normal to the body surface, respectively. $EV$ denotes the evaporative heat loss function.

The heat flow was assumed to continue in the direction perpendicular to the body surface in the boundary condition. That is, the temperature difference between the external air and the superficial tissues is approximated by the temperature gradient between the superficial tissue and the tissue adjacent in the direction perpendicular to the body surface.

*Blood Temperature*

It does not satisfy the first law of thermodynamics as the heat removed from tissue with blood perfusion vanishes in a conventional formulation of the bioheat equation. This violation would not be essential when the radio frequency (RF) energy deposition in the body is smaller than the

total amount of the basal metabolism. For intense localized exposure (as in the rat experiments), the body-core temperature elevates with time (e.g., see [16]; rabbits exposed to intense localized exposures). To analyze the temperature in the body, Bernardi et al. [22] treated the blood temperature in the bioheat equation as variable over time but constant over the body to consider the energy deposited in the blood. We improved the formula for blood temperature in the voxelized models [56].

The volume-averaged blood temperature is changed such that the first law of thermodynamics is satisfied. The change in blood temperature is defined as [22].

$$T_B(t) = T_{B0} + \int \frac{Q_{BT}(t)}{C_B \rho_B V_B} dt , \tag{2.4}$$

$$Q_{BT}(t) = \int B(t)\big(T_B(t) - T(\mathbf{r},t)\big)dV , \tag{2.5}$$

where $Q_{BT}(t)$ denotes the total receiving heat quantity from tissues to blood. Additionally, $C_B$ (=4000 J/(kg·°C), $\rho_B$ (=1058 kg/m$^3$), $T_{B0}$, and $V_B$ denote the specific heat of blood, mass density of blood, initial blood temperature, and total volume of blood, respectively. The average blood volume per unit of rat body mass correspond to 64 mL/kg [57]. The blood volume of the rat model was set at 18.9 mL. The blood temperature in the human head models was fixed at 37 °C, because it marginally affects the temperature elevation for local RF exposure (see Appendix A).

The initial temperature $T_0$ was solved using Equations (2.2) and (2.3) by setting $SAR = 0$ W/kg and $T_{B0} = 37.0$ °C. $T_{B0}$ was estimated from the average rectal temperature (body core temperature) of the anesthetized live rats without exposure. The bioheat equation subject to the boundary condition was solved to obtain the thermally steady-state temperature elevation. Thus, the left-hand-side term of Equation (2.2) was assumed as zero.

*Thermoregulation*

Thermoregulation is a biological characteristic reaction that expand a blood vessel or promotes perspiration in order to positively escape the heat inside body against heat stimulation from outside.

First, the modeling of the vasodilatation is described. The blood flow parameter $B(\mathbf{r},t)$ in the

skin depends on both the hypothalamus temperature and local skin temperature [58]. Skin blood flow was regulated by hypothalamus temperature, and the average temperature of the skin can be expressed as follows:

$$B(\mathbf{r},t) = \left\{ B_0(\mathbf{r}) + F_{HS}\Delta T_H(t) + F_{SS}\overline{\Delta T_S(t)} \right\} \cdot 2^{(T(\mathbf{r},t)-T_0(\mathbf{r}))/6},$$

$$\overline{\Delta T_S(t)} = \frac{\int_S \left( T(\mathbf{r},t) - T_0(\mathbf{r}) \right) \cdot ds}{S}, \tag{2.6}$$

where $B_0$ denotes the basal blood perfusion of each tissue, $\Delta T_S(t)$ denotes the average temperature elevation of the skin, and $\Delta T_H(t)$ denotes the elevation of the core temperature. Additionally, $F_{HS}$ (=17,500 W/m³/°C) and $F_{SS}$ (=1100 W/m³/°C) are the coefficients that determine the changes in the blood perfusion characteristics over time [59]. Thus, the blood and hypothalamus temperature elevations were used as the approximate body core temperature in rat and human models, respectively.

Blood flow in the brain is influenced by the core and brain local temperature elevations and is expressed as [21]

$$B(\mathbf{r},t) = B_0(\mathbf{r}) \cdot \left( 1 + F_{HB} \cdot \Delta T_H \right) \cdot 2^{(T(\mathbf{r},t)-T_0(\mathbf{r}))/F_{BB}}, \tag{2.7}$$

where $F_{HB}$ and $F_{BB}$ denote weighting coefficients relating to the variations in the core and brain temperature elevations, respectively. The parameters of $F_{HB}$ and $F_{BB}$ are extracted in section 3.3.3.

Regulation of blood perfusion in tissues (except for the skin and brain) is defined as [60], [61]

$$\left.\begin{array}{ll} B(\mathbf{r},t) = B_0(\mathbf{r}) & \left( T(\mathbf{r},t) \leq 39\,^{\circ}\text{C} \right) \\ B(\mathbf{r},t) = B_0(\mathbf{r}) \cdot \left[ 1 + S_B \left( T(\mathbf{r},t) - 39 \right) \right] & \left( 39\,^{\circ}\text{C} < T(\mathbf{r},t) \leq 44\,^{\circ}\text{C} \right) \\ B(\mathbf{r},t) = B_0(\mathbf{r}) \cdot \left( 1 + 5 \cdot S_B \right) & \left( 44\,^{\circ}\text{C} < T(\mathbf{r},t) \right) \end{array}\right\} \tag{2.8}$$

where $S_B$ (= 0.8 °C⁻¹) denotes a coefficient defining changes in the blood perfusion characteristics over time.

Next, the modeling of sweating in human is described. Evaporative heat loss is assumed to depend on the temperature elevation on the skin and in the hypothalamus. This relationship is defined as [62]

$$EV(\mathbf{r},t) = \begin{bmatrix} \left\{ \alpha_{11} \tanh\left( \beta_{11} \Delta T_S(t) - \beta_{10} \right) + \alpha_{10} \right\} \Delta T_S(t) \\ + \left\{ \alpha_{21} \tanh\left( \beta_{21} \Delta T_H(t) - \beta_{20} \right) + \alpha_{20} \right\} \Delta T_H(t) + PI \end{bmatrix} \cdot F_{EV} / S, \qquad (2.9)$$

where $F_{EV}$ (= 40.6 W·min/g) is a conversion coefficient, and $S$ is the surface area of the human. The parameter of $PI$ (= 0.63 g/min) is insensible water loss, and the coefficients are defined as $\alpha_{10} = 1.20$ g/(min·°C), $\alpha_{11} = 0.80$ g/(min·°C), $\beta_{10} = 0.19$, $\beta_{11} = 0.59$ °C$^{-1}$, $\alpha_{20} = 6.30$ g/(min·°C), $\alpha_{21} = 5.70$ g/(min·°C), $\beta_{20} = 1.03$, and $\beta_{21} = 1.98$ °C$^{-1}$.

Core temperature elevation is one of the essential parameters in sweating. For the maximum output power of the dipole antenna, corresponding to an SAR of 100 W/kg, the total power absorbed in by the human body is less than 30.3 W, which is a quarter of the basal metabolism of the human. Note that a whole-body averaged SAR of 4–6 W/kg (260–390 W for a 65-kg adult) results in a core temperature elevation of 1 °C. As will be discussed in the Appendix A, the effect of core temperature elevation and sweating is not dominant for the scenarios considered here.

Table 2.1 Thermal properties of rat model

| Tissues | $\rho$ (kg/m$^3$) | $K$ (W/(m·°C)) | $C$ (J/(kg·°C)) | $B_0$ (W/(m$^3$·°C)) | $A$ (W/m$^3$) |
|---|---|---|---|---|---|
| Fat | 916 | 0.25 | 3000 | 6299 | 4983 |
| Muscle | 1047 | 0.50 | 3800 | 2880 | 2278 |
| Bone | 1990 | 0.37 | 3100 | 12,317 | 9743 |
| Eye | 1009 | 0.57 | 4000 | 0 | 0 |
| Brain | 1038 | 0.57 | 3800 | 35,692 | 28,233 |
| Skin | 1125 | 0.42 | 3600 | 11,605 | 9180 |

Density is denoted as $\rho$, thermal conductivity is denoted as $K$, specific heat is denoted as $C$, basal blood flow parameter is denoted as $B_0$, and basal metabolism is denoted as $A$.

*Thermal Constants of Tissues*

Table 2.1 lists the thermal parameters of tissues adapted in the rat model. The specific heat and thermal conductivities shown in a study by Cooper et al. [63] were used. The term associated with blood flow for each tissue was extrapolated from a study by Gordon et al. [35]. The basal metabolism of the entire body of a rat was estimated based on Kleiber's law [64] and associated

with each tissue in the model based on a reference to the proportion of blood flow [35]. The blood flow for eye tissue was ignored for simplicity. Not that blood flow on the retina and choroid is high. However, it has minor impact on the temperature elevation in the target area. The heat transfer coefficients were based on those used in a study by Hirata et al. [21]; the coefficient of air and skin is 0.5 W/(m$^2$·°C) and that of lung and air is 8.1 W/(m$^2$·°C). For these parameter sets, together with the basal metabolism in Table 2.1, the heat balance between the air and rat model is maintained (basal metabolism of the rat model was estimated at 1.4 W).

Table 2.2 shows the thermal parameters of tissues adapted in the human and multilayer models. The thermal parameters used in this study are the same as those used by [65], where the parameters were borrowed primarily from [66]. In addition, the blood perfusion rate through skin was the same as that used in [38]. The blood perfusion varies substantially even in a shallow region (surface to 3 mm). Its impact on the surface temperature elevation is ±15% at frequency higher than 6 GHz [39], which is consistent with Monte-Calro approach by [67]. This study used relatively low blood perfusion rate to discuss conservative temperature elevation in RF exposure safety. Note that for relatively brief exposure (e.g., < 10 s), the effect of the blood perfusion rate on the temperature elevation is negligible. The heat transfer coefficient between skin and air was set to 5 W/m$^2$/°C, which is a typical value at an ambient temperature of 23 °C [62].

## 2.3.3. Averaging Algorism of SAR Averaged over 10 g

The SAR was averaged over 10 g of tissues in a cube shape following IEEE C95.3 [3], IEEE 1528-2013 [68], and IEC 62209-1:2016 [69]. In the current ICNIRP guidelines [1], the averaging volume of SAR corresponds to contiguous tissue. The SAR averaging over contiguous tissue is feasible in computation, but is not practically feasible as later noted by the ICNIRP [70]. Thus, the SAR averaging volume, but has been changed to a cube in the ICNIRP public consultation document. Even though the SAR is not used at frequencies above 6 GHz by the IEEE standard [2], the same metric was used at 10 GHz for a proper comparison. The localized SAR in a single contiguous tissue following the ICNIRP guidelines [1] was difficult to use in the rat model, because the rat skin weight over the whole body was 32 g.

The averaging mass of the SAR has been discussed by [71]–[73]. The main conclusion drawn by international experts is that the averaging mass of 10 g, corresponding to a cube with a side length of approximately 22 mm, is a good metric to correlate with the local temperature elevation [74]. The reference level (intensity of electromagnetic fields), which is an external physical quantity is evaluated based on this localized SAR in the international guidelines/standards.

As no averaging volume/mass has been discussed for the SA, 10 g averaging mass was chosen considering the continuity at the limit for longer than 6-min exposures. If this averaging mass was not used, the compliance may become very complicated; the evaluation metric varies with exposure duration.

Table 2.2 Thermal properties of human model

| Tissues | $\rho$ (kg/m$^3$) | $K$ (W/(m·°C)) | $C$ (J/(kg·°C)) | $B_0$ (W/(m$^3$·°C)) | $A$ (W/m$^3$) |
|---|---|---|---|---|---|
| Skin | 1125 | 0.42 | 3600 | 7367 | 1620 |
| Muscle | 1047 | 0.50 | 3800 | 2700 | 480 |
| Fat | 916 | 0.25 | 3000 | 1626 | 300 |
| Cortical Bone | 1990 | 0.37 | 3100 | 3400 | 610 |
| Cancellous Bone | 1920 | 0.41 | 3200 | 3300 | 530 |
| Cartilage | 1097 | 0.47 | 3600 | 9000 | 1600 |
| Nerve | 1038 | 0.46 | 3400 | 40000 | 7100 |
| Dura | 1125 | 0.50 | 3600 | 9100 | 0 |
| Gray Matter | 1038 | 0.57 | 3800 | 40000 | 7100 |
| White Matter | 1038 | 0.50 | 3500 | 40000 | 7100 |
| Cerebellum | 1038 | 0.57 | 3800 | 40000 | 7100 |
| CSF | 1007 | 0.62 | 4000 | 0 | 0 |
| Hypothalamus | 1038 | 0.57 | 3800 | 40000 | 7100 |
| Vitreous Humor | 1009 | 0.58 | 4000 | 0 | 0 |
| Lens | 1053 | 0.40 | 3000 | 0 | 0 |
| Retina | 1026 | 0.58 | 4000 | 0 | 0 |
| Blood | 1058 | 0.56 | 3900 | 0 | 0 |
| Tongue | 1047 | 0.54 | 3800 | 2700 | 480 |
| Thalamus | 1038 | 0.57 | 3800 | 40000 | 7100 |
| Pituitaria | 1038 | 0.57 | 3800 | 40000 | 7100 |
| Pineal | 1038 | 0.57 | 3800 | 40000 | 7100 |
| Trachea | 1100 | 0.47 | 3650 | 3700 | 1600 |
| Glandula Salivaria | 1000 | 0.42 | 3500 | 2350 | 4200 |
| Brain (Averaged) | 1038 | 0.57 | 3800 | 40000 | 7100 |

Density is denoted as $\rho$, thermal conductivity is denoted as $K$, specific heat is denoted as $C$, basal blood flow parameter is denoted as $B_0$, and basal metabolism is denoted as $A$.

# Chapter 3

# Modeling of Thermoregulation

## 3.1.   Overview

The rapid development of wireless technology has led to widespread concerns regarding adverse human health effects caused by exposure to electromagnetic fields. Temperature elevation in biological bodies is an important factor that can adversely affect health. A thermophysiological model is desired to quantify MW induced temperature elevations.

In this chapter, parameters related to thermophysiological responses for MW exposures were estimated using an electromagnetic-thermodynamics simulation technique. An apparatus for highly-localized MW exposure employing frequencies higher than several GHz is developed in the present study to maximize tissue exposure local to the antenna, while suppressing exposure levels elsewhere in the rat body. This improves the accuracy of the thermo-physiological model and makes it suitable for general applications. Specifically, it is useful for a number of applications to evaluate thermal evaluation in a consistent model that can be used for conventional and higher frequencies. Such a model can be a powerful tool in providing useful data when replicating previous measurements, some of which provide a rationale of MW protection guidelines/standards.

To our knowledge, this is the first study in which parameters related to regional cerebral blood flow in a rat model were extracted at a high degree of accuracy through experimental measurements for localized MW exposure at frequencies exceeding 6 GHz. The findings indicate that the improved modeling parameters yield computed results that match well with the measured quantities during and after exposure in rats. It is expected that the computational model

will be helpful in estimating the temperature elevation in the rat brain at multiple observation points (that are difficult to measure simultaneously) and in explaining the physiological changes in the local cortex region. The results presented here was published in [75], [76].

## 3.2. Methods

### 3.2.1. Animal Experiments

Changes in physiological parameters were measured using live rats under MW exposure corresponding to three frequencies (1.5, 6, and 10 GHz). All animal experiments corresponding to 6 and 10 GHz were approved by the Institutional Animal Care and Use Committee of Tokyo Medical and Dental University. The animal experimental data corresponding to 1.5 GHz were obtained in a previous study [21] and reused to evaluate the effectiveness of the computational model proposed in the present study.

*Animals*

Eight-week old male Sprague–Dawley rats (Japan SLC, Inc., Shizuoka, Japan) were used in the experiments. The rats were fed a standard pellet diet and given water ad libitum in an animal room with a 12 h light/dark cycle at a temperature corresponding to 23.0 ± 1 °C and relative humidity corresponding to 50 ± 20%.

*Definition of Target Area*

The target area is defined as a disk-shaped area of a rat's right parietal cortex tissue (4 mm in diameter and 0.25 mm deep), within which physiological responses to MW exposure were evaluated (see Figure 3.1c). The target area is located immediately under the dura mater, and its center is located 4 mm posterior to the bregma and 4 mm to the right of the midline.

*Measurement of Physiological Parameters*

Two physiological parameters, that is, temperature of the rectum and target area and rCBF in the target area were simultaneously measured using methods described in our previous study

[21], [34]. Briefly, the rats were anesthetized during the experiment and were placed on a heated pad after the head was fixed in the acrylic stereotaxic apparatus. The temperature of the heated pad was kept at 42 °C for a 1.5 GHz-exposure system, and at 39 °C for 6 and 10 GHz-exposure systems to stabilize temperatures in each measured region under sham-exposure conditions in our experimental setup. The right parietal skin was locally excised, and the skull of the right hemisphere was exposed. Three independent holes (0.5 mm in diameter) were drilled into the skull just above the target area 1.0 mm apart from each other. Two optical fibers (0.2 mm in diameter) connected to the Doppler blood flow meter (FLO-C1, Omegawave, Tokyo, Japan) and one optical probe (0.5 mm in diameter) connected to a thermometer (m600, Luxtron, Santa Clara, CA, U.S.A.) were independently inserted through the three holes and placed on the dura mater above the target area. Another thermometer probe was inserted into the rectum. The above-mentioned probes are all made of nonmetallic material. The blood flow and temperature signals were recorded at a 1.0 Hz sampling rate through an A/D converter and time was averaged over 1 min intervals.

*1.5 GHz Experimental Systems*

The animal experimental corresponding to 1.5 GHz performed and described in the previous study [21]. As reference information, the rat brain was locally exposed to 1457 MHz MW by using a figure-8 loop antenna. The rats were anesthetized using an intramuscular injection of ketamine (100 mg/kg) and xylazine (10 mg/kg) in conjunction with a subcutaneous injection of pentobarbital (12.5 mg/kg). The rat head was immobilized in an acrylic stereotaxic apparatus and placed in the manipulator system fitted with an antenna positioned 4 mm over the target area. The radiation power of the antenna corresponded to 3.4 W. The corresponding specific absorption rate averaged over the brain (BASAR) was 75 W/kg. BASAR was calculated using the numerical rat model (described as follows). The total duration of the MW exposure corresponded to 6 min and followed the premeasurement of physiological parameters. The parameters were measured in the exposed rats ($n = 4$) and the sham-exposed rats ($n = 4$), which were prepared according to the same system but without MW exposure (0 W/kg of BASAR).

*6 GHz and 10 GHz Experimental Systems*

A microstrip-fed monopole antenna was used for an ultra-wideband exposure of the rat brain at 6 and 10 GHz [77]. The rats were anesthetized with 3% isoflurane in $O_2$ and maintained at 2% isoflurane in $O_2$ throughout the experiment. The rat head was immobilized in an acrylic stereotaxic apparatus. The antenna was positioned 5 mm over the right parietal bone immediately above the target area. Two exposure intensities were used at each frequency. The radiation power of the antenna corresponded to 1.5 and 2.4 W at 6 GHz, and 0.8 and 2.4 W at 10 GHz. The computed BASARs in the 6 GHz experiment corresponded to 64 and 106 W/kg, and those in the 10 GHz experiment corresponded to 29 and 79 W/kg. The total duration of the MW exposure corresponded to 18 min and followed the premeasurement of physiological parameters conducted for 6 min. Four rats were prepared for each exposure condition, including the sham-exposure.

Note that the metric in the safety guidelines is SAR averaged over 10 g of tissue in the safety guidelines [14], [71]. As mentioned in World [74], this physical quantity provides good correlation with the temperature elevation. However, this is a metric used for localized exposures for frequencies up to 3 GHz in IEEE-C95.1 [2] and 10 GHz in ICNIRP [1]; in addition, a 10-g volume is difficult for use in small animals. In other words, no metric exists for the thermal effect over wide frequencies. Thus, BASAR (mass of the brain of 1.9 g) was used as an empirical measurement because of the lack of metric.

*Data Analysis*

Statistical analysis was done using the Mann-Whitney U test to evaluate the difference in regional temperatures between before and after MW exposure. A P value of <0.05 was considered statistically significant.
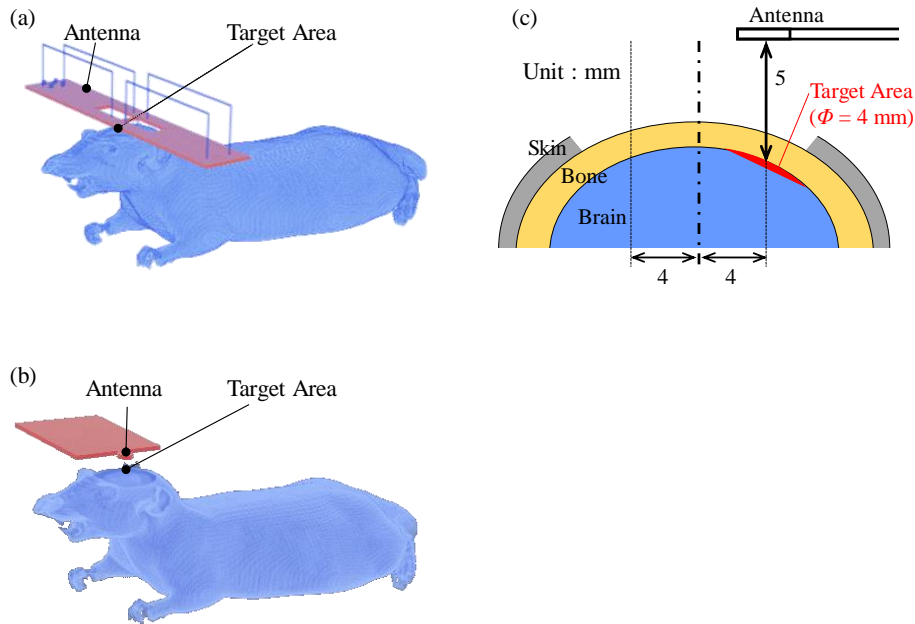
Figure 3.1 Position of rat and antennas during exposure.
(a) The antennas correspond to a figure-8 loop antenna for a 1.5 GHz exposure; (b) monopole-fed antenna for 6 and 10 GHz exposure; (c) definition of the target.

## 3.2.2.  Exposure Scenarios

Figure 3.1 shows the exposure scenarios using the numerical rat model as shown in section 2.2.1. In this chapter, the rat skin that covered the parietal bones was removed to compare with the animal experiment in the same condition. The measuring probes for temperature and rCBF possess a sufficiently small diameter below 0.5 mm, and all the probes are composed of quartz optical fiber ($\varepsilon_r = 3.7$, $\sigma = 10^{-18}$ S/m). Thus, the probes did not significantly violate the electromagnetic field distribution. The probes were replaced with air in the simulation.

## 3.2.3.  Evaluation Index for Effects of Thermoregulation

To confirm the effects of thermoregulatory modeling on the temperature in the brain, the temperature is computed under the assumption that the blood flow in the tissues is constant at

$B_0$, as shown in Table 2.1. Note that this case is termed as "without thermoregulation" in Table 3.2. The evaluation index *I* is defined as follows:

$$I = \overline{\Delta T_{m,c}} \Big/ T_{\max\_TA\_m} \, ,$$

$$\overline{\Delta T_{m,c}} = \int \left| T_{TA\_c}(t) - T_{TA\_m}(t) \right| dt \Big/ t_{duration} , \tag{3.1}$$

where $T_{TA\_c}(t)$ and $T_{TA\_m}(t)$ denote the computed and measured temperature elevations in the target area, $t_{duration}$ denotes the total duration of measurement, and *I* denotes the time average of the difference between the measured and computed temperature elevations ($\overline{\Delta T_{m,c}}$) normalized by the maximum value of the measured temperature elevation ($T_{max\_TA\_m}$) during the measurement.

## 3.3. Results

### 3.3.1. Time-course of Changes in Physiological Parameters

To investigate whether regional temperatures and rCBF were modified by MW exposure, we measured these parameters simultaneously during the exposure. Figure 3.2 shows a typical response to 10 GHz-MW exposure at 0 and 79 W/kg BASAR. Parameters, such as rectal temperature, target area temperature, or rCBF, showed unremarkable changes in sham-exposed conditions. In contrast, the target area temperature rose immediately after the beginning of the exposure, whereas the rectal temperatures increased slightly ($<0.3$ °C) until the end of the exposure. An increase in rCBF also appeared immediately after the beginning of the exposure period and lasted until the end of the experiment.

Table 3.1 Temperature conditions in the experiment

| $f$ (GHz) | BASAR (W/kg) | Target Temperature (°C) | | Rectal Temperature (°C) | |
|---|---|---|---|---|---|
| | | Before | After | Before | After |
| 1.5 | 0 | $33.3 \pm 0.1$ | $33.5 \pm 0.1$ | $37.1 \pm 0.1$ | $37.2 \pm 0.1$ |
| | 75 | $33.0 \pm 0.2$ | $36.2 \pm 0.2*$ | $37.4 \pm 0.1$ | $37.9 \pm 0.0*$ |
| 6 | 0 | $30.3 \pm 0.3$ | $31.1 \pm 0.2$ | $37.5 \pm 0.2$ | $37.6 \pm 0.3$ |
| | 64 | $30.9 \pm 0.6$ | $35.6 \pm 0.6*$ | $37.0 \pm 0.2$ | $37.6 \pm 0.2$ |
| | 106 | $30.6 \pm 0.1$ | $37.6 \pm 0.2*$ | $37.3 \pm 0.2$ | $38.2 \pm 0.1*$ |
| 10 | 0 | $30.2 \pm 0.6$ | $30.4 \pm 0.2$ | $36.7 \pm 0.2$ | $36.7 \pm 0.2$ |
| | 29 | $30.1 \pm 0.3$ | $33.6 \pm 0.4*$ | $36.4 \pm 0.2$ | $36.5 \pm 0.1$ |
| | 79 | $29.4 \pm 0.3$ | $36.5 \pm 0.2*$ | $36.5 \pm 0.1$ | $36.7 \pm 0.0$ |

Regional temperatures in target area and rectum before and after the MW exposure were compared. The temperature shown as the mean ± SEM. *: $P < 0.05$ v.s. before the MW exposure.

### 3.3.2. Temperature Conditions in Animal Experiments

Table 3.1 shows practical temperatures in two regions at the beginning and end of the MW exposure in the animal experiments. Before the exposure, the basal temperatures in the rectum and target area were 36.4–37.5 °C and 29.4–33.3 °C, respectively. To examine the stability of

29
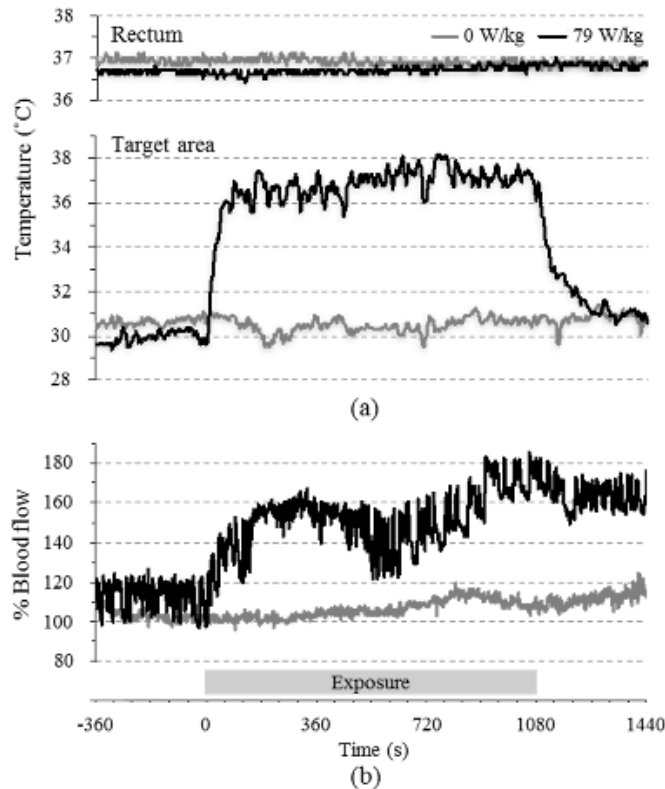
Figure 3.2 Typical responses to localized microwave exposure.

Three physiological parameters, (a) rectal and target area temperatures; (b) regional cerebral blood flow in target area were simultaneously measured before, during, and after the localized 10 GHz MW exposure. The physiological parameters were obtained under sham-exposed and exposed rats ($n = 1$ each).

heat balance in our experimental setup and anesthetized animals, the temperatures in two regions, that is, before and after the sham exposure were compared. The result showed no significant difference in either temperature for any experimental setup. In contrast, a significant temperature elevation was found in the target area after the MW exposure. However, even maximum temperature elevation was less than 38.0 °C because the initial temperature in the target area was around 31 °C.
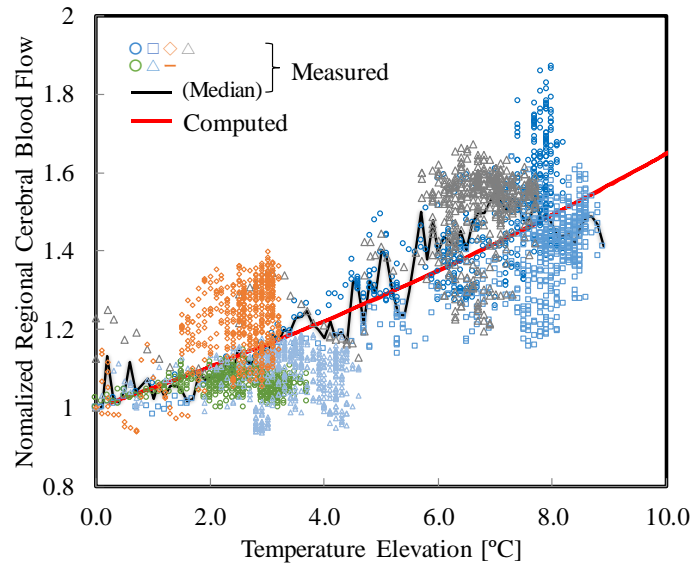
Figure 3.3 Regional cerebral blood flow and temperatures in the target area of the rat brain during localized MW exposure at 10 GHz.
The red solid line shows the values computed based on Equation (2.7). The markers show the experimental values ($n = 7$) including the SARs averaged over the brain that correspond to 29 and 79 W/kg. The black line shows the median of experimental values.

### 3.3.3. Extraction of Parameters Associated with Blood Flow Rate in Brain

The determination of $F_{BB}$ and $F_{HB}$ is required to compute the temperature elevations in the target area of the rat brain, considering the thermoregulation. First, the experimental results for rats under exposure corresponding to 10 GHz including the BASARs of 29 and 79 W/kg ($n = 7$) were selected, in which rectal temperature did not elevate, and thus the effect of the rectal temperature elevation was neglected. Additionally, $F_{BB}$ was estimated using least-squares regression between the time course of rCBF and the brain temperature. The $F_{BB}$ parameter corresponds to 14 °C.

The value of $F_{BB}$ was used to estimate $F_{HB}$ by employing least-squares regression between the time course of rCBF and the temperature at the rectum and target area under MW exposure of 6

GHz including BASARs corresponding to 38, 64, and 106 W/kg ($n = 8$). $F_{HB}$ corresponded to 0.053 °C$^{-1}$.

The values of $F_{BB}$ and $F_{HB}$ determined in a previous study [21] were 31 °C and 0.050 °C$^{-1}$ from measurements performed at 1.5 GHz MW exposure. For the purposes of comparing the parameters, the temperature elevation in the target area was computed and compared using index I (Equation 9). The values of I for the 106 W kg/ BASAR at 6 GHz and 79 W/kg BASAR at 10 GHz corresponded to 9.2% and 9.1%, which exceeded 4.7% and 5.3%, respectively, as obtained using the parameter values derived in this study. Thus, $F_{BB}$ and $F_{HB}$ correspond to 14 °C and 0.053 °C$^{-1}$, respectively, as discussed subsequently.

Figure 3.3 shows the correlation between the changes in rCBF and temperature elevation in the target area exposed to 10 GHz at 29 and 79 W/kg of BASARs. The measured rCBF exhibited temporal fluctuations with the heartbeat and vasomotor and a positive correlation with the temperature.

## 3.3.4.   Effects of Thermoregulation

Figure 3.4 shows the estimation of time course in temperature changes at target area with and without consideration of thermoregulation parameter for different exposure intensities and frequencies. As shown in Figure 3.4, the difference in temperature elevation between the target areas with and without thermoregulation modeling increased with corresponding increase in the value of BASAR. Next, the index *I* (Equation (3.1) was calculated using the data in Figure 3.4.

Table 3.2 Comparison between experimental and computed data based on Equation (3.1)

| $f$ (GHz) | BASAR (W/kg) | $I\_\Delta T_{W/O}$ (%) | $I\_\Delta T_W$ (%) | Reduction (percentage point) |
|---|---|---|---|---|
| 1.5 | 75 | 6.6 | 2.7 | 3.9 |
| 6 | 64 | 9.2 | 3.7 | 5.5 |
|  | 106 | 19.3 | 4.7 | 14.6 |
| 10 | 29 | 10.7 | 7.2 | 3.5 |
|  | 79 | 18.7 | 5.3 | 13.4 |

Temperature elevations with thermoregulation ($I\_\Delta T_W$) and without thermoregulation ($I\_\Delta T_{W/O}$) are shown.
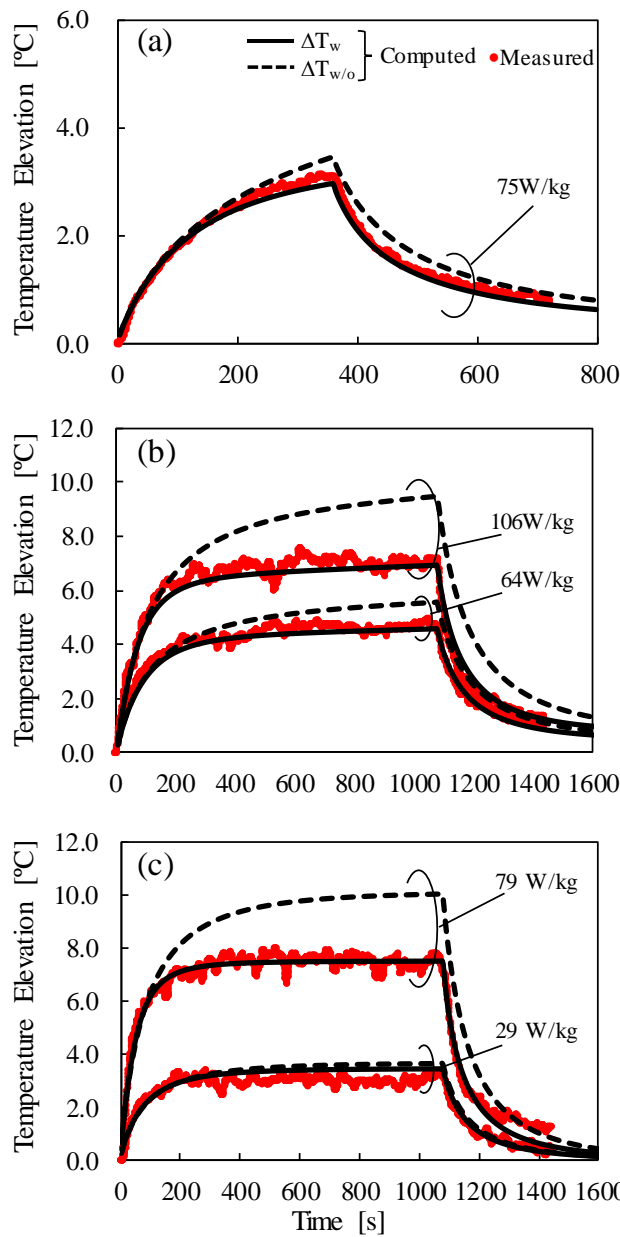
Figure 3.4 Comparison of temperature elevations with and without thermoregulation at different BASARs.
Frequencies, (a) 1.5 GHz; (a) 6 GHz; (a) 10 GHz. The solid line shows the computed temperature with thermoregulation at the central target area ($\Delta T_W$). The broken line shows the computed temperature without thermoregulation ($\Delta T_{W/O}$). Average values of measured temperatures are plotted for comparison with computed values.
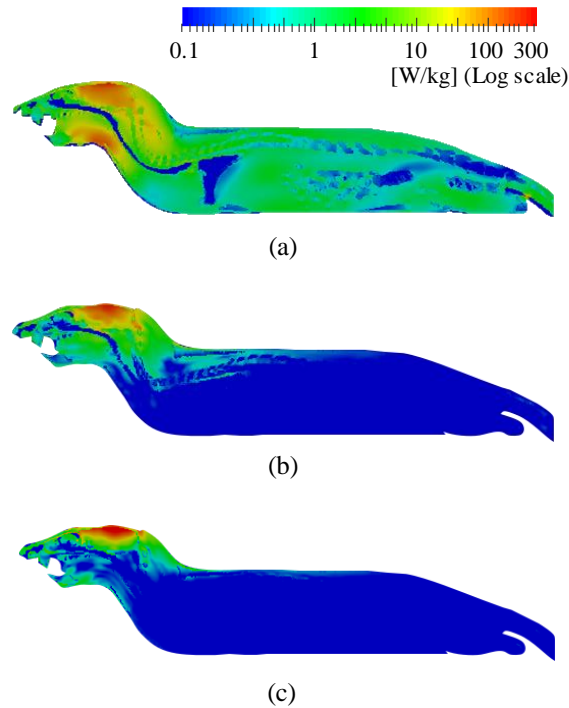
Figure 3.5 Distributions of SAR in the rat model
(a) 1.5 GHz, (b) 6 GHz, and (c) 10 GHz: The average brain SARs correspond to (a) 75 W/kg; (b)
64 W/kg; (c) 79 W/kg. Exposure durations correspond to 6 min in (a) and 18 min in (b) and (c).

Table 3.2 shows the comparison between the temperature elevations in the target areas with and without thermoregulation modeling that correspond to $I\_\Delta T_W$ and $I\_\Delta T_{W/O}$ based on (Equation (3.1)), respectively. The index $I\_\Delta T_W$ was lower than $I\_\Delta T_{W/O}$ across all the conditions .

### 3.3.5. Distributions of SAR and Temperature in the Numerical Rat Model

Figure 3.5 shows the SAR distribution under MW exposure at 1.5, 6, and 10 GHz, respectively. The maximum SAR computed in all models was located approximately near the parietal region; this corresponded to the position immediately below the antennas. Specifically, the absorption region of SAR was localized at the surface. The BASARs at 1.5, 6, and 10 GHz were 16, 32,
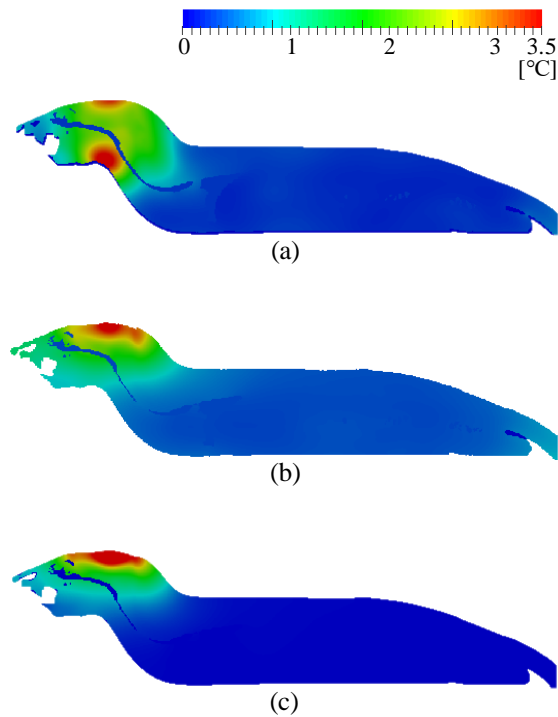
Figure 3.6 Distributions of maximum temperature elevation in the rat model.
(a) 1.5 GHz; (b) 6 GHz; (c) 10 GHz. The average brain SARs correspond to (a) 75 W/kg; (b) 64 W/kg; (c) 79 W/kg. Exposure durations correspond to 6 min in (a) and 18 min in (b) and (c).

and 30 times larger than the whole-body average SARs, respectively. These results suggested that MW power was mainly absorbed approximately near the parietal region with the exception of 1.5 GHz because the SAR was high even at the throat.

Figure 3.6 shows the distribution of temperature elevations at 1.5, 6, and 10 GHz, respectively. The distribution following 6 min of exposure is shown at 1.5 GHz, whereas the distributions following 18 min of exposure are shown at 6 and 10 GHz. The distribution patterns of temperature elevation were similar to those of the SAR albeit with less spatial variation. The maximum temperature elevation appeared in the target area of the brain at 6 and 10 GHz, whereas the maximum temperature elevation appeared around the throat at 1.5 GHz.

### 3.3.6. Comparison of Temperature Elevations Between Live and Numerical Rats

Figure 3.7 shows the temperature elevations in the target area and rectum for each BASAR. Figure 3.7a–e show the temperature in the target area for each BASAR. The black bold line shows the temperature elevation computed in the central target area. The target area consists of 249 cells, from which the minimum and maximum temperature elevations were extracted and indicated by the broken lines. To confirm the validity, the temperature computed using the numerical rat model was compared with the measured temperature values of the living rats (n = 4 for each BASAR). Following a few minutes of initial exposure, the brain temperature elevated rapidly and then linearly during exposure at 6 GHz (Figure 3.7b,c), and is almost constant at 10 GHz (Figure 3.7d,e). The linear increment is attributed to increased blood temperature. The temperature elevation did not reach a steady state at 1.5 GHz because the exposure time was short (Figure 3.7a). After the MW exposure, the target area temperature started to decrease rapidly and remained approximately 1.0 °C higher than the pre-exposure. The time course of the computed temperature elevation in the target agreed well with the measured temperature during and following MW exposure.

As shown in Figure 3.7f–j, the measured rectal temperature elevated linearly during exposure and remained almost constant after the exposure ended. The bar representing 95% confidence interval of measured temperature was wide following the MW exposure.
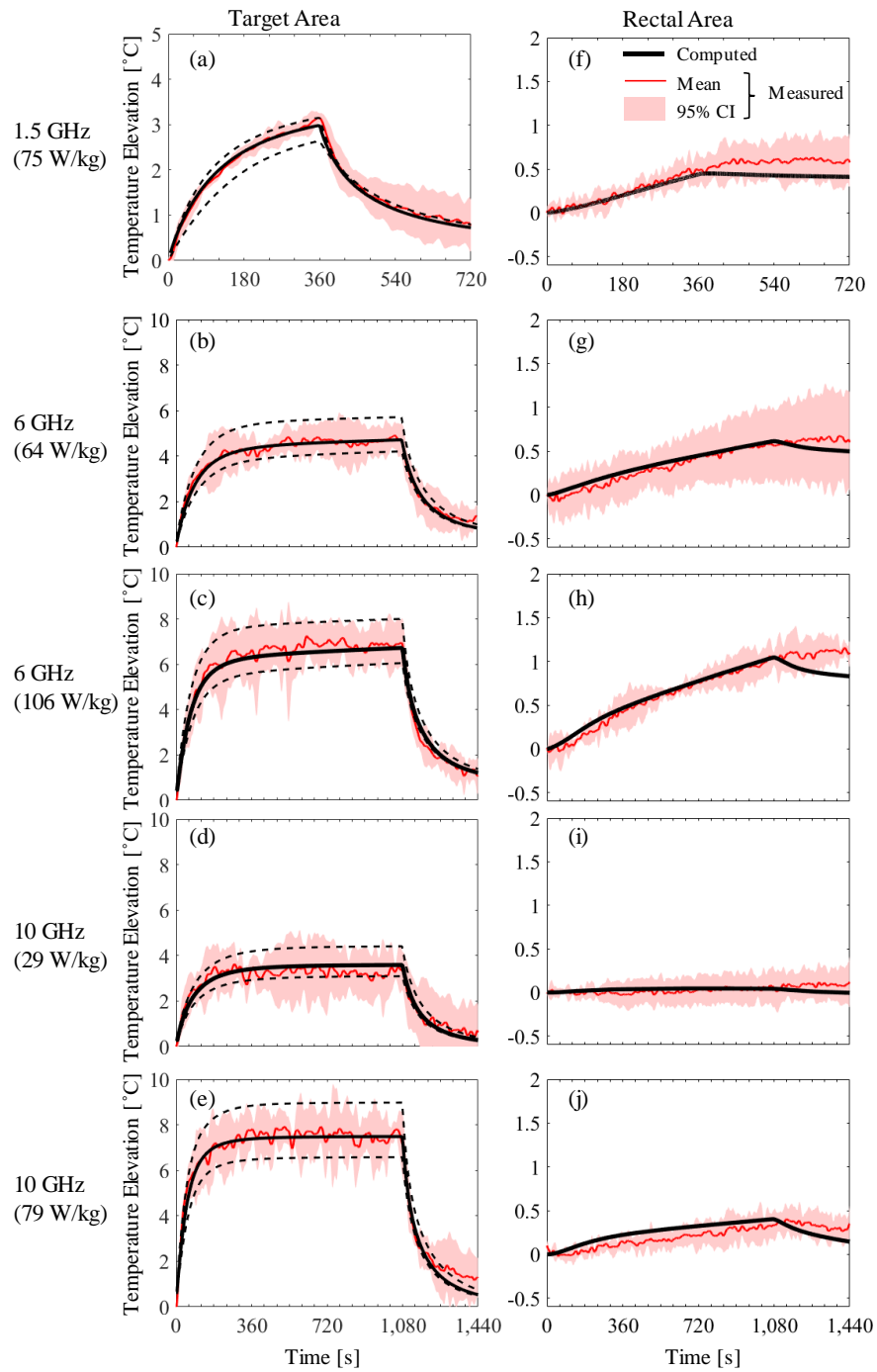
Figure 3.7 Temperature elevations in the target and rectal areas for each BASAR.
Exposure durations correspond to: 6 min (a, f) and 18 min in (b–e, g–j). The black bold line
shows the temperature elevation computed in the central target area. The maximum and
minimum elevations in the target area are indicated by broken lines. Temperature changes
measured in the target and rectal areas of the rats are plotted for model verification ($n = 4$). The
red solid line shows the average of each measured value and the red bars show 95% confidence
interval. The computed blood temperature is compared with the measured rectal temperature.

## 3.4.   Discussion

In this chapter, parameters related to thermophysiological responses for MW exposures were estimated using an electromagnetic-thermodynamics simulation technique. The results indicated that the improved modeling parameters led to a computed temperature elevation that matched well with experimental measurements designed for the local exposure of the rat brain.

As described in the previous report [34], specific experimental conditions were set up in the current study to focus on local physiological changes caused by the localized MW exposure of the cortex. First, we improved the localization of MW exposure of the cortex by using two types of antenna. The exposure intensity in the cortex target area was estimated to be 16 or more times greater than that in the animal's entire body. This facilitated in maintaining the exposure of the entire rat body at a low level. In particular, even the maximum-level MW exposure at 106 W/kg of BASAR caused a very small temperature increase (< 0.9 °C) in the rectum. Furthermore, in the exposure at 10 GHz, no significant temperature elevation was found in the rectum, whereas target area temperature elevated after the exposure. Thus, it is likely that the physiological responses in this study were obtained in the near absence of direct heating of the body, including heat generation at the body surface.

Second, temperature stabilization in each measured region was achieved under sham-exposed conditions. In physiological experiments using rodents, rectal temperature is maintained at 37 °C by using a feedback-regulated heating pad. However, this temperature regulation was unsuitable for our study because MW-related temperature changes would be compensated by it. The present experimental conditions were determined after evaluation of several factors such as heated pad shape, steady temperature, anesthesia type, and experimental duration. As shown in Figure 3.2 and Table 3.1, no significant mean temperature elevation from the initial rectal temperature was observed over the period of sham exposure; however, this did not hinder the detection of the small changes in temperature between exposed and sham-exposed groups during MW exposure.

Third, the rat's target area temperature was kept below 39 °C throughout the experiment for all exposure conditions. This was attributed to the initial temperature of approximately 30°C in the target area. Thus, severe toxic effects such as cell death and higher oedema, which were

observed in brain heated at around 42 °C [78], were unlikely to occur under the present conditions.

In contrast, several researchers found that cerebral hypothermia modified physiological functions such as neuronal activity [79] and blood-brain barrier [80]. However, it is known to be difficult to keep the rat cortex temperature at 37 °C in an anesthetized small animal. In particular, in our experiment, removal of parietal skin and exposure of a part of the skull were needed to provide localized MW exposure, leading to the lower initial temperature. Therefore, there might be limitations to some physiological functions. Nevertheless, it was interesting that the thermoregulation in the cortex was activated and its behavior was mimicked in the computational model we improved, even under the present limited conditions.

The parameters related to brain and rectal temperatures ($F_{BB}$ and $F_{RB}$) were determined from the measured values of 6 and 10 GHz. The parameters used in our previous study [21] were arbitrary and derived from a one-exposure condition. The parameters derived in the present study were demonstrated to be applicable to different exposure frequencies and systems. Specifically, $F_{BB}$ affected the initial rate of increase in brain temperature, and $F_{RB}$ influenced the linear gradient of brain temperature elevation by using blood temperature. The rate of increase in brain temperature was rapid with decreases in the $F_{BB}$ results. The coefficients related to blood flow changes in a biological system were not affected by the frequency of the external electromagnetic field but by the internal heat load (SAR). Therefore, parameters derived through the measurements at multiple frequencies can provide accuracy and generality with respect to parameter extraction.

Blood flow regulation was modulated through tissue temperature and aided in lowering the tissue temperature against heating load. As shown in Figure 3.4, the effectiveness of temperature reduction in the target area between the cases with and without thermoregulatory modeling was more remarkable at the higher BASAR conditions. This is because of the increase in the blood flow produced by the temperature elevation due to exposure (e.g., Equation (2.7) for brain tissue). Simultaneously, temperature elevation was also regulated by the blood flow elevation (Equation (2.2)); this is not considered in the model without thermoregulation. The computed accuracy of the temperature elevation improved when thermoregulatory modeling was considered (see Table

3.2). Moreover, thermoregulation significantly influenced the brain temperature elevation, with increases in the BASAR. These results show that the modeling of thermophysiological response is essential for estimating regional brain temperature in rats. A potential reason for the larger difference in $I\_\Delta T_W$ at higher frequencies can be attributed to the location control of the antenna. Fine location control is required at higher frequencies for high focality.

At 1.5 GHz, the SAR distribution was higher in the brain and throat (Figure 3.5a). This is because the size of the rat was smaller than the size of the antenna, and the MW diffracted around the side of the rat's head [47]. Conversely, SAR absorption was gradually localized at 6 and 10 GHz (Figure 3.5b,c) because the penetration depth of MW decreased as the frequency increased. The distributions of temperature elevation (Figure 3.6) were similar to those of SAR. The temperature-elevation distribution was much smoother because of thermal diffusion and blood perfusion.

The models in the present study allowed for the thermoregulatory response of rCBF (Equation (2.7)) and provided estimates of brain temperature elevations that were in good agreement with the measured data (Figure 3.7a–e). As is widely known, the estimations of temperature and blood flow are highly dependent on the computational location in local exposure. Variations were observed in the computed values inside the target area (249 cells). However, the model value corresponded reasonably well with the experimental data. Therefore, the findings suggest that the thermoregulatory responses in the brain and rectal regions were efficiently modeled for localized MW exposure in this frequency band.

We investigated that the computed blood temperature elevation is a tool to help predict rat core (rectal) temperature elevation. This is because the computed blood temperature was changed to satisfy the thermodynamic law; the heat in the tissue is transferred to and stored in the blood. This works well in this study because of higher blood perfusion rate and smaller dimension of a rat compared to those than in human [21], [81]. Typically, the computed rectal temperature elevations were in extremely good agreement with the measured rectal values.

One of the limitations of the computation is attributable to phantom development, in which an automatic classification algorithm is applied. The heat transfer between the lung and internal air is simplified; one reason for this is that the lung cannot be modeled from CT images. A single

value of thermal conductivity, specific heat, and blood flow is assigned to a corresponding tissue throughout the body at the thermoneutral condition [82], [83]. Nonetheless, the computation agreed well with measurement because we focused on the brain temperature elevation and blood flow. The heat diffusion length in the brain is of a few millimeters because of higher blood perfusion rate. In addition, the volume-averaged blood temperature is changed so as to satisfy the first law of the thermodynamics. We demonstrated the effectiveness of our multiphysics modeling, which is still simple to implement, by comparing with measure data. The main purpose of this study was to develop the model for rat brain and thus the result obtained here is not directly applied to humans. Thermophysiological modeling in humans can be found in [7], [23], [25] although they are useful and validated for relatively small temperature elevation.

It remains unclear whether other physiological parameters such as heart rate and blood pressure could involve the regional temperature elevations including core body's. However, the topics are challenging and considered as the next step, because of several difficulties. As a first step, we focused on the relationship between target cortex temperature and rCBF for electromagnetic safety for localized exposure. That is the main reason why we developed the special antennas to eliminate the direct body heating under MW exposure. As the present results showed, even in our simpler model, the computed estimation matched well with the measured quantities during and after exposure in rats. This result may suggest that rCBF change is the dominant parameter to control the local temperature, by comparing with other physiological parameters. In the next step, we may have to discuss additional mechanism carefully.

## 3.5.    Conclusion

In this chapter, parameters related to thermophysiological responses for MW exposures were estimated using an electromagnetic-thermodynamics simulation technique. Specifically, the parameters related to cerebral blood flow were estimated with a high degree of accuracy. The improved modeling parameters resulted in computed results that corresponded well with the measured values at a super-high-frequency band that was not previously computed. The computational model provides the basis to simulate MW exposure for thermal evaluation in a consistent model ranging from conventional frequencies to frequencies exceeding 6 GHz. This simulation can be helpful in estimating temperature elevation and changes in blood flow rate at multiple observation points that are difficult to measure, and can help analyze the physiological effects caused by MW exposure and improve health risk assessment.

# Chapter 4

# Comparison of Temperature Elevation between Rat and Humans

## 4.1.   Overview

In the international guidelines/standards for human protection against electromagnetic fields, the SAR is used as a metric for radio-frequency field exposure. For radio-frequency near-field exposures, the peak value of the SAR averaged over 10 g of tissue is treated as a surrogate of the local temperature elevation for frequencies up to 3–10 GHz. The limit of localized SAR was derived by extrapolating the thermal damage in animal experiments. However, no reports discussed the difference between the time constant of temperature elevation in small animals and humans for local exposure. This chapter computationally estimated the thermal time constants of temperature elevation in human head and rat models exposed to dipole antennas at 3–10 GHz. The peak temperature elevation in human brain was lower than that in rat mainly because of the difference in depth from the scalp. Consequently, the thermal time constant of the rat brain was smaller than that of the human brain. Additionally, thermal time constant in human skin decreases with the increasing frequency, which is mainly characterized by effective SAR volume, whereas it is almost frequency-independent in the human brain. These findings would be helpful for extrapolating animal studies to humans. The work presented here was published in [84].

## 4.2. Methods

### 4.2.1. Exposure Scenarios

One rat and four human models were considered as computational models. The rat model was used as shown in section 2.2.1. Realistic anatomical human models for different ages and gender were considered. The Japanese male model and the for European models were used as shown in section 2.2.3. Figure 4.1 illustrates the exposure scenarios. As shown in Figure 4.1, the separation between the dipole antenna and the surface of the head model was 5 mm for the rat, and 5, 15, and 25 mm for the human. The frequencies considered here were 3, 6, and 10 GHz, which is the upper frequency range where the SAR is used. The reason for choosing the frequencies above 3 GHz is that the whole-body averaged SAR cannot be neglected at lower frequencies, making difficult to discuss the local temperature elevation and its time course. The antenna-head separation for the rat model was only chosen at 5 mm to realize local exposures [21], [29], [76]. The length of the antenna was adjusted to half the wavelength depending on each frequency in free space. The duration of the RF exposure corresponded to 50 min so that the temperature elevation was in a steady-state. The ambient temperature was set to 27 °C. For



(a)                                              (b)
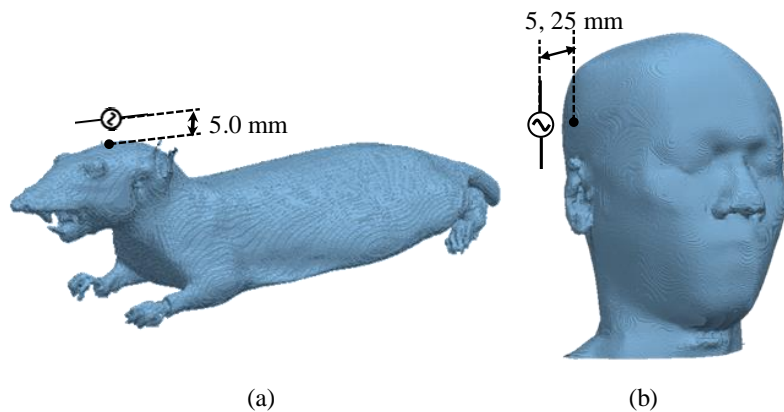
Figure 4.1 Exposure scenarios for computational (a) rat and (b) human head models (TARO).
The separations between the antenna and the rat and human models are 5 mm and 5–25 mm, respectively.

comparison, the output power of the antenna was adjusted so that the localized SAR was 2, 10, 20, 30, 40, and 50 W/kg. The guidelines/ standards set at 2-W/kg-limit local RF exposure for the general public and unrestricted environment, and 10-W/kg-limit for restricted environments or occupational exposures.

## 4.2.2.   Definition of Thermal Time Constant

The thermal time constant is an empirical quantity that characterizes the time to reach steady state temperature (the step response of the tissue). A small thermal time constant means quick thermal response. The thermal time constant is calculated from the time evolution of temperature from continuous wave exposure,

$$\Delta T(t) = \Delta T_{\max} \left( 1 - e^{-(t - \tau_D)/\tau} \right), \tag{4.1}$$

where $\Delta T_{max}$ [°C] is the maximum temperature elevation, $\tau$ [s] is the thermal time constant, and $\tau_D$ [s] is the heat conduction time from the model surface.

The time evolution of temperature is observed as a primary delay function in surface tissues; $\Delta T(t) = \Delta T_{max} (1 - e^{-t/\tau})$ can be obtained by substituting $\tau_D = 0$ in Equation (4.1). The temperature elevation at the thermal time constant is approximately 63% of the maximum temperature elevation, because $\Delta T(t) = \Delta T_{max} (1 - 1/e) \approx 0.63 T_{max}$ when $t = \tau$. The twice and three times value of the thermal time constant approximately correspond to the temperature elevation of 86% and 95%, which may be more relevant to the human safety, as discussed in Appendix A of the ICNIRP draft guidelines [85].

A secondary delay function, $\tau_D \neq 0$ in Equation (4.1), is observed in inner tissue (such as the brain). The heat conduction time is observed as the time taken to reach the heat source (the RF power absorption) to the observation point. The observation points of the thermal time constant were taken as the points of the maximum temperature elevation in the brain and tissues (excluding the pinna). Here, the brain tissue includes gray matter, white matter, cerebellum, thalamus, pineal gland, and hypothalamus.

### 4.2.3. Definition of Effective SAR Volume

The temperature elevation is mainly affected by the SAR, which is larger than 1/e of peak SAR [38]. Hirata et al. estimated the heat diffusion length in terms of the length where the amplitude of heat decreases to $1/e$ [56], [65]. Foster et al. derived an analytic formula to estimate the thermal time constant in a 1D homogeneous model for plane wave exposure [38]. Hashimoto et al. proposed the effective area of the SAR pattern as an evaluation index of temperature elevation, which is defined by the area where SAR is larger than $1/e$ of the peak value in the averaging area using the multilayer cubic model [10]. The effective SAR volume [cm$^3$] is defined as a metric where SAR is larger than $1/e$ of the $SAR_{max}$ to consider both the depth and the spread on the model surface. Here, $SAR_{max}$ is treated as a value excluding the SAR voxels, which has the highest SAR value of 0.01 % for below reasons.

One of the disadvantages of using voxelized anatomical human models is that the computed EM absorbed power suffers from computational artifacts, especially around the model surface. This error is notable at low frequency [86], but may still occur in computation at high frequencies. We define the voxel $SAR_n$ as the $n$th element of the list of SAR values sorted in ascending order. The gradient $\Delta$ is computed for each $SAR_n$ by the following equation:

$$\Delta_n = \frac{SAR_{n+1} - SAR_n}{\left(SAR_n + SAR_{n+1}\right)/2}, \tag{4.2}$$

The first significantly different value of the gradient is defined as the detection point of the outlier [87]. Figure 4.2 shows the voxel values corresponding to a SAR with the highest value of 0.2%, and the gradient in the TARO model. As shown in the figure, the gradient significantly increased above 99.99% owing to the effect of calculation using a voxelized model. The gradient of the SAR value in the other head models also significantly increased above 99.97%–99.99%. $SAR_{max}$ was the value obtained by removing the highest value of 0.01%. The removed volumes were 0.4–0.5 cm$^3$ and 0.02 cm$^3$, which corresponded to 0.5–0.8 g and 0.04 g in human and rat models, respectively. The removed volumes are generally located in complex shapes, such as around pinna. Note that an extensive analysis was conducted for low-frequency exposure where *in situ* electric fields were evaluated in voxelized models [87]. Similarly, the metric for evaluating SAR should be averaged over 10 g of tissue, and thus is not discussed extensively for

RF exposures. The main purpose of this metric is to evaluate the SAR volume appropriately rather than for defining the physical meaning of the temperature.
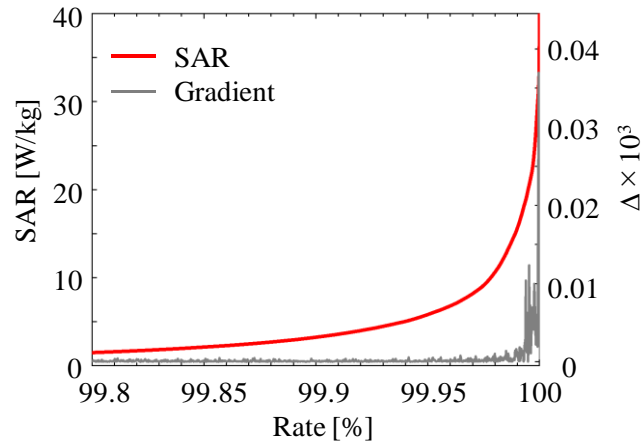


Figure 4.2 Computed results of SAR and its gradient for voxels whose SAR has the highest value of 0.2% in the TARO head model.

# 4.3. Results

## 4.3.1. Distribution of SAR and Temperature Elevation

Figure 4.3 shows the SAR distribution on the cross section of the rat through the antenna feed point at 3, 6, and 10 GHz. The localized SAR was adjusted to 10 W/kg for proper comparison. As shown in the figure, the SAR is distributed over the whole head at 3 GHz, whereas it is more localized at 10 GHz. Because of smaller dimension of the rat head, localized SAR almost coincides to the head averaged SAR.

Figure 4.4 shows the SAR distributions on the cross section of TARO through the feed point at 3, 6, and 10 GHz. The distances between the antenna and surface of the head were 5, 15, and 25 mm at each frequency. The peak SAR averaged over 10-g tissue was adjusted to 10 W/kg, as for the rat model. The SAR also distributed in the brain surface at 3 GHz, whereas for frequencies above 6 GHz it only distributed in the superficial tissues (such as skin and muscle), because of shallower penetration depth of the electromagnetic fields. Further, the lateral extent of SAR becomes widespread at lower frequencies. As shown in Figure 4.4, the exposure volume is smaller for the antenna distance $d = 5$ mm than that at $d = 25$ mm.
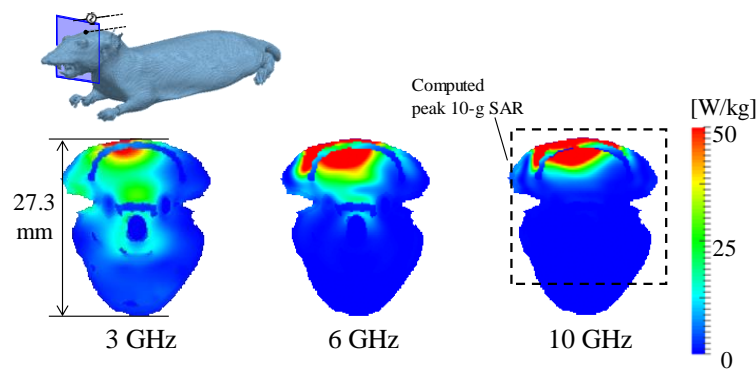


Figure 4.3 SAR distribution in the rat model.
The distance between the skin surface and the dipole antenna as set to 5 mm. The output power of the antenna was adjusted so that the peak SAR averaged over 10 g tissue was equal to 10 W/kg. The dashed square shows the region with computed peak 10-g SAR.

Figure 4.5 shows the temperature elevation distributions in rat and TARO at 3, 6, and 10 GHz. The distance from head to antenna is 5 mm. The temperature elevation has similar tendency as SAR, but is smoother due to the heat diffusion.
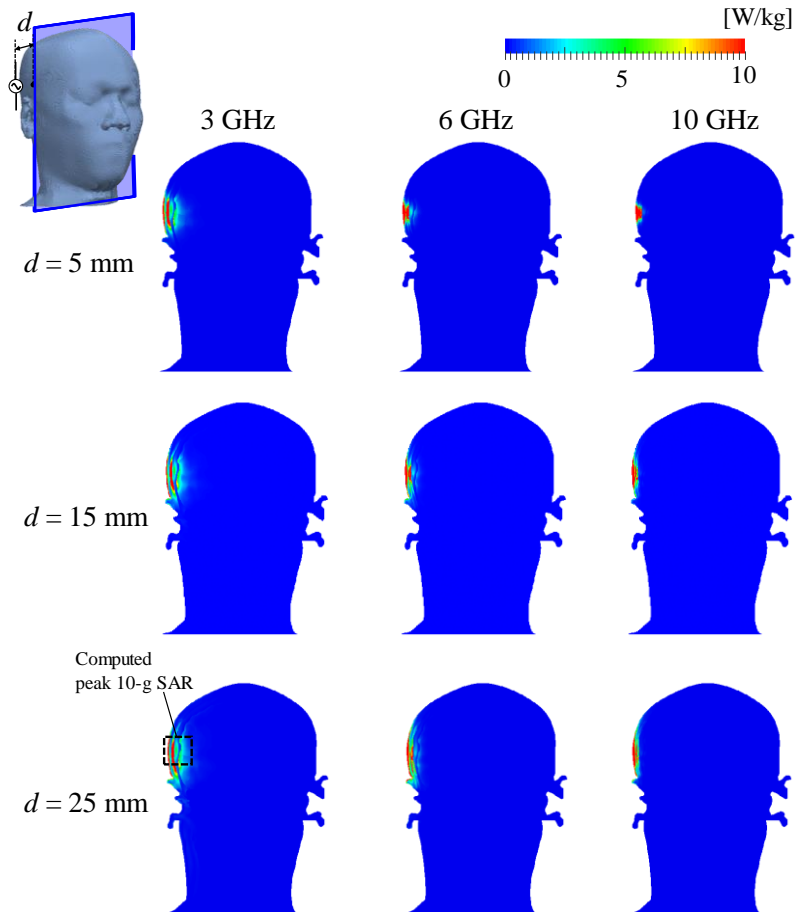


Figure 4.4 SAR distribution in the TARO model.
The distance between the skin surface and the dipole antenna d was set to 5, 15, and 25 mm. The output power of the antenna was adjusted so that the peak SAR averaged over 10 g tissue was equal to 10 W/kg. The dashed square shows the region with computed peak 10-g SAR.
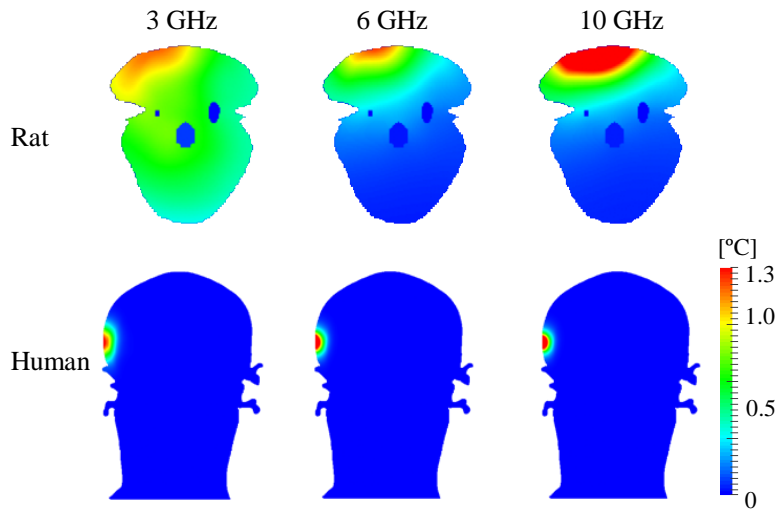
Figure 4.5 Distribution of temperature elevation in the rat and TARO models.
The distance between the skin surface and the dipole antenna was set to 5 mm. The output power of
the antenna was adjusted so that the peak SAR averaged over 10 g tissue was equal to 10 W/kg.

## 4.3.2.   Comparison with Temperature Elevation in Rat and Human Models

Figure 4.6 shows the peak temperature elevation of skin and brain in the human models for
different SARs and antenna-head distances. For comparison, the temperature elevation in the rat
skin for $d = 5$ mm was also plotted. As shown in Figure 4.6a–c, the temperature elevation in the
skin increases as the frequency increases. The peak temperature elevation in the human was
approximately twice as high as that in the rat at $d = 5$ mm. The peak temperature elevation
decreased as the antenna was moved away for the human. For $d = 15$ and 25 mm, the temperature
elevation in the human model was lower than that in the rat model at 10 GHz. As shown in
Figure 4.6d–f, the peak temperature in brain varied significantly with frequency for the rat model,
but was almost independent of frequency for the human model. The peak temperature elevation
in the human brain was lower than that in the rat brain.

50
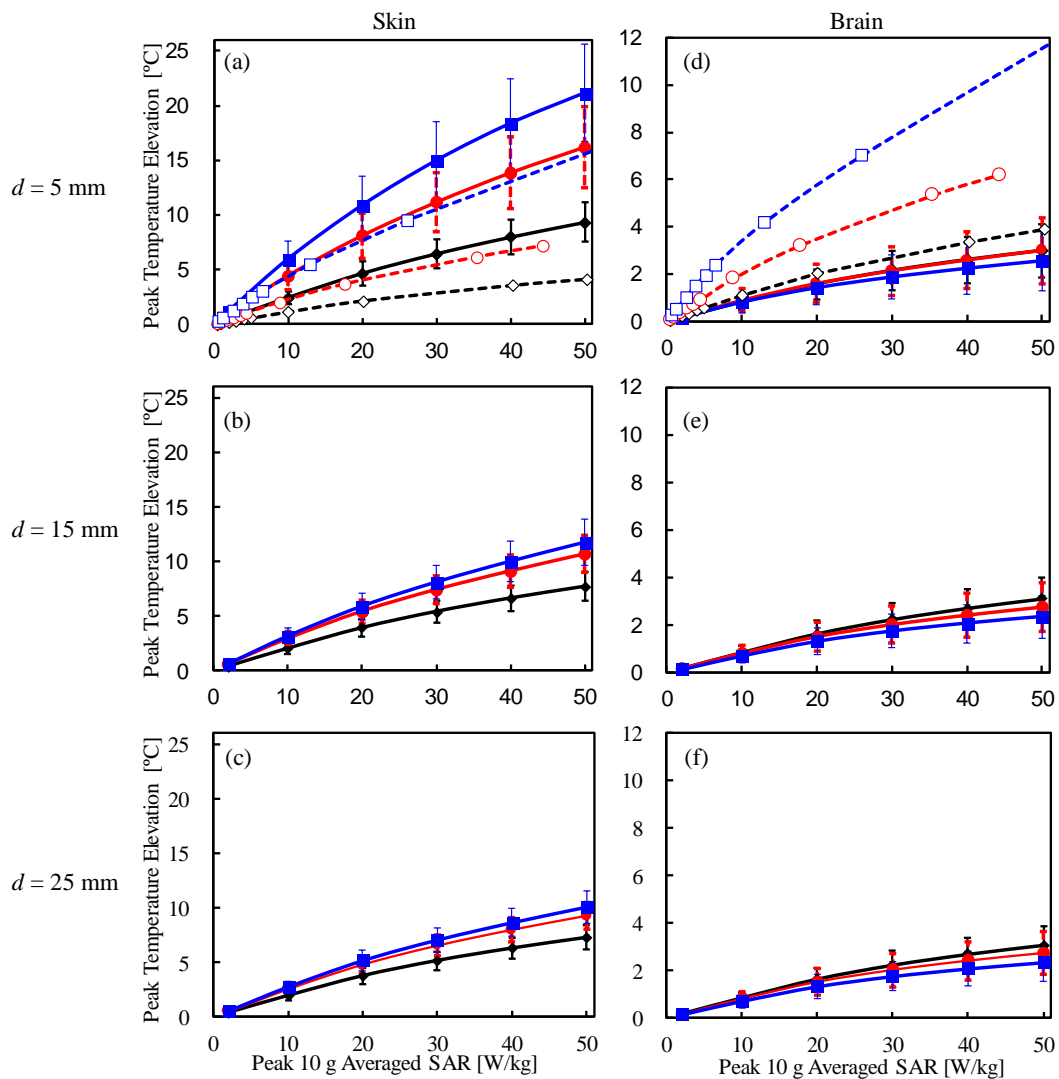
Figure 4.6 Peak temperature elevation of (a–c) skin and (d–f) brain for each peak SAR averaged over 10 g tissue.

The distance between the skin surface and the dipole antenna $d$ is set to (a, d) 5 mm, (b, e) 15 mm, and (c, f) 25 mm. Each point represents the average value and error bar showing the standard deviation ($n = 4$). For comparison, the temperature elevation of rat brain tissue was also plotted.

## 4.3.3.  Thermal Time Constant in Rat and Human Head Model

Figure 4.7 shows typical examples of time evolution of temperature elevation in the rat and
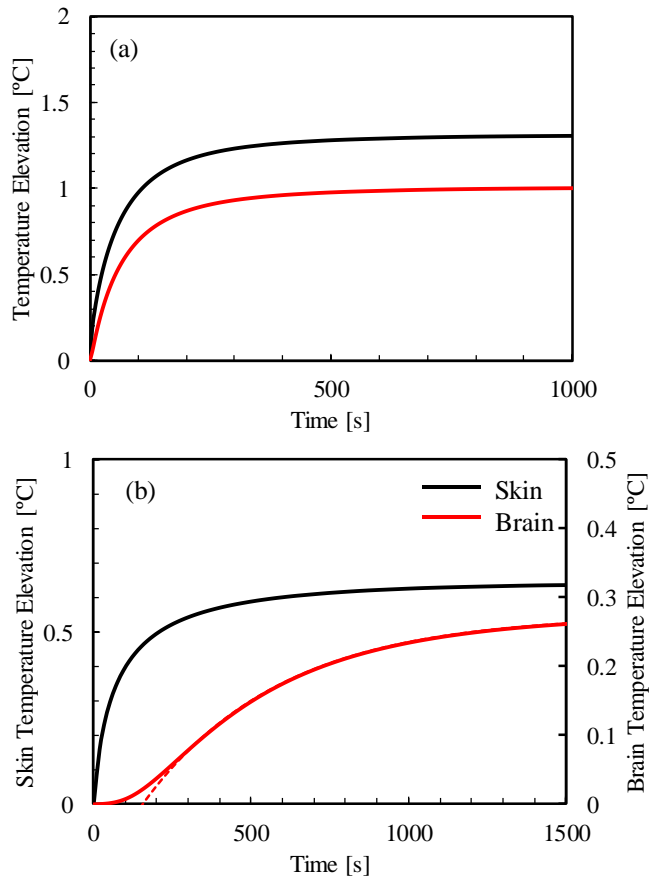
Figure 4.7 Time evolution of temperature elevation in (a) rat and (b) TARO at 10 GHz.
The SAR averaged over 10-g tissue was adjusted to 2 W/kg. The distance from the antenna and
the head is (a) 5 mm and (b) 25 mm. The dotted line in (b) shows the regression curve from
Equation (9).

human models. The frequency was chosen 10 GHz, and TARO was used for the human model.
As shown in Figure 4.7a, the heat conduction time ($\tau_D$ in Equation (4.1)) is not necessary to
describe the temperature elevation in the skin of rat and human. The time evolution of
temperature in the skin is expressed as a primary delay function. As shown in Figure 4.7b, the
heat conduction time in the rat brain is marginal, whereas that in the human brain is significant.
Thermal time constant in the human brain is expressed as $\tau + \tau_D$ for comparison with the rat in
the following discussion.
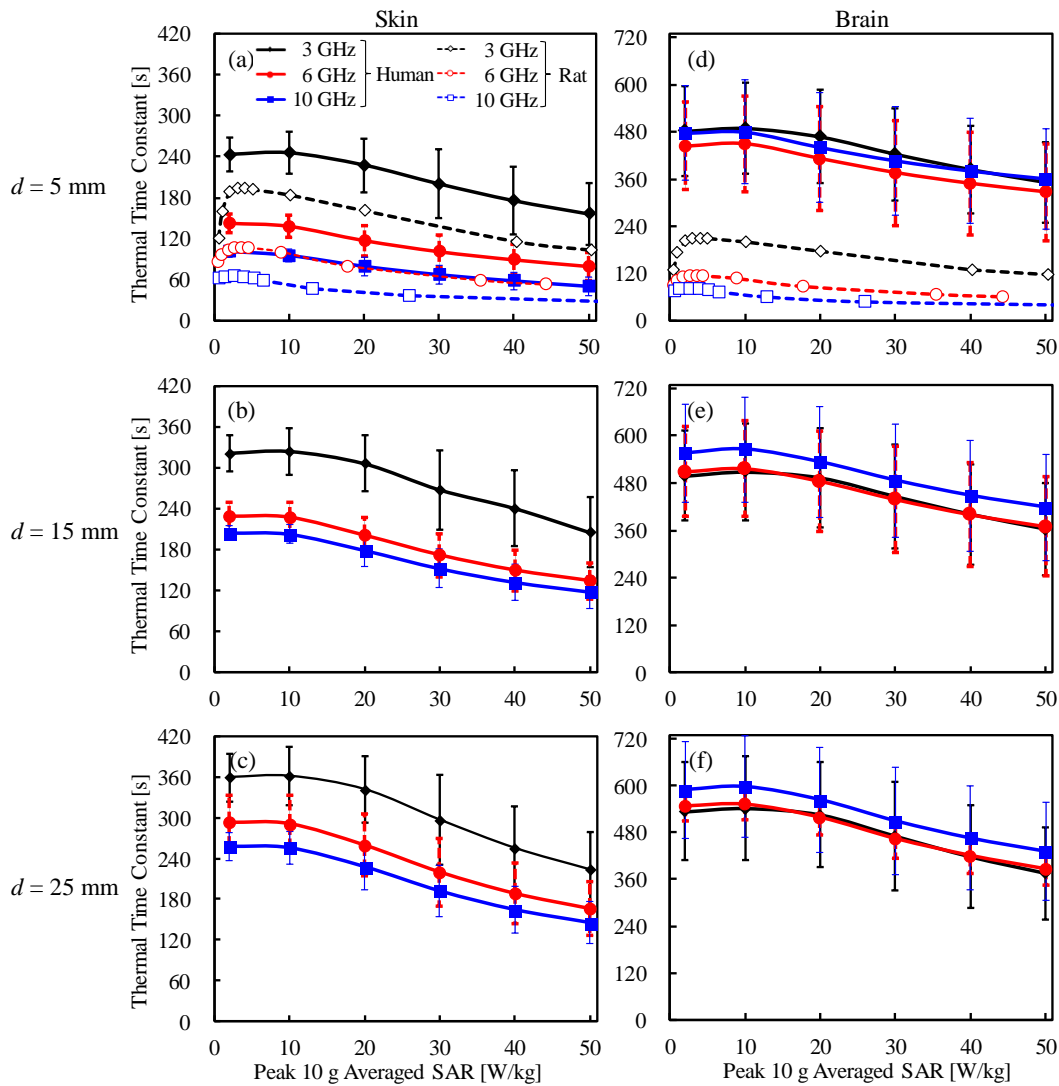
Figure 4.8 Thermal time constants of (a–c) skin and (d–f) brain in human models for each peak SAR averaged over 10 g tissue.

The distance between the skin surface and the dipole antenna *d* is set to (a, d) 5 mm, (b, e) 15 mm, and (c, f) 25 mm. Each point represents the average value and error bar showing the standard deviation (*n* = 4). For comparison, the temperature elevation of rat brain tissue is also plotted.

Figure 4.8 displays a comparison of the thermal time constant of the skin and brain in the rat and human. The thermal time constant was computed at the positions where the peak temperature elevation appeared. The thermal time constant decreases with increasing exposure

53
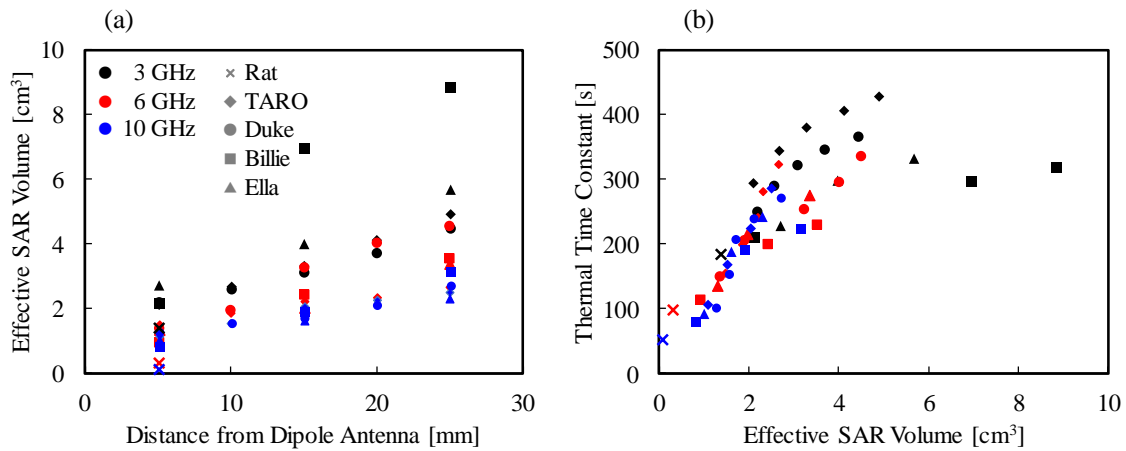
Figure 4.9 (a) Effective SAR volume for each exposure scenario; (b) Relationship between thermal time constant of skin and effective SAR volume in rat and human models.
Output power of the antenna was adjusted so that the peak SAR averaged over 10-g tissue was 10 W/kg.

intensity nonlinearly. As shown in Figure 4.8a–c, the thermal time constant of the skin decreases with increasing frequency in both rat and human models. The thermal time constant also increases with increasing of the distance between the antenna and the skin surface. The thermal time constant in the human skin is 1.5 times higher than that in the rat skin at $d = 5$ mm.

The thermal time constants of skin in the rat and human models were 3 and 6 min, respectively. The time required to reach the thermal steady state was estimated as 6 and 12 min in rat and human models, respectively ($2\tau$ in Equation (4.1) is the time to reach 86% of steady-state temperature).

As shown in Figure 4.8d–f, the thermal time constant in the rat brain had similar tendencies to rat skin. One noteworthy point is that the time constant in the human brain was almost frequency-independent. The thermal time constant in the brain of the human was approximately two to four times larger than that in the rat brain at the same antenna-head distance. The maximum thermal time constant of rat brain tissue was 3.5 min at 3 GHz, and that of human brain was 10 min at 10 GHz for $d = 25$ mm. The time required to reach the thermal steady state was 7 min and 20 min (or more) in rat and human models, respectively.

54

### 4.3.4. Relationship Between Effective SAR Volume and Thermal Time Constant

Figure 4.9 shows the relationship between the effective SAR volume and thermal time constants of the skin at same intensity of RF exposure in rat and human models. Figure 4.9a shows the effective SAR volume for each exposure scenario. The effective exposure volume increases with decreasing frequency and increasing antenna-head separation. Figure 4.9b shows the relationship between the thermal time constant in the skin and the effective SAR volume. As shown in the figure, thermal time constant in the human model depended on the model type rather than on the frequency, especially at frequencies of 6 and 10 GHz. The thermal time constant increased as the effective SAR volume increased.

## 4.4.　Discussion

The thermal time constant has not been discussed until recently [5], except for a few studies on the exposure from handset antennas (e.g., [5], [8], [9], [32]). Instead, thermal damage in animal studies has been commented on in the international guidelines/standards. For example, regarding the eye exposure in rabbits, temperature elevation was observed in the eye and the core, and then cataract formation was reported [16], [26]. To understand the phenomena as well as future design of experiments, the time course of the temperature elevation in the animal is important [16]. Thus, this study computed the temperature elevation in human and rat models for exposure at 3–10 GHz taking into account the thermoregulation (vasodilatation). In addition to the temperature elevation, thermal time constants were evaluated and discussed.

We demonstrated the difference between SAR and temperature distributions in the rat and human models. The ratios of local and whole-body averaged SAR were 18, 26, and 27, at 3, 6, and 10 GHz in the rat model, respectively. The SAR was distributed over the whole head at 3 GHz and in the rat brain, even at 10 GHz (Figure 4.3). The penetration depth of the skin is 18.8 mm at 3 GHz, 8.2 mm at 6 GHz, and 3.8 mm at 10 GHz [88]. The distance between the brain and the head surface is at most 2 mm in the rat. In the human model, the SAR was marginally distributed in the brain only at 3 GHz (Figure 4.4). The distance between the brain and the head surface of TARO is 13.5 mm, which is larger than the penetration depth above 6 GHz. As shown in Figure 4.5, the temperature elevation is distributed throughout the brain in the rat model but is contained locally in the human model. The temperature elevation above 0.1 °C reached approximately 2 cm in depth in the human model.

We then compared the temperature elevation in rat and human models for different antenna distances and SARs. As shown in Figure 4.6, the peak temperature elevation in human skin was twice that of rat skin at the same head-antenna distance. This difference is attributable to the SAR distribution (volume of power absorption). The temperature elevation is characterized by the heat diffusion length in the volume (approximately 1 cm [56]). In addition, the SAR averaged over 10-g tissue in cubic shape was used as an index of comparison. Further, in the rat model, the skin is close to the brain, where blood perfusion is high, thus reducing skin temperature. In

the brain, the peak temperature elevation in the human model was lower than in the rat model. Unlike the rat, the SAR is only slightly distributed in the human brain, and temperature elevation by heat conduction from external tissues becomes dominant.

We compared the thermal time constants of rat and human models. As shown in Figure 4.8, the thermal time constant decreases at higher exposure intensity owing to the cooling effect of vasodilation or nonlinear thermoregulation. The thermal time constant also increases with the increase of the antenna-head distance, which can be attributed to a larger effective SAR volume. The effective SAR volume increases with the head-antenna distance, and may be related to the head size, which has been extensively discussed in [89], [90]. The thermal time constant in skin exhibits good correlation with the effective SAR volume, even if the head shapes are significantly different, such as in rats and humans. As shown in Figure 4.9, the thermal time constant increases as the effective SAR volume increases, but does so in nonlinear fashion. Focusing on each condition, the thermal time constant can be expected to saturate as the effective SAR volume increases. The increment of the effective SAR volume results in thermal diffusion, causing the delay in temperature elevation [5]. This result suggests that the effective SAR volume can be estimated as a metric in superficial tissues. Note that the SAR volume is not a good metric for 5 cm3 or less, because it is larger than the heat diffusion length. The difference of the time constant in skin between rat and human models is caused by the difference of the effective SAR volumes (see Figure 4.9). The effective SAR is useful for estimating the thermal time constant of superficial tissue, which varies greatly depending on the shape and size of the head, type and position of antenna, and the frequency applied.

In the inner tissue, such as the brain, the thermal time constant is also characterized by the heat conduction time, which is mainly attributable to the distance from the heat source to the target point. The heat conduction time ($\tau_D$ in Equation (4.1)) observed in the human brain was approximately 40, 120, and 150 s at 3, 6 and 10 GHz, respectively. In contrast, $\tau$ decreases as the frequency increases. Therefore, the thermal time constant ($\tau + \tau_D$) in the human brain is less sensitive to frequency. The difference of the time constant between rat and human brains is caused by the heat conduction time and differences in temperature elevations.

The antenna position was chosen to be different from the how people actually use mobile

phones, because we decided to set the antenna position for accurate comparison of the thermal response between human and rat models. In that situation, the antenna is likely to be present near pinna, cheek, and mouth. For a dipole antenna located at the side of the pinna, most of the power is absorbed in the pinna [91]. For a dipole antenna located close to the cheek or mouth, the temperature elevation in the brain obviously decreases because of distance.

The thermal damage depends on tissue sensitivity, temperature, and exposure time [30]. The cumulative equivalent minutes at 43 °C are used as a model to calculate the thermal dose. In that evaluation, the thermal time constant is essential. Focusing on the brain, which is a highly heat sensitive tissue, the thermal time constant in humans was more than twice that in rats. Thus, the exposure time required for thermal damage is correspondingly increased. Furthermore, because the characteristics of the temperature elevation of deep tissues in rats and humans are different, extrapolation from small animals to humans in deep tissues needs further attention. However, these findings suggest that excessive temperature elevation is caused with increasing frequency in rat brains, but only marginally occurs in the human brain. These results exclude the possibility of thermally induced brain-tissue damage for the limits stated in current international guidelines, especially at higher frequencies. To determine exactly how conservative these limits are when applied to humans, further experimental studies are necessary.

The thermal time constant obtained here would also be useful to interpret the experimental data discussing the thermal and non-thermal effects of RF fields, because the temperature elevation may not always be monitored in the measurements (e.g., [92], [93]; see also [94]).

## 4.5.    Conclusion

This chapter investigated the differences in temperature elevation and thermal time constant between rat and human models exposed to dipole antennas at frequencies of 3–10 GHz. We computationally estimated the time course of temperature elevation by considering the vasodilation. It should be noted that the temperature elevation and time course are quite different between rat and human models, especially in deep tissue such as the brain. The characteristics of temperature elevation vary in humans owing to the shape and size of the head and distance to the antenna. We then proposed the effective SAR volume as a metric to estimate the thermal time constant, indicating that there is a good correlation between them, even if head shapes are significantly different, such as in rats and humans. These findings should be useful for extrapolating the small animal studies to humans.

# Chapter 5

# Temperature Elevation of Brain and Skin in Humans

## 5.1.  Overview

This chapter aims to discuss the temperature elevation in a human head model considering vasodilation to discuss the conservativeness of the current limit. We computed the temperature elevations in an anatomical human head model exposed to radiation from a dipole antenna and truncated plane waves at 300 M–10 GHz. The maximum temperature elevation in the brain appeared around its periphery. At exposures with higher intensity, the temperature elevation became larger and reached around 40 °C at the localized SAR of 100 W/kg at 1 GHz, and became lower with an increase in the frequency. The temperature elevation in the brain at the current limit of 10 W/kg is at most 0.93 °C. The effect of vasodilation became notable for tissue temperature elevations higher than 1–2 °C and for a localized SAR of 10 W/kg. The temperature at the periphery was below the basal brain temperature (37 °C).

The temperature elevation in the brain at the limit in the current guideline for occupational exposure is within the ranges of brain temperature variability for environmental changes in daily life. The effect of vasodilation is significant, especially at higher frequencies where the skin temperature elevation is dominant. The work presented here was published in [52].

## 5.2. Methods

### 5.2.1. Exposure Scenarios

Figure 5.1 illustrates the exposure scenarios using the head part of the numeric Japanese male modeled as shown in section 2.2.3. As shown in Figure 5.1, the separation between the dipole antenna and the surface of the head model, excluding the pinna, was chosen as 25 mm (14–16 mm from the pinna). For comparison, a plane wave, vertically polarized and incident from the side of the head, was also calculated. The frequencies considered in this study were 300 MHz– 10 GHz. The length of the antenna was adjusted to half the wavelength depending on each frequency. For comparison, the output power of the antenna was adjusted so that the localized SAR was 2 (limited for the general public or unrestricted environment), 10 (limited for restricted environments or occupational exposures), 50, and 100 W/kg. The ambient temperature was set to 27 °C.

A vertically polarized plane wave, as a far-field source, is also considered for comparison. The effect of the polarization is marginal at frequencies higher than the GHz region where the penetration depth is a few centimeters or less.
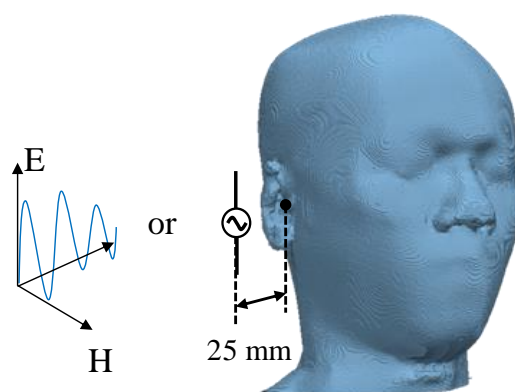


Figure 5.1 Exposure scenarios using the head part of the numeric Japanese male model.

## 5.2.2. Heating Factor

The heating factor is an approximation that expresses the temperature elevation from MW exposure, as follows [10], [91], [95]:

$$\alpha = T_{Brain} \Big/ SAR_{Head},$$

(5.1)

where $\alpha$ [°C·kg/W] denotes the heating factor, $\Delta T_{Brain}$ [°C] denotes the maximum temperature elevation in the brain, and $SAR_{Head}$ [W/kg] denotes the peak SAR in the head. Note the several heating factors have been introduced for different locations of peak SAR and peak temperature elevation.

# 5.3. Results

## 5.3.1. SAR Distributions

Figure 5.2 shows the SAR distributions from the dipole antenna and truncated plane wave at 1, 3, and 10 GHz, respectively. The reason for choosing three frequencies will be given below. As shown in the figures, the distribution of SAR concentrates on the surface layer as the frequency increases or as the penetration depth decreases. The penetration depth into muscle is 40.7 mm at 1 GHz and 3.3 mm at 10 GHz [88]. The penetration depths of the dipole antenna and
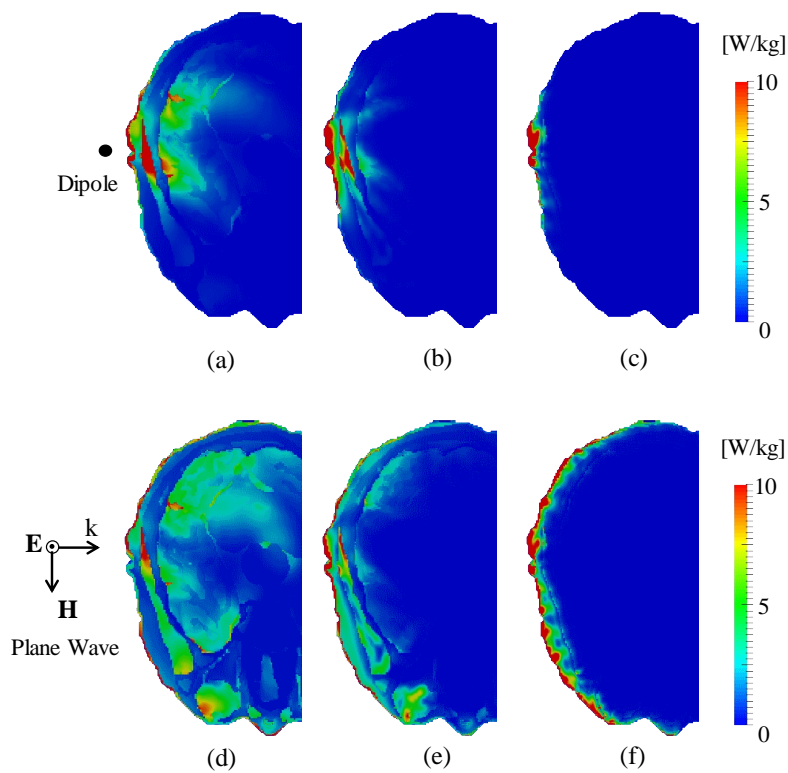


Figure 5.2 SAR distributions for each exposure scenario.

The exposure from a dipole antenna at a 1 GHz, b 3 GHz, and c 10 GHz. Exposure from a truncated plane wave at d 1 GHz, e 3 GHz, and f 10 GHz. The output power was adjusted so that the peak 10 g average SAR becomes 10 W/kg.

the plane wave are nearly the same. The exposure from plane waves has a wider area than that from the dipole antenna. These tendencies are most evident, at 1 GHz.

Table 5.1 shows the peak SAR averaged over the cubic and contiguous regions. The average SAR over a contiguous region was larger than in a cube shape for both the dipole antenna and plane wave exposure. For comparison, the dipole antenna output power was chosen as 1 W, and the plane wave incident power density was 100 W/m$^2$. As seen from the table, the differences between SARs calculated from the different algorithms are obvious at higher frequencies. Unlike the ICNIRP guidelines, the IEEE standards treat the pinna as the extremity. For the dipole antenna in close proximity to the pinna, most of the power is absorbed in the pinna [91]. A more detailed discussion on the effect of the averaging algorithm on the relation between SAR and temperature elevation can be found in our previous study [91]. The temperature elevation for a contiguous tissue can be estimated from the results presented in the table. As mentioned above, the cubic shape is commonly used and thus in the following discussion the SAR is averaged over a cubic shape.

Table 5.1 Computed specific absorption rate (SAR) averaged over 10 g using two averaging algorithms prescribed in the IEEE standard and ICNIRP guidelines.

| Frequency | 300 MHz | 1 GHz | 3 GHz | 6 GHz | 10 GHz |
|---|---|---|---|---|---|
| Dipole Antenna | | | | | |
| Cube | 0.75 | 2.59 | 3.20 | 2.67 | 3.83 |
| Contiguous | 1.02 | 6.04 | 10.82 | 8.30 | 12.70 |
| Plane Wave | | | | | |
| Cube | 8.07 | 4.43 | 6.18 | 4.66 | 4.15 |
| Contiguous | 13.34 | 7.85 | 14.15 | 25.77 | 23.80 |

The output power from the dipole antenna is 1 W. The incident power density of the plane wave is 100 W/m$^2$.

## 5.3.2. Temperature Elevation and Blood Perfusion Rate in Skin and Brain

Tables 5.2 and 5.3 show the maximum temperature elevations in the brain for dipole antenna

and plane wave exposure, respectively. It took 64, 34, 44, 45, 49 minutes at 0.3, 1, 3, 6, 10 GHz, respectively to the thermal steady-state. The time needed for skin to reach the steady state was shorter than that for the brain. This occurs because of the heat conduction from the surface to the brain. The time needed to reach the steady state becomes shorter as the localized SAR increased. This is because the blood perfusion effect becomes obvious, resulting in shorter thermal time constant.

The maximum localized SAR appeared in the skin of the head surface at frequencies ranging from 1 to 10 GHz and in fat at 0.3 GHz. The maximum temperature elevation presented in the head appeared in the skin at frequencies of 3–10 GHz while in the muscle at 0.3 and 1 GHz. The maximum temperature elevation in the brain appeared in gray matter for all the frequencies.

Table 5.2 Spatial maximum (voxel) temperature elevation in the brain due to exposure from the dipole antenna.

| Localized SAR | 2 W/kg | | 10 W/kg | | 50 W/kg | | 100 W/kg | |
|---|---|---|---|---|---|---|---|---|
| | $T_{Brain}$ (°C) | $\Delta T$ (°C) | $T_{Brain}$ (°C) | $\Delta T$ (°C) | $T_{Brain}$ (°C) | $\Delta T$ (°C) | $T_{Brain}$ (°C) | $\Delta T$ (°C) |
| 300 MHz | 36.77 | +0.17 | 37.48 | +0.87 | 39.80 | +3.19 | 41.62 | +4.76 |
| 1 GHz | 36.75 | +0.18 | 37.49 | +0.93 | 40.00 | +3.46 | 41.67 | +5.14 |
| 3 GHz | 36.71 | +0.14 | 37.30 | +0.73 | 39.21 | +2.64 | 40.40 | +3.83 |
| 6 GHz | 36.66 | +0.09 | 37.04 | +0.46 | 38.32 | +1.74 | 39.19 | +2.61 |
| 10 GHz | 36.66 | +0.07 | 36.85 | +0.37 | 37.79 | +1.23 | 38.26 | +1.70 |

Temperature computations including thermoregulation. The SAR was averaged over a cubic shape following the IEEE standard.

Table 5.3 Spatial Maximum (voxel) temperature elevation in the brain for exposure from the truncated plane wave.

| Localized SAR | 2 W/kg | | 10 W/kg | | 50 W/kg | | 100 W/kg | |
|---|---|---|---|---|---|---|---|---|
| | $T_{Brain}$ (°C) | $\Delta T$ (°C) | $T_{Brain}$ (°C) | $\Delta T$ (°C) | $T_{Brain}$ (°C) | $\Delta T$ (°C) | $T_{Brain}$ (°C) | $\Delta T$ (°C) |
| 300 MHz | 37.22 | +0.16 | 37.89 | +0.83 | 40.16 | +3.08 | 41.85 | +4.79 |
| 1 GHz | 36.76 | +0.14 | 37.38 | +0.76 | 39.90 | +3.28 | 42.07 | +5.25 |
| 3 GHz | 36.81 | +0.13 | 37.36 | +0.68 | 39.34 | +2.75 | 40.56 | +3.97 |
| 6 GHz | 36.74 | +0.15 | 37.24 | +0.75 | 39.35 | +2.86 | 40.55 | +4.06 |
| 10 GHz | 36.61 | +0.14 | 37.21 | +0.68 | 38.90 | +2.46 | 40.00 | +3.52 |

Temperature computations including thermoregulation. The SAR was averaged over a cubic shape following the IEEE standard.
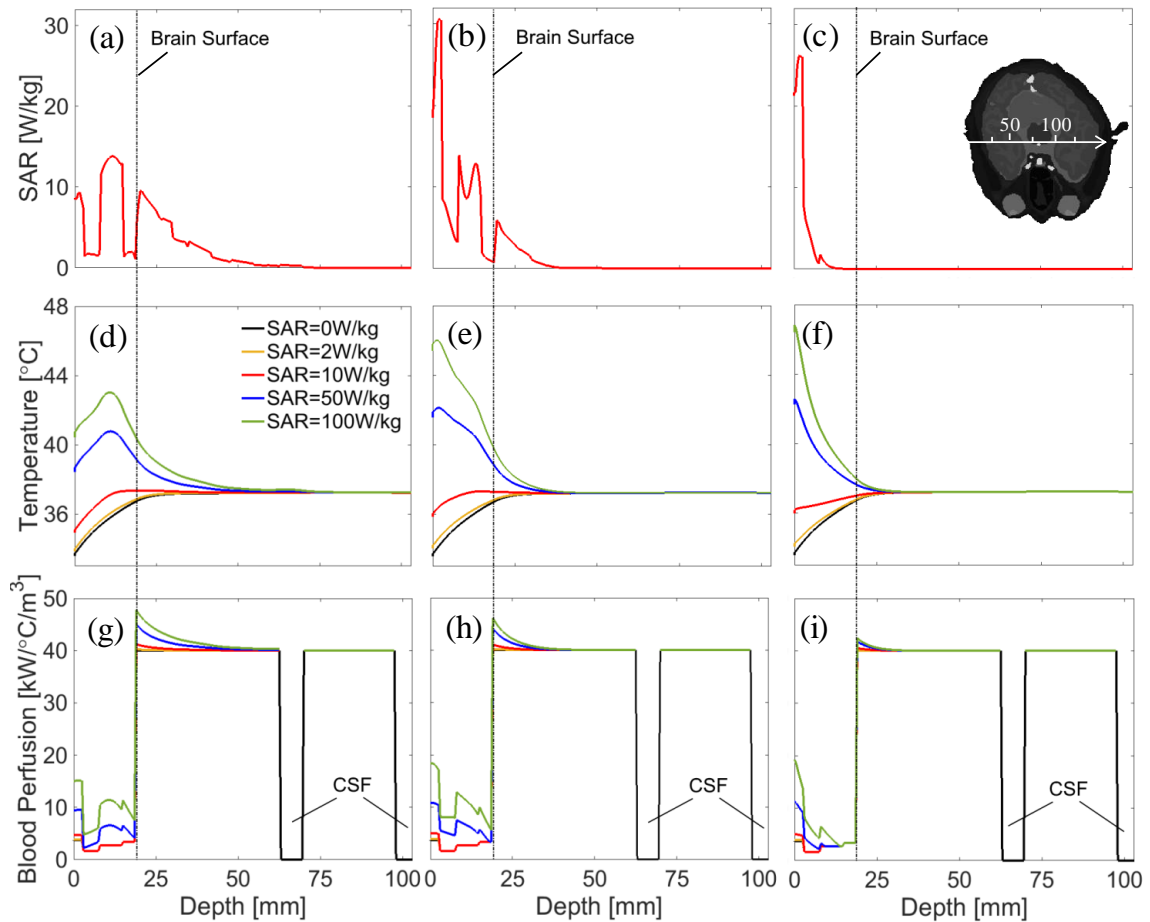
Figure 5.3 Distributions of (a–c) SAR, (d–f) temperature, and (g–i) blood perfusion rate from the dipole antenna.

The axis passes through the cross section center in Figure 5.2. Frequencies are (a, d, g) 1 GHz, (b, e, h) 3 GHz, and (c, f, i) 10 GHz. The output power was normalized so that peak SAR becomes 2, 10, 50, and 100 W/kg, respectively. SAR = 0 W/kg indicates the initial state without microwave exposure

However, their points did not coincide with each other because of the complicated SAR distribution. For localized SAR equal to 100 W/kg, the differences between the two scenarios were 0.6, 2.1, 13.8, 55.5 and 107.5% at 0.3, 1, 3, 6 and 10 GHz.

For SAR averaged over a contiguous tissue, the maximum temperature elevations in the brain were 0.45 and 0.11 °C at 1 and 10 GHz, respectively. These values occur at a localized SAR of 10 W/kg. These values were a half to one third of the SAR averaged over a cube. The main
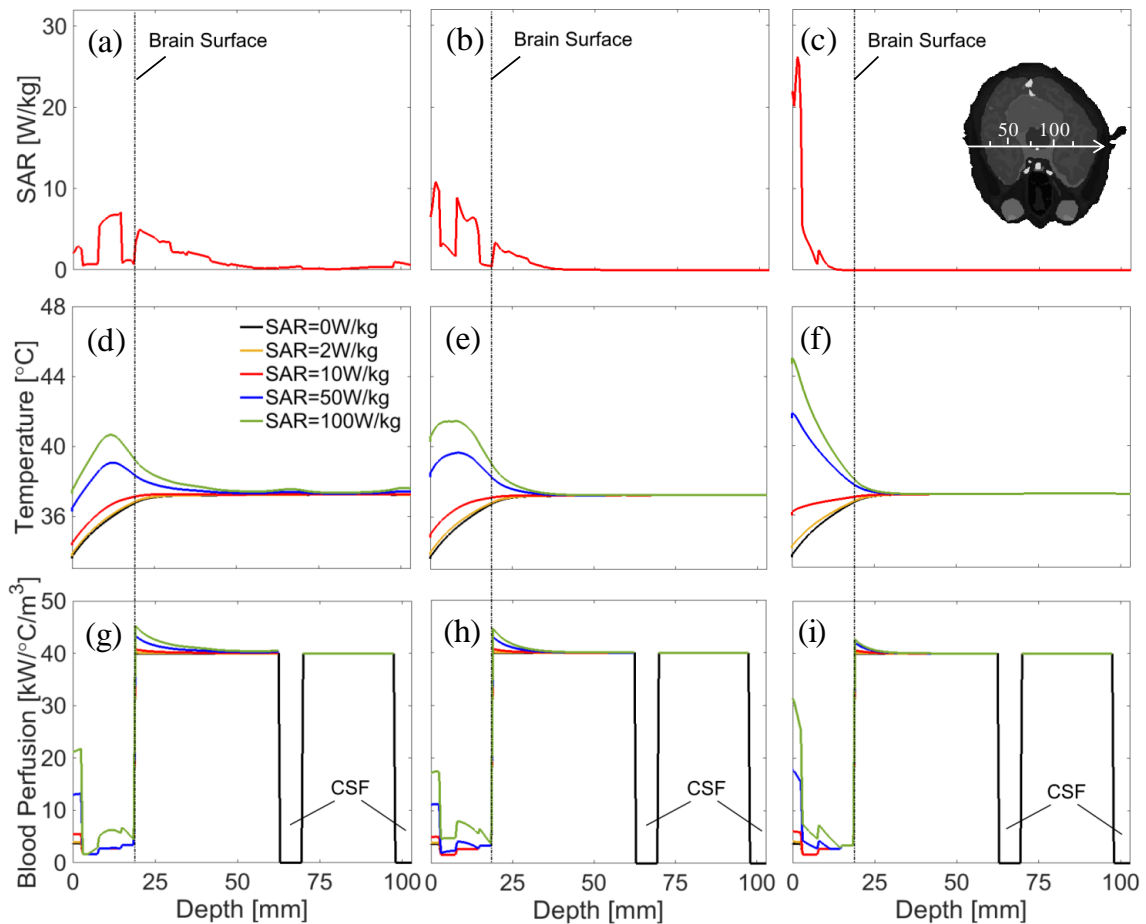
Figure 5.4 Distributions of (a–c) SAR, (d–f) temperature, and (g–i) blood perfusion rate from the truncated plane wave.
The axis passes through the cross section center in Figure 5.2. Frequencies are (a, d, g) 1 GHz, (b, e, h) 3 GHz, and (c, f, i) 10 GHz. The output power was normalized so that peak SAR becomes 2, 10, 50, and 100 W/kg, respectively. SAR = 0 W/kg indicates the initial state without microwave exposure

reason for the SAR difference is attributable to the inclusion of the pinna in the averaging volume.

Figure 5.3 shows the SAR distribution, temperature elevation, and blood perfusion rate along the center axis (see Figure 5.2) for localized SAR values of 2, 10, 50, and 100 W/kg. The wave source was the dipole antenna. As shown in Figure 5.3a–c, the penetration depth decreases as the frequency increases. As shown in Figure 5.3d–f, the temperature elevation becomes larger for higher SARs. The common temperatures around the periphery of the brain (19–33 mm from
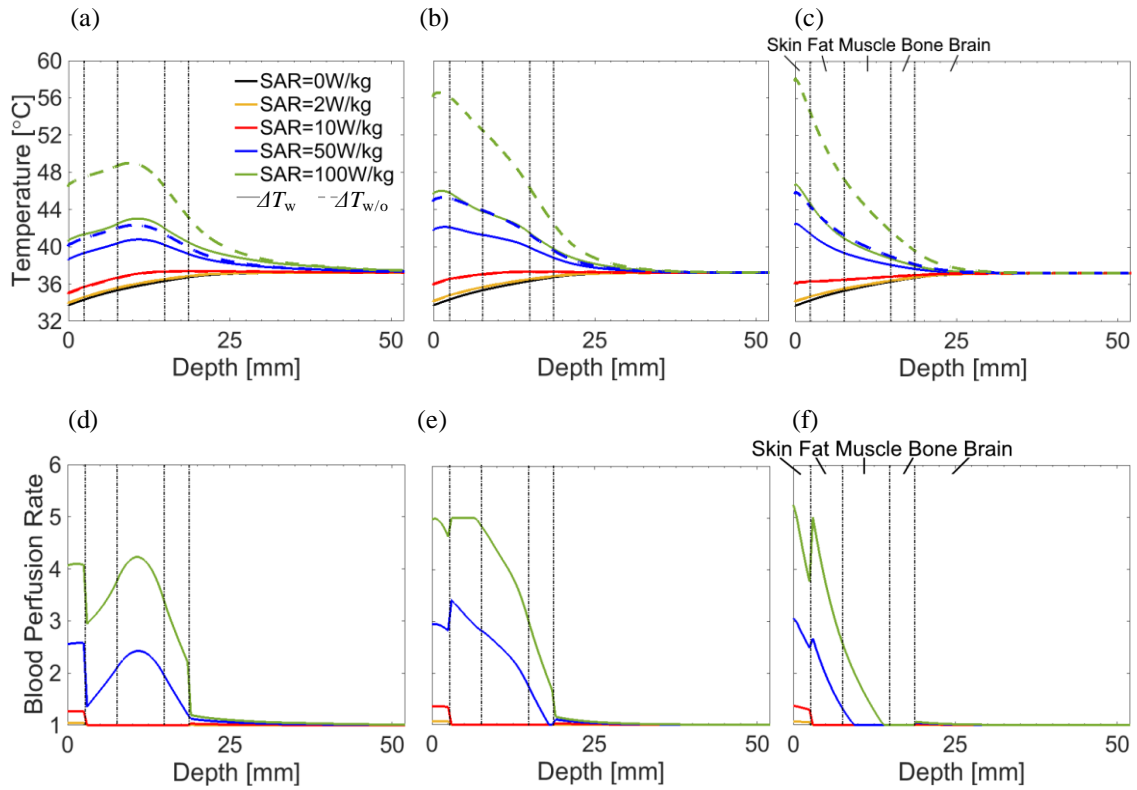
Figure 5.5 Comparison of temperature elevations with and without thermoregulation (a–c) and normalized blood perfusion (d–f).
Frequencies are (a, d) 1 GHz, (b, e) 3 GHz, and (c, f) 10 GHz. The heat source is the dipole antenna. The solid line indicates temperature with thermo-regulation through the cross section center in Figure 5.2. ($\Delta T_W$ are the same data in Figure 5.3). The broken line indicates the temperature without thermoregulation ($\Delta T_{W/O}$)

the surface) are lower than the brain basal temperature of 37.3 °C.

The steady-state peripheral brain temperature without exposure was 36.6 °C, which is consistent with the tendency in [96]; the peripheral temperature is approximately 0.5–0.6 °C smaller than the central temperature in the brain. The temperature around the brain surface increases and reaches around 40 °C at a peak SAR of 100 W/kg at 1 GHz. The temperature also reduces with increasing frequency.

In addition, the figures show that the elevation in skin temperature is dominant, especially at 10 GHz. As seen from Figure 5.3, the blood perfusion rate becomes large with the local temperature elevation. This is characterized by Equations (2.6), (2.7), and (2.8), or governed by

the tissue type and local temperature elevation. The brain blood perfusion rate at 1 GHz increased by 0.58%, 3.1%, 12.6%, and 19.5% for peak SARs of 2, 10, 50, and 100 W/kg, respectively. The skin blood perfusion rate at 1 GHz increased by 4.2%, 26.8%, 157.8%, and 309.8% for peak SARs of 2, 10, 50, and 100 W/kg, respectively. The increase in the other tissues was not notable, which is attributed to the formula we used in this study.

Figure 5.4 shows the distribution of the SAR, temperature, and blood perfusion rate along the same axis of Figure 5.2 due to plane-wave exposure. Comparing Figures 5.3 and 5.4, the difference in the SAR distribution between the dipole antenna and the plane wave is significant at 1 GHz.

### 5.3.3.   Effect of Thermoregulation and Heating Factor

Figure 5.5a–c shows a comparison of the temperature elevation in the head with and without thermoregulation ($B(\mathbf{r}, t) = B_0(\mathbf{r})$ in Equation (2.2) over the model). The difference in the temperature with and without thermoregulation is marginal at a peak SAR below 10 W/kg, while it is obvious at 50 and 100 W/kg. For peak SAR equal to 100 W/kg, the temperature elevation on the skin surface was 6.0, 10.6, and 11.4 °C at 1, 3, and 10 GHz, respectively. This corresponds to suppression of temperature elevation by 54.2, 53.3, and 53.6%, respectively. For 100 W/kg peak SAR, temperature elevations in the brain were suppressed by 2.5, 2.5, and 1.5 °C at 1, 3 and 10 GHz, respectively, each corresponding to a suppression of 58.9, 53.5, and 45.1%, respectively.

Figure 5.5d–f shows the blood perfusion rate normalized by the basal blood perfusion rate B0 for the dipole antenna. The tendency of Figures 5.5a–c and 5.5d–f are similar due to an increase in blood perfusion with local temperature elevation, as shown in Equations (2.6), (2.7), and (2.8). The increased blood perfusion is noticeable only in skin for a peak SAR equal to 10 W/kg. The blood perfusion increase is significant in the skin, fat, and muscle at 50 and 100 W/kg.

Table 5.4 shows the heating factors with thermoregulation for the peak localized SAR. The heating factors at 2 and 10 W/kg are relatively constant. However, they decrease by 30.6 % and 52.7 % at peak SARs of 50 and 100 W/kg at 10 GHz when considering thermoregulation from

the dipole antenna. These results are confirmed to have a nonlinear relationship, as mentioned above.

Table 5.4 Heating factor in the brain from exposure to the dipole antenna and the truncated plane wave.

|  |  | Heating factor (°C·kg/W) | | | |
|  | Localized SAR | 2 W/kg | 10 W/kg | 50 W/kg | 100 W/kg |
|---|---|---|---|---|---|
| Dipole antenna | 1 GHz | 0.092 | 0.093 | 0.069 | 0.051 |
|  | 3 GHz | 0.072 | 0.073 | 0.053 | 0.038 |
|  | 10 GHz | 0.036 | 0.037 | 0.025 | 0.017 |
| Plane wave | 1 GHz | 0.072 | 0.076 | 0.066 | 0.052 |
|  | 3 GHz | 0.065 | 0.068 | 0.055 | 0.040 |
|  | 10 GHz | 0.068 | 0.068 | 0.049 | 0.035 |

## 5.4.  Discussion

In this chapter, we computed the temperature elevation in the human head while accounting for vasodilation. Vasodilation is the most significant parameter that influences the temperature elevation due to local exposure (see also [65]). In the worst case, temperature elevation at the thermal steady state was investigated. It takes more than 30 minutes of constant exposure for the steady state to be reached [5]. The main contribution of this study revealed the limitation of the approach in terms of the heating factor in the regime where thermal damage may occur. Specifically, the local temperature cannot be well estimated in terms of the heating factor at the steady-state temperature. The inaccuracy arises due to ignoring thermoregulation (vasodilation).

The SAR and temperature elevation distributions were different for different wave sources, whereas the influence of internal tissues such as the brain on the temperature were marginal (Figures 5.3 and 5.4). This is due to the heat diffusion length in biological tissue [38]. The effect of vasodilation becomes notable for tissue temperature elevations higher than 1–2 °C, which is consistent with a previous study [97]. For localized exposure in the head, averaged skin and core temperature elevations were smaller than 0.3 and 0.1 °C, respectively. Thus, thermoregulation was dominated by local temperature elevation or vasodilation. A significant difference in the temperature elevation considering thermoregulation was found in the skin and brain. In addition, for all the cases considered here, the temperature elevation was mainly induced by heat conduction of the power absorption in the outer layer of the head (skin and skull). Considering the linearity of the bioheat equation without thermoregulation [62], we can estimate the contribution of SAR in the brain to the temperature elevation in the brain. Although detailed data is not shown, its contribution at peak SAR of 2 W/kg was 25% or less at 1 GHz and becomes smaller at higher frequencies.

With increasing frequency, the SAR distributions and resulting temperature elevations were shifted to more peripheral locations in the head. At the current occupational exposure limit of 10 W/kg localized SAR in the head, the peak temperature elevation in the brain is at most 0.93 °C (see Table 5.2). The temperature elevation was marginally affected by the ambient temperature. The differences of temperature elevation were less than 10% in both skin and brain when the

ambient temperature was set to 23 °C. In comparison, using a statistical approach considering more than 30 cases [91], the maximum brain temperature was observed at 1.25 °C at 10 W/kg (1.06 °C as the 95%ile value), corresponding to the maximum brain temperature of 37.8 °C. Exposure limits for the general public are 20% of those for occupational groups, resulting in a correspondingly lower peak temperature increase at the margins of the brain.

The local brain temperature at 39–43 °C may be close to the threshold of tissue damage, however it depends on the exposure duration, etc. [30]. As shown in Table 5.2, the temperature may reach this 43 °C threshold at more than 100 W/kg. From the Tables 5.2 and 5.3, as well as a previous study [91], the brain temperature elevation decreases as the frequency increases. The temperature elevation, however, does not decrease significantly at higher frequencies because heat is conducted away from the surface of the human head. Instead, the temperature elevation in the skin reached approximately 50 °C at 10 GHz. This is attributable to the SAR averaging algorithm. In the IEEE standard, the pinna is not included in the averaging volume. Instead, in the ICNIRP guidelines, the SAR values are averaged over single tissues that include the pinna. Thus, a straightforward comparison is not available. However, additional consideration is needed when extending SAR in a cube up to 10 GHz.

The peak temperature elevation is in the periphery of the brain. It is generally 0.5 °C cooler than the core of the brain due to thermal interactions with the environment [96], as is apparent from Figure 5.3 and 5.4. The peak temperature in the brain induced by RF exposure, even at occupational exposure limits, is anticipated to be comparable to the baseline temperature in the core of the brain. The peak temperature increase in the brain at exposure limits for the general public are anticipated to be well within the diurnal variation in brain temperature (about 1 °C peak to peak) [98].

As shown in Figure 5.5, the temperature elevation reduced significantly due to the increased blood perfusion rate in the skin and muscle. In contrast, the increase of blood perfusion in the brain was marginal. As mentioned above, the SAR in the brain contributes slightly to the brain temperature elevation, and the suppressed brain temperature with thermoregulation mainly is attributable to thermoregulation in the surface tissues.

Head models commonly used in dosimetry have a less detailed structure of the brain. There

are many tissues between the skull itself and the brain in a real head (e.g. superior cerebral veins). The vasculature is considered to be a source of heat transfer [99], which is not considered in this study. Due to the finite resolution of the anatomical models, the anatomy of dura and cerebrospinal fluid etc. cannot be modeled accurately. The temperature elevation would be different between a plane wave applied to the whole body and the truncated head model.

Finally, if the heating factor is used to set the limit in the international standards, the location of the maximum temperature elevation is not considered. It is the nature of electromagnetic fields to decay exponentially from the body surface, especially for near field exposures from portable devices (see Figure 5.2). Thus, the limit derived based on the heating factor may provide conservative limits. Instead, this study showed that the effect of thermoregulation is not significant for a local temperature elevation of ~1 °C because thermoregulation has not been activated.

## 5.5. Conclusion

This chapter investigated temperature elevations in the brain considering vasodilation for MW exposure at the limits prescribed in the international guidelines/standards. We computationally estimated the temperature elevation in the brain for excessive SAR. The current limit of 10 W/kg has the margin of more than 10 when compared to the thermal damage of threshold [30]. This margin is caused by thermoregulation and is not be expected from the linear model that ignores thermoregulation. Note that damage is characterized by the duration of the exposure, which has not been significantly addressed in this paper. Temperature elevation in the brain at the current guideline limit for occupational exposure (i.e., 10 W/kg averaged over 10 g) was comparable to the variability from daily environmental changes and/or diurnal changes.

# Chapter 6

# Temperature Elevation for Brief Exposure

## 6.1.   Overview

In international guidelines for human protection from radio-frequency (RF) electromagnetic fields, the specific absorption rate (SAR) averaged over 6 minutes and 10 g of tissue is used as a physical quantity to prevent excess local temperature elevation. The resultant SAR restriction has been set to avoid potential adverse health effects due to the temperature elevation resulting from RF energy absorption. In the public consultation version of the upcoming ICNIRP RF guidelines (10th July, 2018), a specific absorption (SA) limit was set to avoid heating from brief exposures (shorter than 6 min). However, to the best of our knowledge, no prior research has evaluated the temperature elevation for single/multiple pulses with energy equivalent to the 6 min exposure SAR restriction for continuous waves.

This chapter computed the temperature elevation for brief pulse exposures based on bioheat computations. We first confirmed that the peak temperature elevation for a pulse with SA corresponding to occupational exposure exceeds the steady-state temperature elevation for temporally uniform continuous wave exposure. We then proposed the SA limit from a regression curve that is dependent on the duration of brief exposure to RF pulse(s). The temperature elevation in a multilayer cube and an anatomical human model were also computed for exposures to multiple pulses. The temperature elevation from multiple pulses satisfying the

formula was found to be below the relevant threshold level. The SA based on this regression curve can be used as a metric to prevent excess temperature elevation for different brief exposure scenarios below 6 min. The work presented here was published in [100].

## 6.2.    Methods

### 6.2.1.    Exposure Scenarios

Figure 6.1 illustrates exposure scenarios using the multilayer cube model and the anatomical human head model. The multilayer cube model was used as shown in section 2.2.2, and the anatomical human head model was used Japanese male model TARO in section 2.2.3. The frequencies of the RF fields were 0.1, 0.3, 0.4, 0.5, 1, 3 and 6 GHz. To simulate plane-wave exposure using the multilayer cube, we conducted a one-dimensional analysis with the same seven-tissue composite for simplicity. Hereafter, the one-dimensional analysis will be referred to as plane wave exposure.

Considering the effect of field non-uniformity, a half-wave dipole antenna was also considered as a canonical near-field source. The length of the half-wave dipole antenna was adjusted to approximately half the wavelength of the RF field so as to resonate at the respective frequencies. The separation distances between the dipole antenna and the surface of the cube model and the human head model were set to 15 mm and 25 mm, respectively. The ambient temperature was set to 27 °C.



(a)                                                                (b)
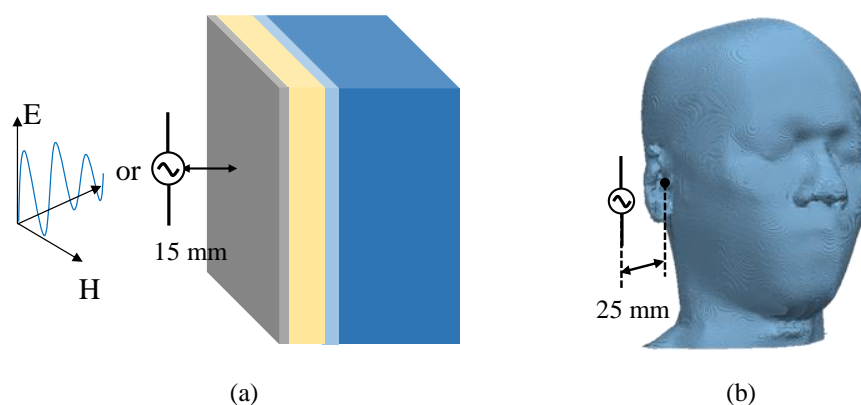
Figure 6.1 Exposure scenario with (a) a multilayer cube model and (b) an anatomical head model.

Thermoregulation, such as vasodilation and sweating, were not considered in this chapter as the exposure duration is brief, and thus the temperature elevation is confined around the surface in most cases (e.g. [52], [62]).

# 6.3. Results

## 6.3.1. Temperature Elevation in Skin at Constant SA

Figure 6.2 shows the SAR distributions and temperature elevation at 400 MHz and 6 GHz in the multilayer cube model for exposure from the dipole antenna and plane wave. The distributions of temperature elevation were obtained at constant SA (3.6 kJ/kg, corresponding to the energy of 10 W/kg for 6 min) and were normalized at the peak temperature elevation in each
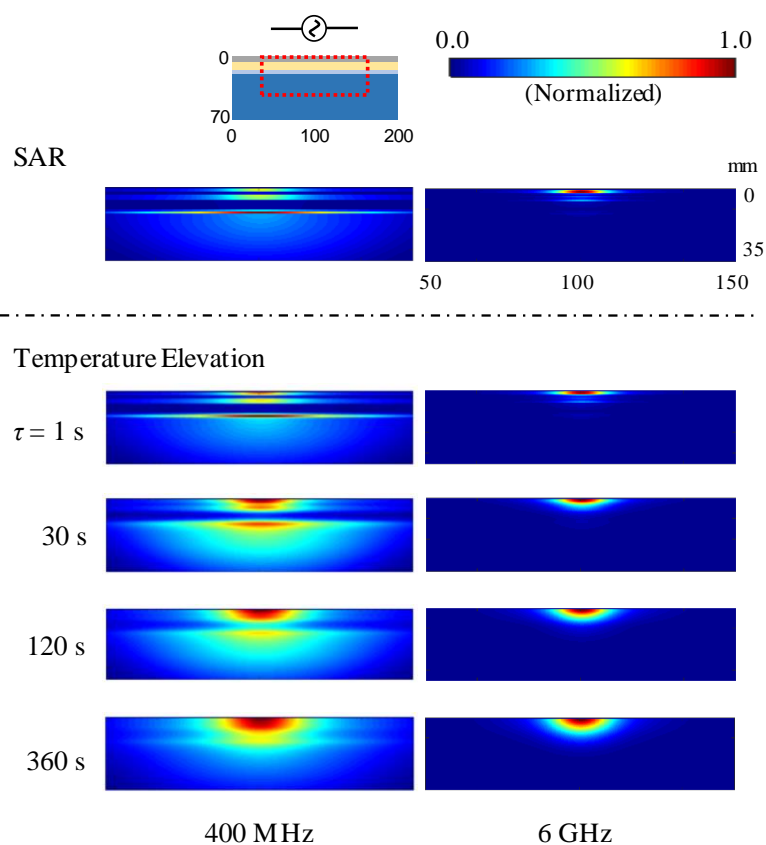


Figure 6.2 Distribution of SAR and temperature elevation in the multilayer cube model. The SARs were adjusted to 10-g averaged SAR at 10 W/kg. The temperature elevations were at constant specific absorption (SA) at 3.6 kJ. Distribution of temperature rise were normalized at the peak temperature rise in each scenario.
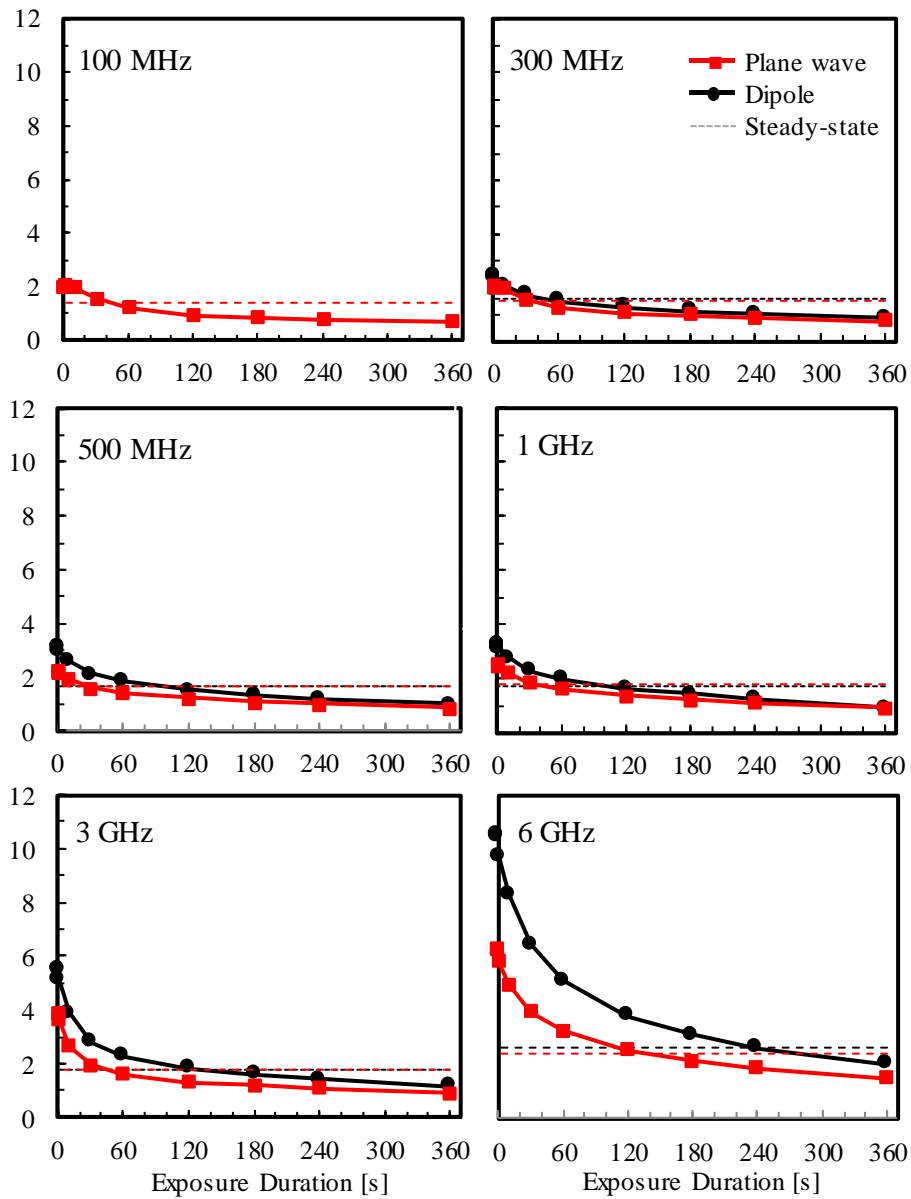
Figure 6.3 Temperature elevation in multilayer cube model for dipole antenna and plane wave exposure.

The SA was adjusted to 3.6 kJ/kg. The observed points correspond to the maximum temperature elevation. The steady-state temperature rise (duration longer than 30 min) are also plotted for comparison.

scenario. Note that the basic restriction is 10 W/kg for occupational exposure, and the averaging time is set to 6 min below 3 GHz in IEEE C95.1 [2] and 10 GHz in ICNIRP [1]. As shown in Figure 6.2, the temperature elevation distributions for short exposure duration (e.g., 1 s) is almost identical to the SAR distributions, whereas it becomes smoother with increased time due to heat diffusion. The peak temperature elevation at 400 MHz and 6 GHz were 2.5 and 9.8 °C for 1 s short exposure, while they became 0.9 and 2.0 °C at 6 min, respectively. These results suggest that an enhanced temperature elevation can be observed at higher frequencies. The spatial peak temperature elevation appeared in the skin (i.e., at the model surface) except at 3 GHz, which is attributable to the standing wave in the tissues.

Figure 6.3 shows the peak temperature elevation in a multilayer cube at constant SA (3.6 kJ/kg) for exposure to a dipole antenna and plane wave. For comparison, the steady-state temperature elevation for 10 W/kg was also plotted. The temperature elevation at 6 min is lower than that at the steady state because the time required to reach the steady state is longer than 6 min at frequencies below 6 GHz [5]. The temperature elevation for the dipole antenna is not shown at 100 MHz because its dimension (approximately 150 cm) is much larger than that of the head size. Thus, results for the dipole antenna at 100 MHz may become similar to the results from plane wave exposure at 100 MHz just as their results at 300 MHz were similar. As shown in Figure 6.3, an energy concentration of less than 30 s below 500 MHz is required to induce a temperature elevation larger than that of the steady state for plane wave exposure, but the exposure time is somewhat longer for a dipole antenna. This difference is attributable to the difference in SAR distribution (see Figure 6.2). For short pulse duration at 6 GHz, a factor of 4 enhancements was observed. Also from Figure 6.3, the effect of frequency on pulse-induced temperature elevation is dominant over the field distributions (dipole antenna versus plane wave). At the same frequencies, the difference was smaller than a factor of 2.

## 6.3.2. Effectiveness of SA as Basic Restrictions

Figure 6.4a summarizes the SA required for a skin temperature elevation of 1 °C for different parameters; frequencies, sources, and exposure durations. Even at 1 s, the variability of
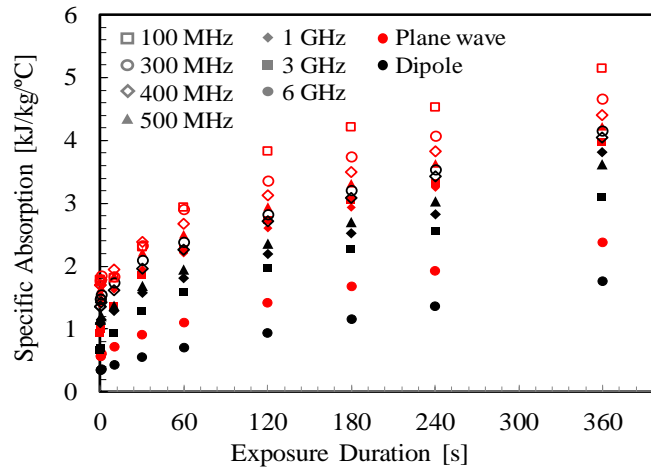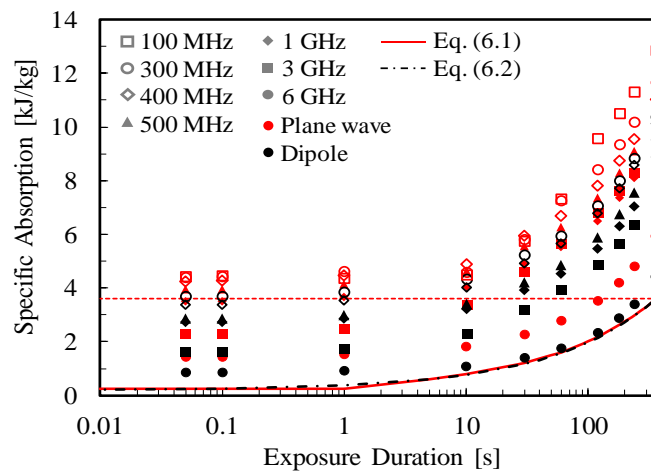
Figure 6.4 SA required for temperature elevation of (a) 1 °C and (b) 2.5 °C for exposure from dipole antenna and plane wave using multilayer cube model.
The allowable SA for occupational exposure and proposed regression curve are also plotted in (b).

temperature elevation by SA is significant (see Figure 6.3) For increasing frequency, the SA is concentrated on more superficial layers and consequently less absorbed energy is needed for the same temperature elevation as at lower frequencies where the energy is distributed to a larger volume. For decreasing exposure durations, the decrease of heat flow has a similar effect on

temperature elevation. As shown in Figure 6.4, the required SA decreases as the exposure duration decreases. The heat diffusion length depends on the exposure time, resulting in the SA difference required for a given temperature elevation (see Figure 6.2).

The draft of IEEE C95.1 limits skin temperature elevation to 2-3 °C. The ICNIRP public consultation document applied a reduction factor of 2 to the 5 °C temperature elevation in tissues which typically have lower thermo-normal temperatures. The localized SAR was set to 10 W/kg for occupational exposure according to the standards and guidelines available for RF protection at that time. This resulted in a steady-state temperature elevation of approximately 2.5 °C at 0.1–6 GHz (see Figure 6.3). In the following discussion, we chose 2.5 °C as a reference, and then the corresponding SA is discussed based on the bioheat calculation. This can be confirmed also by Figure 6.2, which shows that the peak temperature elevation occurs at skin rather than internal organs whose allowable temperature elevation is 1 °C.

Figure 6.4b shows the SA required for a temperature elevation of 2.5 °C by rescaling Figure 6.4b and the allowable SA (= 3.6 kJ/kg) for head and trunk tissue. The allowable SA at 6 min was designed to match SAR for the head and torso tissues (not in the limb) in a conservative manner. As shown in Fig. 4, the scenario resulting in the lowest SA required for a temperature elevation of 2.5 °C is from the dipole antenna exposure at 6 GHz. This condition corresponds to a non-uniform SAR distribution in the averaging cube (10 g). The SA required below a few seconds of exposure is almost duration-independent, and then increases gradually as the exposure duration increases. The local temperature elevation for a short-pulse ($\tau > 0.01$ s) with intense exposure of 3.6 kJ/kg exceeds 2.5 °C at frequencies higher than 500 MHz. We thus proposed a regression curve for the allowable SA to match 3.6 kJ/kg exposure at 6 min as follows:

$$SA = \begin{cases} 0.25 & \tau < 1\,\text{s}, \\ 0.25 + 0.177\sqrt{\tau - 1} & 1\,\text{s} \le \tau < 360\,\text{s}, \end{cases} \tag{6.1}$$

where $\tau$ denotes the RF exposure duration. For irregular pulse patterns or non-constant exposure levels, any exposure for exposure durations ("temporal analysis windows") between the pulse duration and $\tau$ is considered, as is the same in the incoherent guidelines. Note that the regression

curve is assumed to be proportional to the square root of duration with an intercept below 1 s, which is approximately chosen as adiabatic regime of temperature elevation. The function form is based on the analytic solution by [38].

Another expression for the regression curve is chosen as follows considering allowable SA at 6 min as well as the adiabatic conditions:

$$SA = 3.6\left(0.05 + 0.95\sqrt{\tau/360}\right),$$ (6.2)

The proposed regression curves in Equations (6.1) and (6.2) are plotted in Figure 6.4b, which almost coincide each other.

## 6.3.3.   Demonstrations for Multiple Pulses

We computed the following four scenarios to confirm the change in temperature over time: (i) five different short pulses of 0.1 s exposure; (ii) continuous exposure to a 0.1 s pulse with intervals of 2 s; (iii) after exposure of a continuous wave for 30 min, followed by a 6 min pause and a 1 s pulse exposure; (iv) four repetitions of 200 s pulses and 160 s pauses. The SA values in all scenarios were adjusted so as not to violate the regression curve in Equation (6.1). Note that Equation (6.2) is more conservative than Equation (6.1) except around 1 sec, and thus Equation (6.1) is used in the remaining of the study. The exposure scenarios (iii) and (iv) considered more than 6 min to confirm the cumulative effect of temperature elevation in possible complicated environments.

Figure 6.5 shows the time dependence of the subjected localized SAR and the resulting temperature elevation at the position where the peak temperature appeared in the multilayer cube model in exposure scenarios (i), (ii), (iii), and (iv). To clearly show the effect of temperature for exposure to multiple pulses, the peak temperature was normalized at the peak steady-state temperature elevation for continuous exposure (adjusted to localized SAR at 10 W/kg). As

Figure 6.5 Time dependence of the peak SAR averaged over 10 g of tissue and the resulting temperature elevation for four scenarios of multiple pulse exposure from a dipole antenna at 6 GHz using the multilayer cubic model.

The SAR averaged over 10 g was adjusted so that the SA did not exceed the proposed regression curve. The temperature was normalized at the peak steady-state temperature rise for continuous exposure (adjusted to 10 g averaged peak SAR at 10 W/kg).
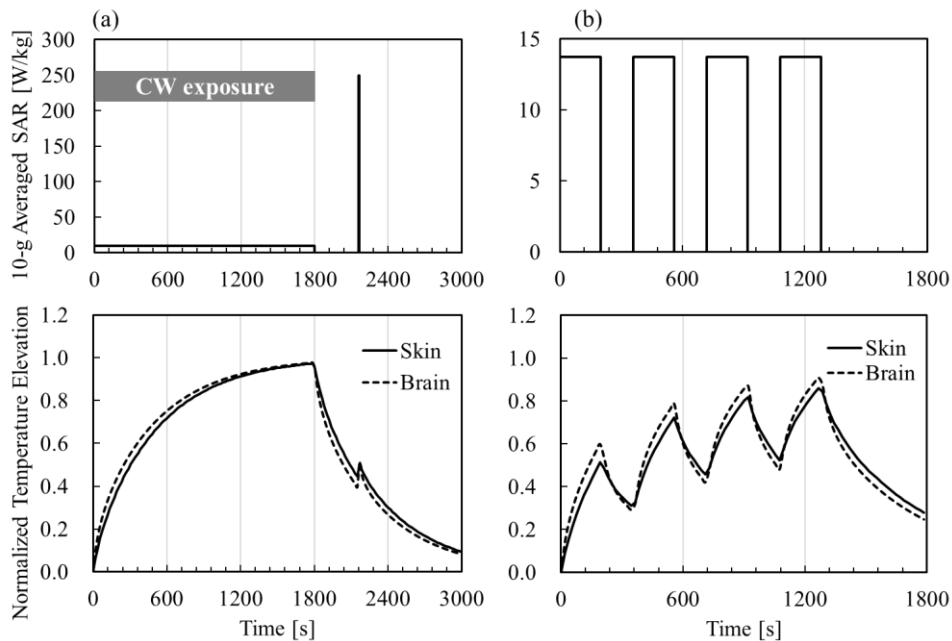
Figure 6.6 Time dependence of the peak SAR averaged over 10 g of tissue and the resulting temperature elevation for four scenarios of multiple pulse exposure from a dipole antenna at 6 GHz using the multilayer cubic model.

The SAR averaged over 10 g was adjusted so that the SA did not exceed the proposed regression curve. The temperature was normalized at the peak steady-state temperature rise for continuous exposure (adjusted to 10 g averaged peak SAR at 10 W/kg).

steady-state temperature in most investigated cases. In the case of Figure 6.5d, the instantaneous peak temperature elevation reached 2.3% above the steady state temperature elevation. The peak temperature elevation did not exceed the steady-state temperature when the separation distance between the dipole antenna and the surface of the cube model was set to 25 mm in the same scenario. Figure 6.6 shows the temperature elevation in skin and brain tissue at 400 MHz in exposure scenarios (iii) and (iv). The peak temperature elevation in the brain was 0.82 °C for continuous exposure adjusted to localized SAR at 10 W/kg for 6 min. The normalized temperature elevation in the brain was 95% and 89% of steady-state temperature in Figure 6.6a and b, respectively. The brain temperature elevates higher at lower frequencies because the penetration depth of electromagnetic field is deeper than at higher frequencies. The computed SAs below 3 GHz are sufficiently higher than the regression curve in Figure 6.4b. Thus, the

regression curve also suppressed the brain temperature elevation for exposure to multiple pulses. In addition, we computed the temperature rise using the anatomical head model in several scenarios. Figure 6.7 shows the temperature elevation in the anatomical head model in exposure scenarios (i), (iii), and (iv). The peak temperature for exposure to multiple pulses was normalized at the peak steady-state temperature elevation for continuous exposure (adjusted to localized SAR at 10 W/kg), as in the case of the multilayer cube model. As shown in Figure 6.7a–d, the peak temperature elevation for multiple pulses in the human head was less than 98% of the steady-state temperature elevation. The normalized temperature elevation of the anatomical model was lower than that of the multilayer model.
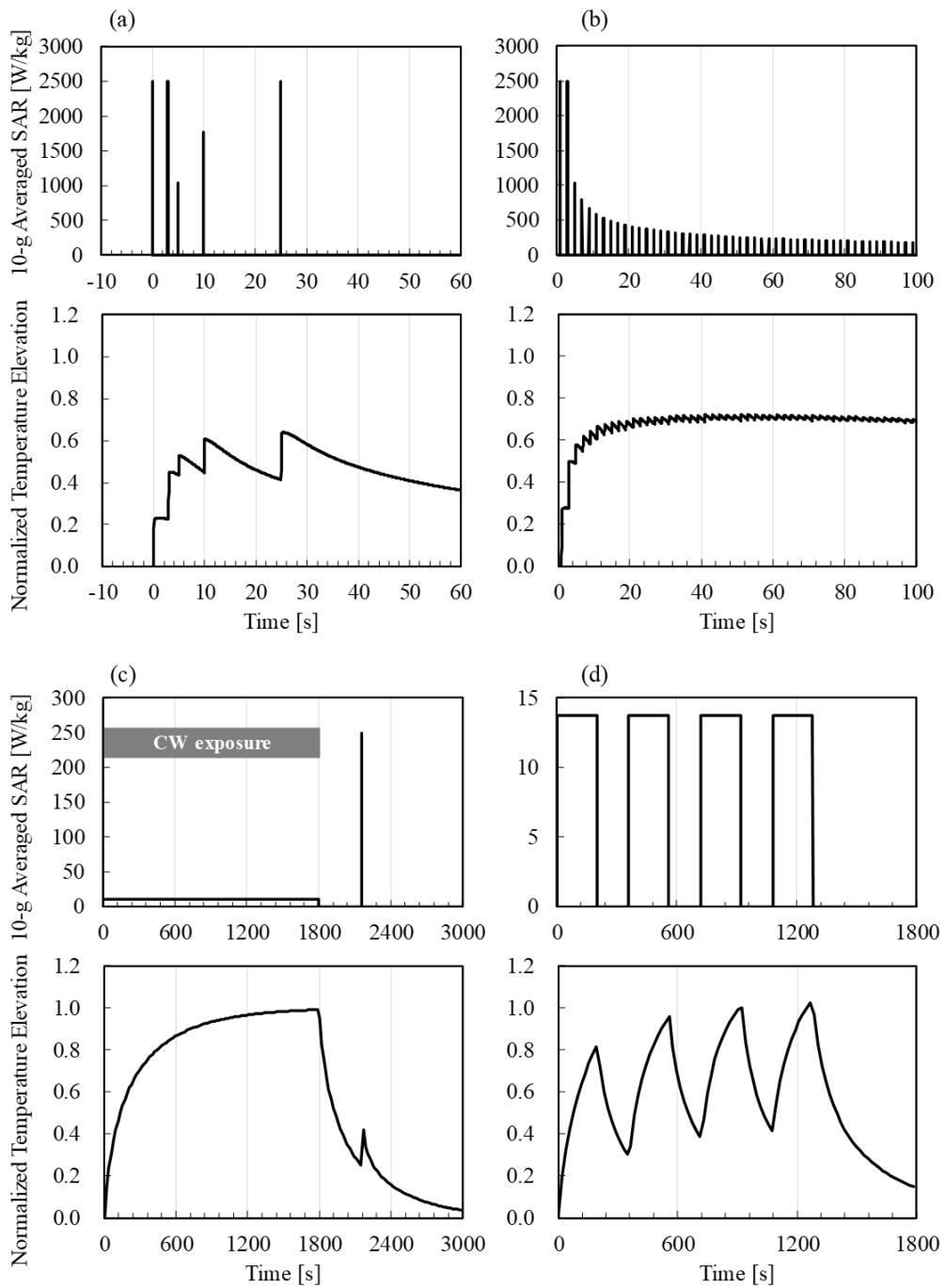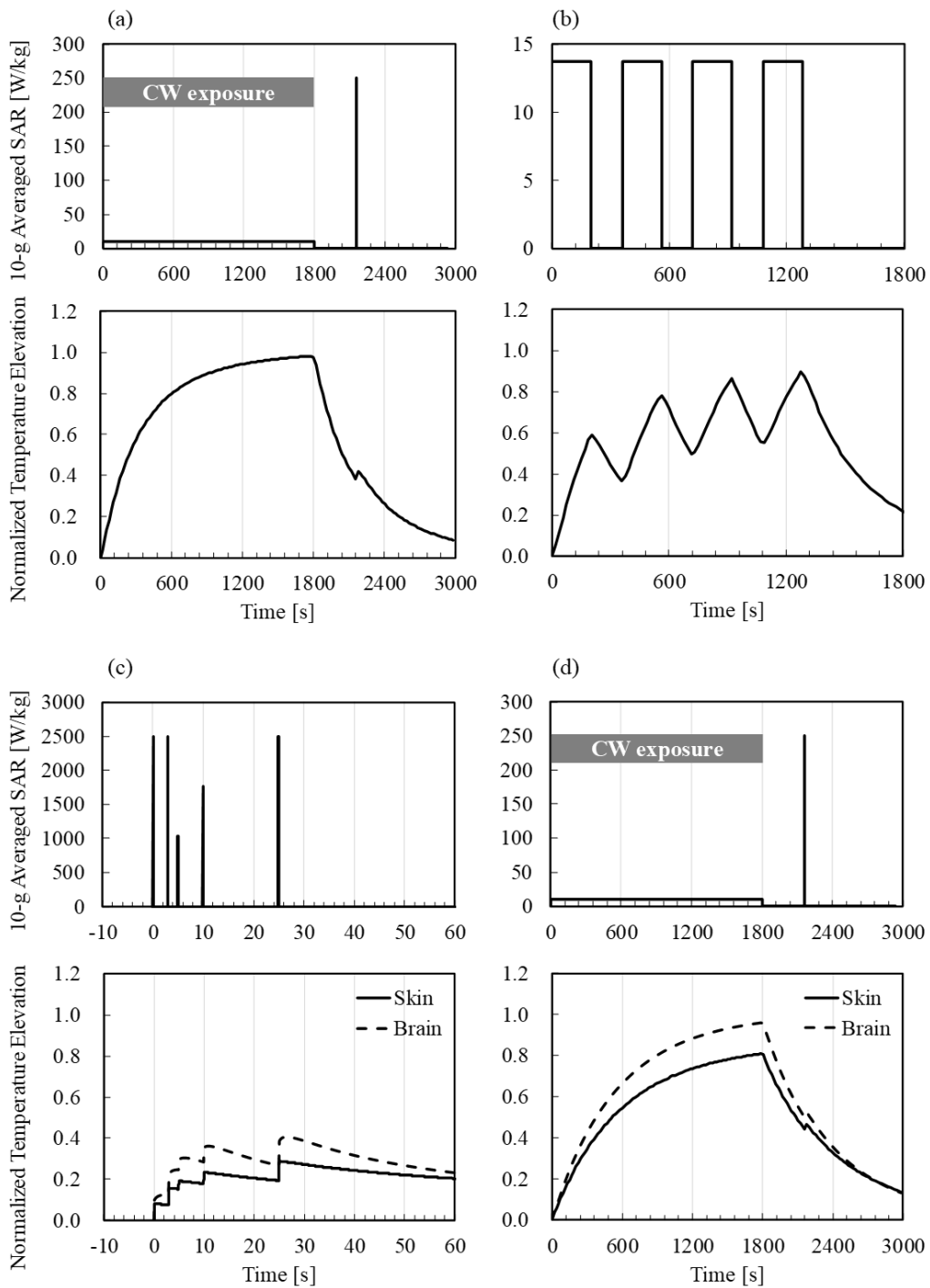
Figure 6.7 Time dependence of the peak SAR averaged over 10 g of tissue and the resulting temperature rise for four scenarios of multiple pulse exposure from a dipole antenna at 6 GHz using the multilayer cubic model.

The SAR averaged over 10 g was adjusted so that the SA did not exceed the proposed regression curve. The temperature was normalized at the peak steady-state temperature rise for continuous exposure (adjusted to 10 g averaged peak SAR at 10 W/kg).

88

## 6.4.  Discussion

We computed the temperature elevation for pulse exposures using the multilayer cubic and anatomical human models. The main contribution of this study was to reveal the limitation of SA in the current guidelines for pulse exposures and to propose a new limit.

The definition of the basic restriction in the ICNIRP 1998 guidelines [1] states "*Restrictions on exposure to time-varying electric, magnetic, and electromagnetic fields that are based directly on established health effects are termed "basic restrictions". Depending upon the frequency of the field, the physical quantities used to specify these restrictions are current density (J), specific energy absorption rate (SAR), and power density (S).*" Repetitive exposure (i.e., repetitive pulses, intermittent exposure, or non-constant exposure) is stated in ICNIRP 2013 guidelines [101] *"As a basic principle, any exposure within the anticipated maximum exposure duration, has to be below the corresponding exposure limit for that duration."*

Below 6 GHz, the SAR averaged over 10 g of tissue and the entire body are used as physical quantities describing basic exposure restrictions for local and whole-body exposures. The localized SAR has been demonstrated to be the one which can relate to a local temperature elevation. Although the localized SAR at a fixed temperature elevation depends on local heat diffusion e.g., blood flow, the heating factor, which is the ratio of temperature elevation to SAR is rather frequency independent [91]. Consequently, the steady-state temperature elevation can be estimated once the SAR is obtained. The whole-body averaged SAR is also a good surrogate for steady-state body-core temperature elevation, even though it depends on the sweating capability and body surface area-to-mass ratio, core temperature elevation can be estimated once the whole-body averaged SAR is obtained [102], [103].

There is, however, no clear trend between SA and local temperature elevation. The difference between SA and SAR is that the temperature elevation for SAR considers the steady state, whereas the temperature elevation for SA is an instantaneous peak temperature elevation. The distance that heat can diffuse then differs for different exposure durations. If the adiabatic condition is considered for uniform SAR distribution, the temperature elevation at 1 s should be 1.06 °C from the SA (3.6 kJ/kg) and the specific heat (3400 J/kg/°C). The computed temperature

elevation was higher than this value but gradually came close to this value with decreased frequency. This is because of the non-uniformity in the SAR distribution, even in the averaging cube.

Figure 6.3 shows that the temperature elevation in the skin does not reach 2.5 °C at frequencies below 300 MHz, although it depends on the choice of the thermal parameters. An energy concentration shorter than 240 s induced a temperature elevation larger than that of the steady state at 6 GHz, and the enhancement decreased as frequency decreased. The enhancement at 100 MHz is at most 40% and may be in the range of computational variability originating from the thermal parameters, the antenna position, and source modeling [104].

From the computational results, we derive a regression curves of SA to limit time-dependent allowable energy. The curves were designed considering the continuity with exposures longer than 6 min. The averaging time of 6 min has been prescribed in the international guidelines/standard for constant exposures. This value is supported by computational studies for local exposures [5], [8], [9]. In addition, the averaging mass for the SA was considered to match that of SAR. This is approximately the optimal mass to correlate the local SAR and local temperature elevations for constant exposure [71], [72], [103], [105], [106]. If the latter were not specified, the compliance may become very complicated; the evaluation metric varies with time, as mentioned above. Though not shown here to avoid repetition, we also computed the relationship between SA and temperature elevation for a planar inverted-F antenna, which is used in a commercial wireless devices. We confirmed that the results of PIFA was in the range between the plane wave and the dipole antenna. For example, the SA required for a temperature elevation of 2.5 °C for exposure from PIFA was 2.48 kJ/kg/°C, which is 17% larger than the result of dipole and 4% smaller than the plane wave at 2 GHz.

We have computed the temperature elevation over time in the skin and brain for multiple pulses when the SA did not exceed the proposed regression curve in Equation (6.1). The time-function form of the regression curve should match that above and below 6 GHz, considering exposure scenarios with frequency components both above and below 6 GHz. Equations below 6 GHz include an adjustment that incorporates the more conservative nature of the derivations for exposures above 6 GHz (see ICNIRP public consultation document).

We treated the peak temperature for multiple pulses normalized by the steady-state temperature corresponding to the localized SAR at 10 W/kg. This was performed because the localized SAR is used as the local exposure limit. As a result, the proposed regression curve kept the temperature elevation below a given level for exposure to multiple pulses and below the steady-state temperature except for one exposure scenario investigated. The temperature elevation from multiple pulses may exceed 10% or less above the steady state temperature elevation, but that excess is within the range of numerical uncertainty discussed in IEEE ICES Technical Committee 95. One of the reasons of this exceedance is attributable to the temperature decay which is attributable to the non-uniformity of the specific heat in realistic models.

The SA may be applicable for realistic exposure assessment based on reference levels for external field strength or incident power density in the case of relatively uniform field such as generated by scanning high power radar antennas. The SA derived here is used for deriving the reference level by using the conventional relationship between SAR and external field strength [107]. The purpose of this limit is more related to the exposure of 10 sec or shorter. Practically, the SA may be applied for protection in occupational exposure where the intensity is higher than the limit for constant waves, but the exposure duration is shorter than 6 min. For example, pulses from radar antennas are assumed; 0.3 s pulses with intervals of 2 s at 3 GHz. The allowable energy per pulse restricted by the proposed curve decreases as the pulse repetition increases; it may match the limit for an averaging time of 6 min.

# 6.5.   Conclusion

This chapter discussed the limit for human protection from brief RF exposures (the duration is shorter than 6 minutes) at frequencies lower than 6 GHz. There is no clear trend between SA and local temperature, unlike the relation between localized SAR and peak steady-state temperature elevation. For brief exposures above 400 MHz, the maximum temperature elevation at the SA corresponding to that from a 6 min local basic exceeds the steady state temperature, depending on the exposure scenario. Duration time dependence is more important to introduce new SA restriction. We proposed the SA based on the regression curve required for temperature elevation of 2.5 °C. In addition, we computed the temperature elevation over time for four typical scenarios with exposure to multiple pulses in the multilayer cube and human anatomical models. The regression curve derived here would be a useful index to suppress tissue temperature elevation from brief exposures. Further research may be required to explore a better physical quantity to relate the temperature elevation for such exposures.

# Chapter 7

# Summary

The rapid development of wireless technology has led to widespread concerns regarding adverse human health effects from RF wave exposure. Temperature elevation is a dominant effect for exposure at frequencies higher than 100 kHz. The international guidelines/standards define the SAR averaged over 10 g of tissue (localized SAR) as a metric for protection against localized RF field exposure from portable devices below 3–10 GHz.

The intensity and exposure duration of MW are essential for discussion of thermal damages. The rationale for the limit is based on studies of thermal damage in animals, which were then extrapolated to humans owing to ethical reasons. Human dosimetry has been widely investigated by computational approaches. However, to the best of our knowledge, no study has computed temperature elevation for local RF exposure considering thermoregulation; or compared temperature elevation and the time constant between animals and humans. There are also no discussions focusing on the location of peak temperature elevation and thermoneutral conditions. As another consideration for human safety, the energy concentration in a shorter than 6 min such as pulse exposure also may cause higher temperature elevation than constant exposure. However, to the best of our knowledge, no study has evaluated temperature elevation for a pulse or pulse trains with energy concentrated shorter than the averaging time.

In this study, we computed temperature elevation in rat and human models using multiphysics code considering thermoregulation in order to clarify the difference between them and to evaluate induced physical quantity of high-frequency exposure.

Firstly, we improved the modeling of the cerebral blood flow using measured temperature elevation and blood flow of rats. Based on the assumption that the cerebral blood flow depends

on the core and local temperatures in the brain, the parameters of the cerebral blood flow modeling were extracted by employing least-squares regression. It was combined with multiphysics code and computed the brain temperature elevations at 1.5, 6, and 10 GHz. The computed results agreed with the measured values during and after exposure in rats within an error of 10%. These findings will be helpful in estimating temperature elevation in the rat brain at multiple observation points (that are difficult to measure simultaneously) and in explaining the physiological changes in the local cortex region.

Secondly, the temperature elevation and thermal time constant were compared between rats and humans exposed from a dipole antenna at 3–10 GHz, at which local exposure in rats is possible. The peak temperature elevation in the human skin was higher than that in the rat skin at the same distance. The peak temperature elevation in the human brain was lower than that in the rat brain, primarily because of difference in depth from the scalp. The thermal time constant of the human brain was bigger than that of the rat brain, and almost frequency-independent. The thermal time constant in the skin decreases with increasing frequency and is characterized by effective SAR volume. These findings are helpful towards extrapolating animal studies to humans.

Thirdly, the temperature elevations in a human head model exposed from a dipole antenna and truncated plane waves at 300 MHz–10GHz were investigated, focusing on the location where peak temperature elevation appeared. The peak temperature elevation in the brain appeared around its periphery which is generally 0.5 °C cooler than the core of the brain. At exposures of higher intensity, the temperature elevation became larger and reached around 40 °C at localized SAR of 100 W/kg, and became lower at higher frequencies. Temperature elevation in the brain at the current limit of 10 W/kg is at most 0.93 °C. The effect of vasodilation became notable for tissue temperature elevations higher than 1–2 °C and for an SAR of 10 W/kg. The temperature at the periphery was below the basal brain temperature (37 °C). The temperature elevation under the current guidelines for occupational exposure is within the ranges of brain temperature variability for environmental changes in daily life.

Finally, temperature elevation for brief exposure in the multilayer cube and the human model at 0.1–6 GHz was investigated. First, it was confirmed that the peak temperature elevation for a

pulse with SA corresponding to occupational exposure exceeds the steady-state temperature elevation for continuous wave exposure. Then, the SA limits were proposed from regression curves which are dependent on the duration of brief exposure to RF pulse. The temperature elevation in a multilayer cube and an anatomical human model were also computed for exposures to multiple pulses. The temperature elevation from multiple pulses satisfying the regression curve was found to be below the relevant threshold level. The SA based on the proposed regression curve can be used as a metric to prevent excess temperature elevation for different scenarios of brief exposure below 6 min.

The limitation of this study is in the modeling of the thermoregulatory response. The vasodilation models of brain and skin that were based on the rat measurements for local RF exposure [76] and cutaneous veins of a dog with local warming [58], respectively, were used. The thermoregulatory response model for blood perfusion was assumed to be the same for both rats and humans because of the lack of specific data. It is difficult to determine the similarity in the thermoregulation details between humans and animals or how the results can be extrapolated to humans. We also chose a model of inner tissue where the vasodilation works only at 39 °C for stricter temperature elevation (Equation (2.8)) to ensure more safety. A recent study suggested the possibility of working with smaller temperature elevations (estimation to the muscle and fat) [108]. If such a model is used, the temperature elevation reduces by 20% or more at higher whole-body SAR [97].

However, human thermoregulation is known to be superior to that of other species, especially rodents [35]. Thus, the actual temperature elevation is expected to be lower in healthy young adults, as thermoregulation in the elderly becomes weak due to degradation of the periphery sensor. Moreover, Philips et al. [109] noted that the vasomotor is positively correlated with body mass. Gordon et al. [35] explained that even though there is a large difference in the body masses between human and rat, the values of different thermoregulatory variables are very close. In fact, our computational model has been demonstrated as useful for modeling human leg exposure to hot water (42 °C) [110]. In addition, we reviewed the thermoregulation modeling and compared our results to their performance for whole-body exposures [97]. The validation for vasodilation due to localized MW exposure was discussed only for rats [76] and rabbits [14]. The exposure

scenario is not feasible for invasive temperature measurement in humans. Accuracy improvement of thermo-regulation modeling will be focused upon in future works.

The evaluation of variability in temperature elevation for local RF exposure will also be done in future studies. For discussing the safety for human exposure, it is necessary to consider various ages, race, gender, wave source, and usage situations. In Chapter 4, we investigated the temperature elevation using four individual human head models, but further investigation of variability in temperature elevation is required.

# Acknowledgements

Firstly, I would like to express my sincere gratitude to my advisor Prof. Akimasa Hirata for the continuous support of my Ph.D. study and related research, for his patience, motivation, and immense knowledge. His guidance helped me in all the time of research and writing of this thesis.

Besides my advisor, I would like to thank the rest of my thesis committee: Prof. Nobuyoshi Kikuma and Prof. Jianqing Wang, for their insightful comments and encouragement, but also for the hard question which incented me to widen my research from various perspectives.

I would like to express my gratitude to Prof. Fujiwara who is my advisor in Bachelor's and Master's degree and always encouraged me during my Ph.D. study. I am deeply grateful to Prof. Kari Jokela, Prof. Rodney Croft, Prof. Soichi Watanabe, Prof. Hiroshi Masuda, and Prof. Takuji Arima.

My sincere thanks also goes to Dr. Jose Gomez-Tames, Dr. Essam Ali Hammam Ahmed Rashed, Dr. Takahiro Ito, and all of the laboratory member.

Finally, I would like to thank my family for encouraging and supporting the whole process of this research.

# References

[1]     ICNIRP, "Guidelines for limiting exposure to time-varying electric, magnetic, and electromagnetic fields (up to 300 GHz)," *Health Phys.*, vol. 75, no. 5, pp. 494–522, 1998.

[2]     IEEE C95.1, "IEEE standard for safety levels with respect to human exposure to radio frequency electromagnetic fields, 3 kHz to 300 GHz," *IEEE Std C95.1-2005*, 2006.

[3]     IEEE C95.3, *IEEE recommended practice for measurements and computations of radio frequency electromagnetic fields with respect to human exposure to such fields, 100 kHz-300 GHz*. Institute of Electrical and Electronics Engineers, 2002.

[4]     K. R. Foster, A. Lozano-Nieto, P. J. Riu, and T. S. Ely, "Heating of tissues by microwaves: A model analysis," *Bioelectromagnetics*, vol. 19, no. 7, pp. 420–428, 1998.

[5]     R. Morimoto, A. Hirata, I. Laakso, M. C. Ziskin, and K. R. Foster, "Time constants for temperature elevation in human models exposed to dipole antennas and beams in the frequency range from 1 to 30 GHz," *Phys. Med. Biol.*, vol. 62, pp. 1676–1699, 2017.

[6]     K. R. Foster, M. C. Ziskin, Q. Balzano, and A. Hirata, "Thermal analysis of averaging times in radiofrequency exposure limits," *IEEE Access*, vol. (submitted, 2018.

[7]     A. Hirata, T. Asano, and O. Fujiwara, "FDTD analysis of human body-core temperature elevation due to RF far-field energy prescribed in the ICNIRP guidelines.," *Phys. Med. Biol.*, vol. 52, no. 16, pp. 5013–5023, 2007.

[8]     J. Wang and O. Fujiwara, "FDTD computation of temperature rise in the human head for portable telephones," *IEEE Trans. Microw. Theory Tech.*, vol. 47, no. 8, pp. 1528–1534, 1999.

[9]     V. Leeuwen, J. J. W. Lagendijk, V. Leersum, A. P. M. Zwamborn, S. N. Hornsleth, and A. N. T. J. Kotte, "Calculation of change in brain temperatures due to exposure to a mobile phone," *Phys. Med. Biol.*, vol. 44, pp. 2367–2379, 1999.

[10]    Y. Hashimoto, A. Hirata, R. Morimoto, S. Aonuma, I. Laakso, K. Jokela, and K. Foster, "On the averaging area for incident power density for human exposure limits at frequencies over 6 GHz," *Phys. Med. Biol.*, vol. 62, pp. 3124–3138, 2017.

[11]    C.-K. Chou, A. W. Guy, L. L. Kunz, R. B. Johnson, J. J. Crowley, and J. H. Krupp, "Long-term, low-level microwave irradiation of rats," *Bioelectromagnetics*, vol. 13, no. 6, pp. 469–496, 1992.

[12]    M. Kojima, I. Hata, K. Wake, S. I. Watanabe, Y. Yamanaka, Y. Kamimura, M. Taki, and K. Sasaki, "Influence of anesthesia on ocular effects and temperature in rabbit eyes exposed to microwaves," *Bioelectromagnetics*, vol. 25, no. 3, pp. 228–233, 2004.

[13]     A. Trakic, S. Crozier, and F. Liu, "Numerical modelling of thermal effects in rats due to high-field magnetic resonance imaging (0.5–1 GHz)," *Phys. Med. Biol.*, vol. 49, no. 24, pp. 5547–5558, 2004.

[14]     A. Hirata, S. Watanabe, M. Kojima, I. Hata, K. Wake, M. Taki, K. Sasaki, O. Fujiwara, and T. Shiozawa, "Computational verification of anesthesia effect on temperature variations in rabbit eyes exposed to 2.45 GHz microwave energy," *Bioelectromagnetics*, vol. 27, no. 8, pp. 602–612, 2006.

[15]     ICNIRP 16/2009, "ICNIRP_Review : Exposure to high frequency electromagnetic fields, biological effects and health consequences (100 kHz-300 GHz)." 2012.

[16]     A. W. Guy, J. C. Lin, P. O. Kramar, and A. F. Emery, "Effect of 2450-MHz radiation on the rabbit eye," *IEEE Trans. Microw. Theory Tech.*, vol. 23, no. 6, pp. 492–498, 1975.

[17]     K. R. Foster and J. J. Morrissey, "Thermal aspects of exposure to radiofrequency energy: Report of a workshop," *Int. J. Hyperth.*, vol. 27, no. 4, pp. 307–319, 2011.

[18]     Z. Sienkiewicz, E. Van Rongen, R. Croft, G. Ziegelberger, and B. Veyret, "ICNIRP Statement : A closer look at the thresholds of thermal damage: Workshop report by an ICNIRP task group," *Health Phys.*, vol. 111, no. 3, 2016.

[19]     V. Rakesh, J. D. Stallings, B. G. Helwig, L. R. Leon, D. A. Jackson, and J. Reifman, "A 3-D mathematical model to identify organ-specific risks in rats during thermal stress," *J. Appl. Physiol.*, vol. 115, no. 12, pp. 1822–1837, 2013.

[20]     V. Rakesh, J. D. Stallings, and J. Reifman, "A virtual rat for simulating environmental and exertional heat stress.," *J. Appl. Physiol.*, vol. 117, no. 11, pp. 1278–1286, 2014.

[21]     A. Hirata, H. Masuda, Y. Kanai, R. Asai, O. Fujiwara, T. Arima, H. Kawai, S. Watanabe, I. Lagroye, and B. Veyret, "Computational modeling of temperature elevation and thermoregulatory response in the brains of anesthetized rats locally exposed at 1.5 GHz," *Phys. Med. Biol.*, vol. 56, no. 23, pp. 7639–7657, 2011.

[22]     P. Bernardi, M. Cavagnaro, S. Pisa, and E. Piuzzi, "Specific absorption rate and temperature elevation in a subject exposed in the far-field of radio-frequency sources operating in the 10-900-MHz range," *IEEE Trans. Biomed. Eng.*, vol. 50, no. 3, pp. 295–304, 2003.

[23]     A. Hirata, T. Asano, and O. Fujiwara, "FDTD analysis of body-core temperature elevation in children and adults for whole-body exposure.," *Phys. Med. Biol.*, vol. 53, no. 18, pp. 5223–38, 2008.

[24]     D. A. Nelson, S. Charbonnel, A. R. Curran, E. A. Marttila, D. Fiala, P. A. Mason, and J. M. Ziriax, "A high-resolution voxel model for predicting local tissue temperatures in humans subjected to warm and hot environments," *J. Biomech. Eng.*, vol. 131, no. 4, p. 041003, 2009.

[25]     S. M. Moore, R. L. McIntosh, S. Iskra, and A. W. Wood, "Modeling the effect of adverse environmental conditions and clothing on temperature rise in a human body exposed to radio frequency electromagnetic fields," *IEEE Trans. Biomed. Eng.*, vol. 62, no. 2, pp. 627–637, 2015.

[26]     P. Kramár, C. Harris, and A. W. Guy, "Thermal cataract formation in rabbits," *Bioelectromagnetics*, vol. 8, no. 4, pp. 397–406, 1987.

[27]     M. Kuribayashi, J. Wang, O. Fujiwara, Y. Doi, K. Nabae, S. Tamano, T. Ogiso, M. Asamoto, and T. Shirai, "Lack of effects of 1439 MHz electromagnetic near field exposure on the blood-brain barrier in immature and young rats," *Bioelectromagnetics*, vol. 26, no. 7, pp. 578–588, 2005.

[28]     T. Wu, A. Hadjem, M. F. Wong, A. Gati, O. Picon, and J. Wiart, "Whole-body new-born and young rats' exposure assessment in a reverberating chamber operating at 2.4 GHz," *Phys. Med. Biol.*, vol. 55, no. 6, pp. 1619–1630, 2010.

[29]     H. Masuda, S. Hirota, A. Ushiyama, A. Hirata, T. Arima, H. Watanabe, K. Wake, S. Watanabe, M. Taki, A. Nagai, and C. Ohkubo, "No changes in cerebral microcirculatory parameters in rat during local cortex exposure to microwaves," *In Vivo*, vol. 29, no. 2, pp. 207–15, 2015.

[30]     G. C. Van Rhoon, T. Samaras, P. S. Yarmolenko, M. W. Dewhirst, E. Neufeld, and N. Kuster, "CEM43ºC thermal dose thresholds: A potential guide for magnetic resonance radiofrequency exposure levels?," *Eur. Radiol.*, vol. 23, no. 8, pp. 2215–2227, 2013.

[31]     L. S. Goldstein, M. W. Dewhirst, M. Repacholi, and L. Kheifets, "Summary, conclusions and recommendations: adverse temperature levels in the human body," *Int. J. Hyperth.*, vol. 19, no. 3, pp. 373–384, 2003.

[32]     P. Bernardi, M. Cavagnaro, S. Pisa, and E. Piuzzi, "Specific absorption rate and temperature increases in the head of a cellular-phone user," *IEEE Trans. Microw. Theory Tech.*, vol. 48, no. 7 PART 1, pp. 1118–1126, 2000.

[33]     P. R. Wainwright, "Computational modelling of temperature rises in the eye in the near field of radiofrequency sources at 380, 900 and 1800 MHz," *Phys. Med. Biol.*, vol. 52, no. 12, pp. 3335–3350, 2007.

[34]     H. Masuda, A. Hirata, H. Kawai, K. Wake, S. Watanabe, T. Arima, F. Poulletier de Gannes, I. Lagroye, and B. Veyret, "Local exposure of the rat cortex to radiofrequency electromagnetic fields increases local cerebral blood flow along with temperature.," *J. Appl. Physiol.*, vol. 110, no. 1, pp. 142–8, 2011.

[35]     C. J. Gordon, *Temperature regulation in laboratory rodents*. Cambridge University Press, 1993.

[36]     K. R. Foster and E. R. Adair, "Modeling thermal responses in human subjects following extended exposure to radiofrequency energy," *Biomed. Eng. Online*, vol. 3, pp. 1–7, 2004.

[37]     S. M. Moore, R. L. McIntosh, S. Iskra, A. Lajevardipour, and A. W. Wood, "Effect of adverse environmental conditions and protective clothing on temperature rise in a human body exposed to radiofrequency electromagnetic fields," *Bioelectromagnetics*, vol. 38, no. 5, pp. 356–363, 2017.

[38]     K. R. Foster, M. C. Ziskin, and Q. Balzano, "Thermal response of human skin to microwave energy: A critical review," *Health Phys.*, vol. 111, no. 6, pp. 528–541, 2016.

[39]     I. Laakso, R. Morimoto, J. Heinonen, K. Jokela, and A. Hirata, "Human exposure to pulsed fields in the frequency range from 6 to 100 GHz," *Phys. Med. Biol.*, vol. 62, no. 17, pp. 6980–6992, 2017.

[40]  A. Hirata, D. Funahashi, and S. Kodera, "Setting exposure guidelines and product safety standards for radio-frequency exposure at frequencies above 6 GHz: Brief review," *Ann. Telecommun.*, vol. to be publ, 2018.

[41]  C.-K. Chou, A. W. Guy, and R. Galambos, "Auditory perception of radio-frequency electromagnetic fields," *J. Acoust. Soc. Am.*, vol. 71, pp. 1321–1334, 1982.

[42]  A. Taflove and S. C. Hagness, *Computational electrodynamics : the finite-difference time-domain method*, 3rd edn. Norwood, MA: Artech House, 2005.

[43]  Kane Yee, "Numerical solution of initial boundary value problems involving maxwell's equations in isotropic media," *IEEE Trans. Antennas Propag.*, vol. 14, no. 3, pp. 302–307, May 1966.

[44]  H. H. Pennes, "Analysis of tissue and arterial blood temperatures in the resting human forearm.," *J. Appl. Physiol.*, vol. 1, no. 2, pp. 93–122, 1948.

[45]  D. A. Nelson, "Invited editorial on "Pennes' 1948 paper revisited"," *J. Appl. Physiol.*, vol. 85, no. 1, pp. 2–3, 1998.

[46]  E. H. Wissler, "Pennes ' 1948 paper revisited," *J. Appl. Physiol.*, pp. 35–41, 2012.

[47]  T. Arima, H. Watanabe, K. Wake, H. Masuda, S. Watanabe, M. Taki, and T. Uno, "Local exposure system for rats head using a figure-8 loop antenna in 1500-MHz band," *IEEE Trans. Biomed. Eng.*, vol. 58, pp. 2740–2747, 2011.

[48]  K. Wake, H. Hongo, S. Watanabe, M. Taki, Y. Kamimura, Y. Yamanaka, T. Uno, S. Member, and M. Kojima, "Development of a 2.45-GHz local exposure system for in vivo study on ocular effects," vol. 55, no. 3, pp. 588–596, 2007.

[49]  A. Drossos, V. Santomaa, and N. Kuster, "The dependence of electromagnetic energy absorption upon human head tissue composition in the frequency range of 300-3000 MHz," *IEEE Trans. Microw. Theory Tech.*, vol. 48, no. 11, pp. 1988–1995, 2000.

[50]  T. Nagaoka, S. Watanabe, K. Sakurai, E. Kunieda, S. Watanabe, M. Taki, and Y. Yamanaka, "Development of realistic high-resolution whole-body voxel models of Japanese adult males and females of average height and weight, and application of models to radio-frequency electromagnetic-field dosimetry," *Phys. Med. Biol.*, vol. 49, no. 1, pp. 1–15, 2004.

[51]  A. Christ, W. Kainz, E. G. Hahn, K. Honegger, M. Zefferer, E. Neufeld, W. Rascher, R. Janka, W. Bautz, J. Chen, B. Kiefer, P. Schmitt, H. P. Hollenbach, J. Shen, M. Oberle, D. Szczerba, A. Kam, J. W. Guag, and N. Kuster, "The Virtual Family - Development of surface-based anatomical models of two adults and two children for dosimetric simulations," *Phys. Med. Biol.*, vol. 55, no. 2, 2010.

[52]  S. Kodera, J. Gomez-Tames, and A. Hirata, "Temperature elevation in the human brain and skin with thermoregulation during exposure to RF energy," *Biomed. Eng. Online*, vol. 17, no. 1, pp. 1–17, 2018.

[53]  J. A. Roden, S. D. Gedney, A. J. Roden, and S. D. Gedney, "Convolutional PML(CPML): An efficient FDTD implementation of the CFS-PML for arbitrary media," *Microw. Opt. Technol. Lett.*, vol. 27, no. 5, pp. 334–339, 2000.

[54]   S. Gabriel, R. W. Lau, and C. Gabriel, "The dielectric properties of biological tissues: III. Parametric models for the dielectric spectrum of tissues.," *Phys. Med. Biol.*, vol. 41, no. 11, pp. 2271–93, 1996.

[55]   K. Sasaki, K. Wake, and S. Watanabe, "Development of best fit Cole-Cole parameters for measurement data from biological tissues and organs between 1 MHz and 20 GHz," *Radio Sci.*, vol. 49, no. 7, pp. 459–472, Jul. 2014.

[56]   A. Hirata, M. Fujimoto, T. Asano, J. Wang, O. Fujiwara, and T. Shiozawa, "Correlation between maximum temperature increase and peak SAR with different average schemes and masses," *IEEE Trans. Electromagn. Compat.*, vol. 48, no. 3, pp. 569–578, 2006.

[57]   H. B. Lee and M. D. Blaufox, "Blood volume in the rat.," *J. Nucl. Med.*, vol. 26, no. 1, pp. 72–6, 1985.

[58]   J. A. Stolwijk, "A mathematical model of physiological temperature regulation in man," *NASA Contract. Rep.*, vol. CR-1855, no. August, p. 77, 1971.

[59]   A. Hirata and O. Fujiwara, "Modeling time variation of blood temperature in a bioheat equation and its application to temperature analysis due to RF exposure," *Phys. Med. Biol.*, vol. 54, pp. N189–N196, 2009.

[60]   M. Hoque and O. P. Gandhi, "Temperature distributions in the human leg for VLF-VHF exposures at the ANSI-recommended safety levels," *IEEE Trans. Biomed. Eng.*, vol. 35, no. 6, pp. 442–449, 1988.

[61]   I. Chatterjee and O. P. Gandhi, "An inhomogeneous thermal block model of man for the electromagnetic environment.," *IEEE Trans. Biomed. Eng.*, vol. 30, no. 11, pp. 707–15, 1983.

[62]   D. Fiala, K. Lomas, and M. Stohrer, "Computer prediction of human thermoregulatory and temperature responses to a wide range of environmental conditions," *Int. J. Biometeorol.*, vol. 45, pp. 143–159, 2001.

[63]   T. E. Cooper and G. J. Trezek, "Correlation of thermal properties of some human tissue with water content.," *Aerosp. Med.*, vol. 42, no. 1, pp. 24–27, 1971.

[64]   M. Kleiber, "Body size and metabolic rate," *Physiol. Rev.*, vol. 27, no. 4, pp. 511–541, 1947.

[65]   A. Hirata, O. Fujiwara, and T. Shiozawa, "Correlation between peak spatial-average SAR and temperature increase due to antennas attached to human trunk," *IEEE Trans. Biomed. Eng.*, vol. 53, no. 8, pp. 1658–1664, 2006.

[66]   F. A. Duck, *Physical properties of tissues: A comprehensive reference book*. New York: Academic, 1990.

[67]   K. Sasaki, M. Mizuno, K. Wake, and S. Watanabe, "Monte Carlo simulations of skin exposure to electromagnetic field from 10 GHz to 1 THz," *Phys. Med. Biol.*, vol. 62, no. 17, pp. 6993–7010, 2017.

[68]   IEEE 1528-2013, "IEEE recommended practice for determining the peak spatial-average specific absorption rate (SAR) in the human head from wireless communications devices: measurement techniques," 2013.

[69]   IEC 62209-1:2016, "Measurement procedure for the assessment of specific absorption rate of human exposure to radio frequency fields from hand-held and body-mounted wireless communication devices - Part 1: Devices used next to the ear (Frequency range of 300 MHz to 6 GHz)," 2016.

[70]   R. Matthes, "Response to questions and comments on ICNIRP.," *Health Phys.*, vol. 75, no. 4, pp. 438–9, 1998.

[71]   A. Hirata and O. Fujiwara, "The correlation between mass-averaged SAR and temperature elevation in the human head model exposed to RF near-fields from 1 to 6 GHz," *Phys. Med. Biol.*, vol. 54, no. 23, pp. 7227–7238, 2009.

[72]   A. Razmadze, L. Shoshiashvili, D. Kakulia, R. Zaridze, G. Bit-Babik, and A. Faraone, "Influence of specific absorption rate averaging schemes on correlation between mass-averaged specific absorption rate and temperature rise," *Electromagnetics*, vol. 29, no. 1, pp. 77–90, 2009.

[73]   R. L. McIntosh and V. Anderson, "SAR versus S inc : What is the appropriate RF exposure metric in the range 1-10 GHz? Part II: Using complex human body models," *Bioelectromagnetics*, vol. 31, no. 6, pp. 467–478, 2010.

[74]   WHO, "WHO research agenda for radiofrequency fields," *Geneva: World Health Organisation*, 2010. [Online]. Available: http://apps.who.int/iris/bitstream/10665/44396/1/9789241599948_eng.pdf. [Accessed: 17-Feb-2017].

[75]   S. Kodera, R. Morimoto, A. Hirata, H. Masuda, T. Arima, and S. Watanabe, "Accurate multi-physics analysis of temperature elevation in rat brain for localized microwave exposure (in Japanese)," *Inst. Electron. Inf. Commun. Eng.*, vol. J100–C, no. 5, pp. 200–207, 2017.

[76]   S. Kodera, J. Gomez-Tames, A. Hirata, H. Masuda, T. Arima, and S. Watanabe, "Multiphysics and thermal response models to improve accuracy of local temperature estimation in rat cortex under microwave exposure," *Int. J. Environ. Res. Public Health*, vol. 14, no. 4, p. 358 (1-18), 2017.

[77]   K. Funakura, Y. Kushiyama, T. Uno, and T. Arima, "Development of antenna for local exposure of small animals in UWB frequency band," *IEICE Tech. Rep. A.P*, vol. 114, no. 62, pp. 1–4, 2014.

[78]   H. S. Sharma, "Hyperthermia induced brain oedema: current status and future perspectives," *Indian J. Med. Res.*, vol. 123, pp. 629–652, 2006.

[79]   A. S. Kalmbach and J. Waters, "Brain surface temperature under a craniotomy," *J. Neurophysiol.*, vol. 108, no. 11, pp. 3138–3146, 2012.

[80]   E. A. Kiyatkin and H. S. Sharma, "Permeability of the blood–brain barrier depends on brain temperature," *Neuroscience*, vol. 161, no. 3, pp. 926–939, Jul. 2009.

[81]   A. Hirata, H. Sugiyama, M. Kojima, H. Kawai, Y. Yamashiro, O. Fujiwara, S. Watanabe, and K. Sasaki, "Computational model for calculating body-core temperature elevation in rabbits due to whole-body exposure at 2.45 GHz.," *Phys. Med. Biol.*, vol. 53, no. 12, pp. 3391–404, 2008.

[82] R. L. McIntosh and V. Anderson, "A comprehensive tissue properties database provided for the thermal assessment of a human at rest," *Biophys. Rev. Lett.*, vol. 05, no. 03, pp. 129–151, 2010.

[83] R. L. McIntosh and V. Anderson, "Erratum: a comprehensive tissue properties database provided for the thermal assessment of a human at rest," *Biophys. Rev. Lett.*, vol. 05, no. 03, pp. 129–151, 2010.

[84] S. Kodera and A. Hirata, "Comparison of thermal response for RF exposure in human and rat models," *Int. J. Environ. Res. Public Health*, vol. 15, no. 10, p. 2320 (1-17), 2018.

[85] ICNIRP, "Draft Appendix A : Guidelines for limiting exposure to time-varying electric, magnetic, and electromagnetic fields (up to 300 GHz)," *Health Phys.*, 2018.

[86] J. P. Reilly and A. Hirata, "Low-frequency electrical dosimetry: research agenda of the IEEE International Committee on Electromagnetic Safety," *Phys. Med. Biol.*, vol. 61, no. 12, pp. R138–R149, Jun. 2016.

[87] J. Gomez-Tames, I. Laakso, Y. Haba, A. Hirata, D. Poljak, and K. Yamazaki, "Computational artifacts of the in situ electric field in Anatomical Models Exposed to Low-Frequency Magnetic Field," *IEEE Trans. Electromagn. Compat.*, vol. 60, no. 3, pp. 589–597, 2018.

[88] "Dielectric properties of body tissues." [Online]. Available: http://niremf.ifac.cnr.it/tissprop/htmlclie/htmlclie.php.

[89] A. K. Lee, H. Do Choi, H. S. Lee, and J. K. Pack, "Human head size and SAR characteristics for handset exposure," *ETRI J.*, vol. 24, no. 2, pp. 176–179, 2002.

[90] G. Bit-Babik, A. W. Guy, C.-K. Chou, A. Faraone, M. Kanda, A. Gessner, J. Wang, and O. Fujiwara, "Simulation of exposure and SAR estimation for adult and child heads exposed to radiofrequency energy from portable communication devices," *Radiat. Res.*, vol. 163, no. 5, pp. 580–590, 2005.

[91] R. Morimoto, I. Laakso, V. De Santis, and A. Hirata, "Relationship between peak spatial-averaged specific absorption rate and peak temperature elevation in human head in frequency range of 1-30 GHz.," *Phys. Med. Biol.*, vol. 61, pp. 5406–5425, 2016.

[92] National Toxicology Program, "Technical report on the toxicology and carcinogenesis studies in Hsd:Sprague Dawley SD rats exposed to whole-body radio frequency radiation at a frequency (900 MHz) and modulations (GSM and CDMA) used by cell phones," vol. NTP TR 595, 2018.

[93] National Toxicology Program, "Technical report on the toxicology and carcinogenesis studies in B6C3F1/N mice exposed to whole-body radio frequency radiation at a frequency (1900 MHz) and modulations (GSM and CDMA) used by cell phones," vol. NTP TR 595, 2018.

[94] ICNIRP, "Note: ICNIRP note on recent animal carcinogenesis studies," 2018. [Online]. Available: https://www.icnirp.org/cms/upload/publications/ICNIRPnote2018.pdf.

[95] K. R. Foster, M. C. Ziskin, and Q. Balzano, "Thermal modeling for the next generation of radiofrequency exposure limits: Commentary," *Health Phys.*, vol. 113, no. 1, pp. 41–53, 2017.

[96]    H. Wang, B. Wang, K. P. Normoyle, K. Jackson, K. Spitler, M. Sharrock, C. M. Miller, C. Best, D. Llano, and R. Du, "Brain temperature and its fundamental properties: A review for clinical neuroscientists," *Front. Neurosci.*, vol. 8, no. 11, pp. 1–17, 2014.

[97]    I. Laakso and A. Hirata, "Dominant factors affecting temperature rise in simulations of human thermoregulation during RF exposure.," *Phys. Med. Biol.*, vol. 56, no. 23, pp. 7449–71, 2011.

[98]    J. J. Aschoff, "Circadian control of body temperature," *J. Therm. Biol.*, vol. 8, no. 1–2, pp. 143–147, 1983.

[99]    A. Kotte, G. Van Leeuwen, and D. Bree, "Modelling the thermal impact of a discrete vessel tree," *Phys. Med. Biol.*, vol. 44, pp. 57–74, 1999.

[100]   S. Kodera, A. Hirata, D. Funahashi, S. Watanabe, K. Jokela, and R. J. Croft, "Temperature rise for brief radio-frequency exposure below 6 GHz," *IEEE Access*, vol. 6, pp. 65737–65746, 2018.

[101]   ICNIRP, "ICNIRP guidelines on limits of exposure to incoherent visible and infrared radiation," *Health Phys.*, vol. 105, no. 1, pp. 74–96, 2013.

[102]   A. Hirata, H. Sugiyama, and O. Fujiwara, "Estimation of core temperature elevation in humans and animals for whole-body averaged SAR," *Prog. Electromagn. Reserch*, vol. 99, pp. 53–70, 2009.

[103]   A. Hirata, I. Laakso, T. Oizumi, R. Hanatani, K. H. Chan, and J. Wiart, "The relationship between specific absorption rate and temperature elevation in anatomically based human body models for plane wave exposure from 30 MHz to 6 GHz," *Phys. Med. Biol.*, vol. 58, no. 4, pp. 903–921, 2013.

[104]   I. Laakso, R. Morimoto, A. Hirata, and S. Member, "Computational dosimetry of the human head exposed to near-field microwaves using measured blood flow," *IEEE Trans. Electromagn. Compat.*, vol. 59, no. 2, pp. 739–746, 2016.

[105]   R. L. Mcintosh and V. Anderson, "SAR versus VAR, and the size and shape that provide the most appropriate RF exposure metric in the range of 0.5-6 GHz," *Bioelectromagnetics*, vol. 32, pp. 312–321, 2011.

[106]   J. F. Bakker, M. M. Paulides, E. Neufeld, A. Christ, N. Kuster, and G. C. van Rhoon, "Children and adults exposed to electromagnetic fields at the ICNIRP reference levels: theoretical assessment of the induced peak temperature increase," *Med. Biol. Phys. Med. Biol*, vol. 56, pp. 4967–4989, 2011.

[107]   G. Neubauer, P. Preiner, S. Cecil, N. Mitrevski, J. Gonter, and H. Garn, "The relation between the specific absorption rate and electromagnetic field intensity for heterogeneous exposure conditions at mobile communications frequencies," *Bioelectromagnetics*, vol. 30, no. 8, pp. 651–662, 2009.

[108]   M. Murbach, E. Neufeld, M. Capstick, W. Kainz, D. O. Brunner, T. Samaras, K. P. Pruessmann, and N. Kuster, "Thermal tissue damage model analyzed for different whole-body SAR and scan durations for standard MR body coils," *Magn. Reson. Med.*, vol. 71, no. 1, pp. 421–431, 2014.

[109]   P. K. Phillips and J. E. Heath, "Dependency of surface temperature regulation on body size in terrestrial mammals," *J. Therm. Biol.*, vol. 20, no. 3, pp. 281–289, 1995.

[110] A. Hirata, T. Nomura, and I. Laakso, "Computational estimation of body temperature and sweating in the aged during passive heat exposure," *Int. J. Therm. Sci.*, vol. 89, no. C, pp. 154–163, 2015.

# Publication Lists

*Published Papers for Thesis*

i.  <u>S. Kodera</u>, R. Morimoto, A. Hirata, H. Masuda, T. Arima, and S. Watanabe, "Accurate multi-physics analysis of temperature elevation in rat brain for localized microwave exposure," The Institute of Electronics, Information and Communication Engineers, vol. J100-C, no.5, pp.200–207, 2017. (in Japanese)

ii. <u>S. Kodera</u>, J. Gomez-Tames, A. Hirata, H. Masuda, T. Arima, and S. Watanabe, "Multiphysics and thermal response models to improve accuracy of local temperature estimation in rat cortex under microwave exposure," International Journal of Environmental Research and Public Health, vol.14, no.4, pii: E358, pp.1–18, 2017.

iii. <u>S. Kodera</u>, J. Gomez-Tames, and A. Hirata, "Temperature elevation in the human brain and skin with thermoregulation during exposure to RF energy," BioMedical Engineering OnLine, vol.17, no.1, pp.1–17, 2018.

iv. <u>S. Kodera</u> and A. Hirata, "Comparison of thermal response for RF exposure in human and rat models," International Journal of Environmental Research and Public Health, vol.15, no.10, pii: E2320, pp.1–17, 2018.

v.  <u>S. Kodera</u>, A. Hirata, D. Funahashi, S. Watanabe, K. Jokela, and R. J. Croft, "Temperature rise for brief radio-frequency exposure below 6 GHz," IEEE Access, vol.6, pp.65737–65746, 2018.

*Peer Reviewed Journal Paper*

vi. J. Wang, O. Fujiwara, <u>S. Kodera</u>, and S. Watanabe, "FDTD calculation of whole-body average SAR in adult and child models for frequencies from 30 MHz to 3 GHz," Physics in

Medicine and Biology, vol.51, no.17, pp.4119–4128, 2006.

vii.   A. Hirata, S. Kodera, J. Wang, and O. Fujiwara, "Dominant factors for influencing whole-body average SAR due to far-field exposure in whole-body resonance frequency and GHz regions," Bioelectromagnetics, vol.28, pp.484–487, 2007.

viii.   W. Nishio, S. Kodera, A. Hirata, D. Sasaki, T. Yamashita, R. Egawa, H. Kobayashi, and H. Sone, "Accelerating Risk Assessment of Heat Stroke for Human Exposure to Ambient Heat and Solar Radiation Using Vector Supercomputer SX-ACE," The Institute of Electronics, Information and Communication Engineers, vol. J100-C, No.5, 2017. (in Japanese)

ix.   K. Kojima, A. Hirata, K. Hasegawa, S. Kodera, I. Laakso, D. Sasaki, T. Yamashita, R. Egawa, Y. Horie, N. Yazaki, S. Kowata, K. Taguchi, and T. Kashiwa, "Risk management of heatstroke based on fast computation of temperature and water loss using weather data for exposure to ambient heat and solar radiation," IEEE Access, vol.6, pp.3774–3785, 2018.

x.   A. Hirata, K. Hasegawa, S. Kodera, Ilkka Laakso, R. Egawa, Y. Horie, N. Yazaki, K. Taguchi, and T. Kashiwa, "Risk evaluation of heat stroke with multiphysics computation and application," IEEJ Transactions on Fundamentals and Materials, vol.138, no.6, pp.288–294, 2018.

xi.   A. Hirata, D. Funahashi, S. Kodera, "Setting exposure guidelines and product safety standards for radio-frequency exposure at frequencies above 6 GHz: brief review," Annals of Telecommunications, 2018. DOI: 10.1007/s12243-018-0683-y (Early Access)

xii.   D. Funahashi, A. Hirata, S. Kodera, and K. R. Foster, "Area-averaged transmitted power density at skin surface as metric to estimate surface temperature elevation," IEEE Access, 2018. DOI: 10.1109/ACCESS.2018.2883733 (Early Access)

*Peer Reviewed Conference Presentation for Thesis (Abstract)*

xiii.  <u>S. Kodera</u>, J. Gomez-Tames, A. Hirata, H. Masuda, T. Arima, and S. Watanabe, "High accuracy estimation of brain temperature elevation in rats for localized microwave exposure," BioEM2017, S08-5, Jun. 2017.

xiv.  <u>S. Kodera</u>, J. Gomez-Tames, and A. Hirata, "Effect of vasodilatation on temperature elevation in human brain during localized RF exposure: A computational study," BioEM2018, S02-1, Jun. 2018.

xv.  <u>S. Kodera</u> and A. Hirata, "Comparison of thermal response in human and rat for RF field," Progress in Electromagnetics Research Symposium (PIERS), pp.221, Aug. 2018.

*Peer Reviewed Conference Presentation (Abstract)*

xvi.  J. Wang, <u>S. Kodera</u>, O. Fujiwara, and S. Watanabe, "Some crucial problems in large-scale FDTD calculation of whole-body average SAR with PML absorbing boundaries," EMC Europe Workshop, Electromagnetic Compatibility of Wireless Systems, pp.434–437, Sep. 2005.

xvii.  J. Wang, O. Fujiwara, <u>S. Kodera</u>, and S. Watanabe, "On FDTD-calculated whole-body average SAR at resonance frequency," BioEM2005, 8-5, Jun. 2005.

xviii.  A. Hirata, <u>S. Kodera</u>, J. Wang, and O. Fujiwara, "EM absorption mechanism of human body model for far-field exposure in whole-body resonance frequency and GHz regions," BEMS Annual Meeting 2006, S12-4, Jun. 2006.

xix.  A. Hirata, <u>S. Kodera</u>, J. Wang, and O. Fujiwara, "Mechanism of double-humped frequency characteristics of whole-body average SAR due to far-field exposure at ICNIRP reference level", EMC Europe, pp.598-602, Sep. 2006.

xx.  K. Kojima, <u>S. Kodera</u>, and A. Hirata, "Validation and application of thermal modeling in human for localized heat exposure," URSI General Assembly and Scientific Symposium,

K23-3, Aug. 2017.

xxi.    A. Hirata, <u>S. Kodera</u>, K. Hasegawa, K. Kojima, D. Sasaki, T. Yamashita, and R. Egawa, "Fast computation of temperature and water loss in human models for simultaneous exposure to ambient heat and solar radiation," The 17th International Conference on Environmental Ergonomics (ICEE2017), pp.101, Nov. 2017.

xxii.    H. Masuda, I. Kageyama, T. Ishitake, A. Hirata, <u>S. Kodera</u>, T. Arima, Y. Kushiyama, and Y. Morimatsu, "Effects of high intensity local exposure of a 10 Ghz-electromagnetic field on glial activity in rat brain," 2018 ISES-ISEE, pp.1558, Aug. 2018.

# Appendix A:

# Effect of Truncated Model and

# Variation of Thermal Parameters

Chapters 4–6 treated the truncated head models and assumed that sweating and changing core temperature were marginal.

To verify the validity of these assumptions, two scenarios were compared: (i) the whole body model considering thermoregulation with sweating and changing core temperature; (ii) the truncated head model considering thermoregulation without sweating and fixed core temperature. The computing condition was the maximum exposure level in this study (localized SAR = 100 W/kg) from the dipole antenna at 1GHz.

The averaged skin and core temperature elevation (whole-body) were at most 0.3 and 0.1 °C, respectively. Over one-hour duration, this is sufficient to reach the thermal steady state. The maximum temperature elevation difference in the skin between these two scenarios was 5% (11.3 °C and 11.9 °C in the whole-body model considering thermoregulation with sweating and in the truncated head model considering thermoregulation but without sweating and core temperature change, respectively).

These results suggest that the temperature elevation computation in the head model without considering sweating was sufficient for computing the local temperature elevation and vasodilation for local exposures.

Another factor that can influence our results is the initial blood perfusion rate. We computed the temperature elevation using the basal blood perfusion in McIntosh et al. [82], [83]. The maximum temperature elevation in the brain due to dipole antenna exposure at 1 GHz was 3.19 and 4.76 °C for peak SAR values of 50 and 100 W/kg, respectively. The difference was less than

10%. The temperature elevation is approximately estimated by volume averaged blood flow as in [65]. Thus, the value of our skin blood perfusion is different from the value in the review, but the difference in the computed temperature was at most 25% [104].